University of Venda

Recent numerical techniques for differential equations arising in fluid flow problems

by

Hillary MUZARA

A Thesis Presented to the

UNIVERSITY OF VENDA

In Partial Fulfilment of the Requirements for the Degree

of

Doctor of Philosopy

in

APPLIED MATHEMATICS

Promoter: Prof S. Shateyi (University of Venda)

Co-Promoter: Dr G. T. Marewo (North-West University)

August 2019

Declaration of Authorship

I, Hillary MUZARA, declare that this thesis titled, 'Recent numerical techniques for differential equations arising in fluid flow problems' is my own work and it has never been submitted before for any degree or examination in any other university, where I have quoted from the work of others, the source is always given.

- This work was done wholly or mainly while in candidature for a research degree at this University.
- Where any part of this thesis has previously been submitted for a degree or any other qualification at this University or any other institution, this has been clearly stated.
- Where I have consulted the published work of others, this is always clearly attributed.
- Where I have quoted from the work of others, the source is always given. With the exception of such quotations, this thesis is entirely my own work.
- I have acknowledged all main sources of help.
- Where the thesis is based on work done by myself jointly with others, I have made clear exactly what was done by others and what I have contributed myself.

Signed: _____

Date: _____

Articles published from this Thesis

The work presented in this thesis has been published in international refereed journals. The articles published are:

1. **Muzara, H.**, Shateyi, S., & Marewo, G.T. (2018). Spectral quasi-linearization method for solving the Bratu problem. Advances and Applications in Fluid Mechanics, 21(4), 449 – 463.

2. **Muzara, H.**, Shateyi, S., & Marewo, G.T. (2018). On the bivariate spectral quasi-linearization method for solving the two-dimensional Bratu problem. Open Physics, 16(1), 554 – 562.

3. **Muzara, H.**, Shateyi, S., & Marewo, G.T. (2019). A numerical analysis of laminar boundary layer flow of a Jeffrey fluid past a vertical porous plate in the presence of thermal radiation and chemical reaction. JP Journal of Heat and Mass Transfer, 17(2), 309 - 340.

Under Review

1. **Muzara, H.**, Shateyi, S., & Marewo, G.T. A numerical study of laminar boundary layer flow, heat and mass transfer of a non-Newtonian fluid past a vertical porous plate.

Abstract

The work presented in this thesis is the application of the recently introduced numerical techniques, namely the spectral quasi-linearization method (SQLM) and the bivariate spectral quasi-linearization method (BSQLM), in solving problems arising in fluid flow.

Firstly, we use the SQLM to solve the highly non-linear one dimensional Bratu problem. The results obtained are compared with exact solution and previously published results using the B-spline method, Picard's Green's Embedded Method and the iterative finite difference method. The results obtained show that the SQLM is highly accurate and computationally efficient.

Secondly, we use the bivariate spectral quasi-linearization method to solve the two dimensional Bratu problem. Since the exact solution of the two-dimensional Bratu problem is unknown, the results obtained are compared with those previously published results using the finite difference method and the weighted residual method.

Thirdly, we use the BSQLM to study numerically the boundary layer flow of a third grade non-Newtonian fluid past a vertical porous plate. We use the Jeffrey fluid as a typical fluid which shows non-Newtonian characteristics. Similarity transformations are used to transform a system of coupled nonlinear partial differential equations into a system of linear partial differential equations which are then solved using BSQLM. The influence of some thermo-physical parameters namely, the ratio relaxation to retardation times parameter, Prandtl number, Schmidt number and the Deborah number is investigated. Also investigated is the influence of the ratio of relaxation to retardation times, Schmidt number and the Prandtl number on the skin friction, heat transfer rate and the mass transfer rate. The results obtained show that increasing the Schmidt number decelerates the fluid flow, reduces the skin friction, heat and mass transfer rates and strongly depresses the fluid concentration whilst the temperature is increased. The fluid velocity, the skin friction, heat and mass transfer rates are increased with increasing values of the relaxation to retardation parameter whilst the fluid temperature and concentration are reduced. Using the the solution based errors, it was shown that the BSQLM converges to the solution only after 5 iterations. The residual error infinity norms showed that BSQLM is very accurate by giving an error of order of 10^{-4} within 5 iterations.

Lastly we propose a model of the non-Newtonian fluid flow past a vertical porous plate in the presence of thermal radiation and chemical reaction. Similarity transformations are used to transform a system of coupled nonlinear partial differential equations into a system of linear partial differential equations. The BSQLM is used to solve the system of equations. We investigate the influence of the ratio of relaxation to retardation parameter, Schmidt number, Prandtl number, thermal radiation parameter, chemical reaction

parameter, Nusselt number, Sherwood number, local skin fiction coefficient on the fluid concentration, fluid temperature as well as the fluid velocity. From the study, it is noted that the fluid flow velocity, the local skin friction coefficient, heat and mass transfer rate are increased with increasing ratio of relaxation to retardation times parameter whilst the fluid concentration is depressed. Increasing the Prandtl number causes a reduction in the velocity and temperature of the fluid whilst the concentration is increased. Also, the local skin friction coefficient and the mass transfer rates are depressed with an increase in the Prandtl number. An increase in the chemical reaction parameter decreases the fluid velocity, temperature and the concentration. Increasing the thermal radiation parameter has an effect of decelerating the fluid flow whilst the temperature and the concentration are slightly enhanced. The infinity norms were used to show that the method converges fast. The method converges to the solution within 5 iterations. The accuracy of the solution is checked using residual errors of the functions f, θ and ϕ. The errors show that the BSQLM is accurate, giving errors of less than 10^{-4}, 10^{-7} and 10^{-8} for f, θ and ϕ, respectively, within 5 iterations.

Acknowledgements

Firstly, l want to express my gratitude to my promoter Professor Stanford Shateyi who gave me an opportunity to study towards my Doctor of Philosophy degree under his supervision and guidance. I thank him very much for the financial support he gave me during the course of my study. It could have been difficult to finish this project without the financial support.

Secondly, I want to express my deepest gratitude to my co-promoter Dr Gerald Tendayi Marewo. He made me who I am today by guiding and assisting me since the time I was doing Master of Science degree in Mathematics at the University of Zimbabwe.

Special thanks goes to my family, wife, mother and two sisters for their moral support and words of encouragement during the course of my study.

Contents

List of Figures

Nomenclature

A	cross sectional area	Nu	Nusselt number
C	concentration	Pr	Prandtl number
C_f	skin friction coefficient	q_r	radiation heat flux
D_m	mass diffusivity	T	temperature
Sc	Schmidt number	t	time
U_∞	free stream velocity	T_w	wall temperature
Re	Reynolds number	d	diameter
Gr_x	Grashof number	S	Cauchy stress tensor

Greek Symbols

α	thermal diffusivity	μ	dynamic viscosity
λ_1	ratio of relaxation to retardation times	ν	kinematic viscosity
λ_2	retardation time	ρ	density of the fluid
$\dot{\gamma}$	shear rate	κ	thermal conductivity
σ	Stefan- Boltzman constant	ω	angular velocity
θ	dimensionless temperature	τ	force stress tensor
ϕ	dimensionless concentration	τ_w	shearing stress
β_T	thermal expansion coefficient	β_T	concentration expansion coefficient
ξ	dimensionless tangential coordinate	η	dimensionless tangential coordinate

Subscripts

w	surface conditions	∞	free stream conditions

This thesis is dedicated to my mother, wife Rutendo, two daughters Helen and Helga, and my two sisters Susan and Floid.

Chapter 1

INTRODUCTION

The subject of fluid mechanics is highly relevant in such domains as chemical, metallurgical, biological and ecological engineering. Fluid mechanics deals with the behavior of fluids. It is worth studying fluid mechanics because of its wide applications in our everyday life activities. Some of the real life applications include: biological applications, automotive industry, heat exchangers, refrigerators, air conditioners, hydroelectric power sources and turbines. The study of fluid flow has attracted the attention of many researchers because of their wide applications in both nature and technology. Of very much importance is the study of heat and mass transfer by fluids through porous media. At times it is also important to consider chemical reactions that occur within the flow. The models of such fluid flow problems constitute systems of differential equations which are usually coupled, non-linear and complex, hence very difficult to find their exact solutions or solve analytically. It is due to this background that researchers seek numerical techniques which can be used to find approximate solutions to these models.

1.1 Background

A fluid can be defined as a substance that flows or deforms under applied shear stress. Fluids can be studied whilst in motion or stationary. The study of fluids in motion is called fluid kinematics and the study of stationary fluids is called fluid statics. When a fluid is subjected to a shearing stress, its layers slide relative to each other. Viscosity is the term which is used to describe the degree of the resistance of the fluid to shear stress. There are different categories of fluids depending on properties and behavior in the same atmospheric conditions. These categories are as follows:

- Idea fluid - this is an imaginary fluid that is incompressible and does not have viscosity.
- Real fluid - all fluids in practice have viscosity. A fluid which has viscosity is a real fluid.
- Newtonian fluid.
- Non-Newtonian fluid.

A fluid of importance in this work is the non-Newtonian fluid. To be discussed in this section is a non-Newtonian fluid, heat and mass transfer in non-Newtonian fluid flow, chemically reacting fluid and porous media. Some dimensionless thermophysical parameters of relevance in this study which are the Sherwood number, Prandtl number, Reynolds number, Nusselt number, Schmidt number, local skin friction and the ratio of relaxation to retardation parameter are also discussed.

1.1.1 Non-Newtonian fluid

A Newtonian fluid is best described as a fluid that obeys Newton's law of viscosity (named after Isaac Newton, 1687), that is, the shear stress between adjacent fluid layers is proportional to the value of the velocity gradient between the two layers at constant temperature and pressure. The relationship can be expressed in symbols by

$$\tau = \mu \frac{du}{dy}, \ \left(\frac{du}{dy} = \dot{\gamma}\right),$$

where μ is the fluid viscosity which is a physical property that characterizes flow resistance and $\dot{\gamma}$ is the rate of shear deformation. Some typical examples of fluids which show Newtonian characteristics are water, oil, gasoline and alcohol. There are some fluids which deviate from Newton's law of viscosity. Such fluids behave in such a way that the linear relationship between shear stress and deformation is not valid. These fluids are termed non-Newtonian fluids. Some typical examples of fluids which exhibit non-Newtonian fluid behavior include food stuffs (jams, ice creams, marmalades, sauces), molten lava, fire fighting foams, biological fluids (blood, saliva, synovial fluids), Bitumen, polymer melts and solutions, coal slurries, pharmaceutical products (creams, foams), dairy products (cheese, butter, yogurt), etc. Non-Newtonian fluids are more complex than Newtonian fluids in that there does not exist a single relation which can predict the characteristics of all the non-Newtonian materials. Also, the simple Navier-Stokes equations are not suitable to characterize the flow behavior of non-Newtonian liquids.

Depending on the complexities and the form of constitutive relations required to describe the behaviour of real fluids, non-Newtonian fluids may be conveniently classified into three broad categories, Chhabra [1]:

1. Time independent (purely viscous) - this is a fluid for which the rate of shear at any point is determined only by the value of shear stress at that point at that instant.

2. Time dependent - this is a fluid for which the relation between shear stress and shear rate depends upon the duration of shearing and their kinematic history.

3. Viscoplastic - substances exhibiting characteristics of both ideal fluids and elastic solids and showing partial elastic recovery, after deformation.

Qualitative flow curves for different types of non-Newtonian fluids are shown in Figure 1.1.

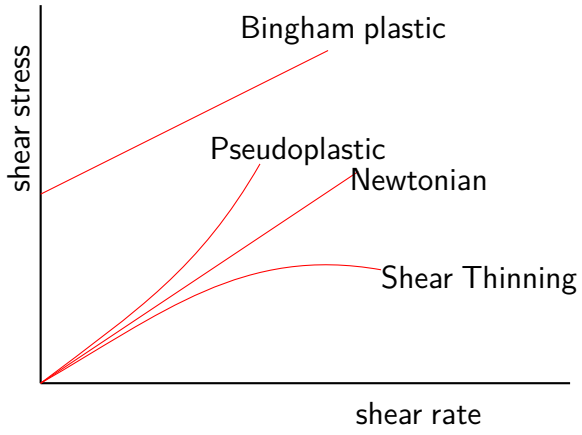

Figure 1.1: Classification of non-Newtonian fluid behaviour.

Although in recent years much attention has been directed towards non-Newtonian fluids rather than Newtonian fluids, there is some research which has been done on both types of fluids. Koplik and Banar [2] used dynamic molecular simulations to compute the flow of both a Newtonian liquid and a non-Newtonian polymer melt through a channel with reentrant corner. Kaur *et al.* [3] studied the flow of Newtonian and non-Newtonian fluids through packed beds. Nouri and Whitelaw [4] presented a communication on the flow of Newton and non-Newtonian fluid in a concentric annulus with rotation of the inner cylinder.

There are various non-Newtonian fluid models like the power law model, Bird-Carreau model, Cross-Carreau model, Herschel-Bulkley Model. A particular non-Newtonian model of importance in this study is the Jeffrey model. The constitutive equation for the Jeffrey fluid is

$$\tau = \frac{\mu}{1+\lambda_1}\left(\dot{\gamma} + \lambda_2 \ddot{\gamma}\right),$$

where λ_1 is the ratio of relaxation to retardation times and λ_2 is the retardation time. The Jeffrey fluid model exhibits the effects of ratio of relaxation to retardation times. The Jeffrey model has practical applications in biomedical sciences. The model has been used in the study of the circulation of fluids in humans. Akbar and Nadeem [5] used the Jeffrey model to study the peristaltic flow of chyme in the small intestines. Akbar *et al.* [6] studied a non-Newtonian fluid model for blood flow through a tapered artery with stenosis by assuming blood as a Jeffrey fluid. Sharma *et al.* [7] discussed the two-layered Jeffrey fluid model with mild stenois in narrow tubes. In the discussion, the blood flow in narrow arteries is treated as a Jeffrey fluid.

1.1.2 Heat transfer

Heat is transferred in fluids due to temperature differences. There are basically three ways in which heat is transferred in fluids namely convection, conduction and radiation.

Convection

Convection is the mechanism of heat transfer through a fluid in the presence of bulk fluid motion. Heat transfer in fluids generally takes place via convection. Convection currents are set up in a fluid due to temperature differences. Due to an upward buoyant force, a warmer part of the fluid, which is less dense, rises while the cooler, denser, fluid sinks. This cycle results in a continuous circulation pattern and heat is transferred to cooler areas. Transfer of heat by convection can be forced or natural or free depending on how the motion is initiated. In forced convection, the fluid motion is generated by an external source like a pump, a fan or a suction device. In natural convection, the motion of the fluid is sustained by the presence of a thermally induced density gradient.

Radiation

Thermal radiation is heat transfer due to the emission of electromagnetic waves. It is the only mode of heat transfer where a transportation medium is not required. In radiation, heat is transferred through open space. As an example, it is through thermal radiation that we feel the heat from the sun. The Stefan-Boltzmann law of thermal radiation (by Josef Stefan (1879) and Ludwig Boltzmann (1884)) states that the total radiant heat energy emitted from a surface is proportional to the fourth power of its absolute temperature. That is

$$q = \sigma T^4,$$

where q is the gross energy emitted from an ideal surface per unit area, time, σ is the Stefan Boltzman constant and T is the absolute temperature of the emitting surface in kelvins.

Part of this work is on the Bratu model. The Bratu equation, also known as Liouville-Bratu-Gelfand equation is a nonlinear Poisson equation named after Joseph Liouville, G. Bratu and Israel Gelfand. The Bratu model is applied in radiative heat transfer within a reacting solid and in spontaneous combustion theory. More on the Bratu model is discussed in Chapters 2 and 3.

Conduction

Heat is always transferred from a higher energy level to a low energy level according to the second law of theromdynamics. In conduction, heat is carried by means of collisions between rapidly moving molecules closer to the hot end of a body of matter and the slower molecules closer to the cold end. Some of the kinetic energy of the fast molecules passes to the slow molecules, and as a result of successive collisions, heat flows through the body of matter from the hot end to the cold end. Solids, liquids, and gases all conduct heat. The equation governing heat conduction along a body of length (thickness) L and cross-sectional area A, in a time t is

$$q = \frac{kA\Delta Tt}{L},$$

where q is energy transferred per unit time, k is the thermal conductivity and ΔT is the temperature change.

In this study, a dimensionless parameter of importance is the heat transfer coefficient, also known as the Nusselt number, named after Wilhelm Nusselt. The Nusselt number is used to describe the ratio of the thermal energy converted to the fluid to the thermal energy conducted within the fluid, that is

$$Nu = \frac{\text{convective heat transfer}}{\text{conductive heat transfer}} = \frac{hL}{\kappa}.$$

This ratio shows how much is the heat transferred due to fluid motion as compared to the heat by the fluid by conduction. If $Nu \gg 1$, it means that convection is more dominant in the fluid flow. If $Nu = 1$, it shows that the fluid layer represents heat transfer by pure conduction across the the layer.

1.1.3 Mass transfer

Mass transfer specifically refers to the relative motion of species in a mixture due to concentration gradients not the transfer of mass due to the bulk fluid motion. The transportation is independent of pressure

gradients. Usually in many technical applications, heat transfer and mass transfer processes occur simultaneously. Mass transfer occurs in many processes, such as evaporation, drying, adsorption, precipitation, membrane filtration and distillation. Some of typical real life examples of mass transfer include evaporation of a drop of perfume in a room, movement of a drop of food coloring in a glass of water, where eventually the entire glass will be colored and in making tea where molecules from the tea cross the tea bag and spread into the water.

Modes of mass transfer

There are two distinct modes of transport, namely, molecular mass transfer and convective mass transfer.

Molecular mass transfer

Molecular mass transfer is also known as mass diffusion. This is a mode of mass transfer where molecules are transferred from a high chemical potential region to a low chemical potential region. Molecular mass transfer is a phenomena that causes the distribution of a chemical species to become uniform in space as time passes. This happens because of the thermal motion of the molecules. At temperatures above absolute zero, the molecules possess kinetic energy and always in motion. They will frequently collide with each other and the direction of motion randomized. The partial differential equations used to model diffusion problems include the Fick's laws of diffusion [8] and Maxwell-Stefan diffusion equation [9].

Convective mass transfer

Convective mass transfer refers to the transfer of molecules in bulk due to the bulk motion of the fluid. It can also be viewed as the transport of materials between a boundary surface and a moving fluid or between two immiscible moving fluids separated by a mobile interface. Convection mass transfer can be classified as either forced convection or natural convection. In forced convection, the fluid moves under the influence of an external force. Examples of force convection include the transfer of a liquid using a pump and the transfer of a gas using a compressor. In natural convection, currents develop as a result of a variation in density within the fluid phase. This can be as a result of differences in temperature or concentration.

The Sherwood number (named after Thomas Kilgore Sherwood), is a dimensionless number used in mass transfer operation. The Sherwood number is defined as the ratio of the convective mass transfer to

the mass diffusivity.

$$Sh = \frac{\text{Convective mass transfer}}{\text{Mass diffusion rate}} = \frac{h}{D_m/L},$$

where h is a convective mass transfer film coefficient.

1.1.4 Porous media

A porous medium is defined as a material that consists of a solid matrix with an interconnected void. The interconnected pores allow the flow of one or more fluids. In a single-phase system, the void space of the porous medium is filled by a single fluid (or by several fluids completely miscible with each other). In a multi-phase system, the void space is filled by two or more fluids that are immiscible with each other. Some typical examples of porous media are sand, cemented sandstone, form rubber, bread and lungs. The porous media can be naturally formed (rocks, sponges) or fabricated (insulation, wicks). Convective heat transfer in fluid saturated porous media has gained considerable attention in recent decades due to its relevance in a wide range of applications such as geothermal engineering, nuclear waste repository, underground spreading of chemical waste, thermal insulation and water movements in geothermal reservoirs.

1.1.5 Boundary layer flow

The boundary layer theory was proposed by Ludwig Prandtl in 1904. A boundary layer refers to the boundary of fluid in the immediate viscinity of the bounding surface where the effects of viscosity are significant. Suppose we consider the flow of a viscous fluid over the plate surface with 'non slip' conditions. When the fluid flows along the surface, the fluid particles adjacent to the surface stick to the surface and have a velocity of zero. The velocity of the fluid varies from zero at the surface to the stream velocity U_∞ further away from the surface. The thin layer out of which the fluid flows faster than the fluid close to the surface is called the boundary layer or the hydrodynamic layer.

A thermal boundary layer is analogous to the hydrodynamic boundary layer. Consider a fluid flowing over a solid heated surface. The surface is at a temperature T_w and the fluid has a temperature T_∞ in an undisturbed flow. As shown in Fig 1.2, the temperature of the fluid at a distance y from the surface is $T(y)$. The thermal boundary is the layer where the difference between the local temperature and the surface temperature is 99% of the difference between the undisturbed fluid temperature and the surface

temperature. Let us consider a dimensionless temperature given by the ratio:

$$\theta(x, y) = \frac{T(y) - T_w}{T_\infty - T_w},$$

the thermal boundary layer can be define as the locus of all the points a distance y from the surface where $\theta = 0.99$.

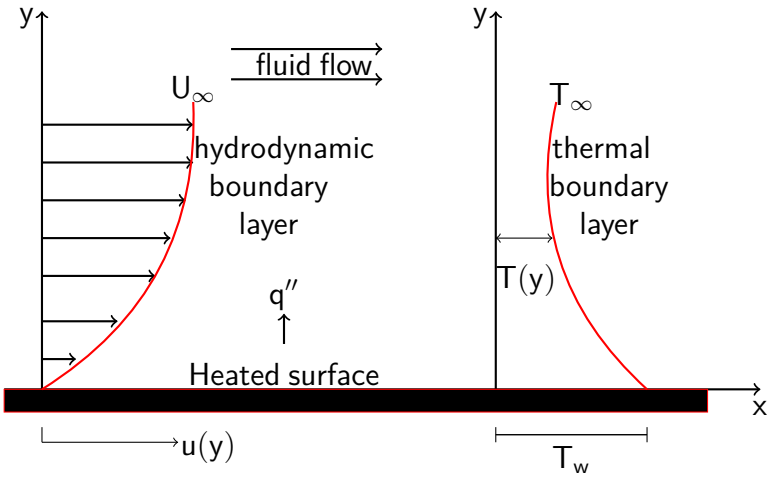

Figure 1.2: Qualitative flow curves for different types of non-Newtonian fluids.

In heat transfer problems, the Prandtl number (Pr) controls the relative thickness of the velocity and thermal boundary layers. That is,

$$Pr = \frac{\text{viscous diffusion rate}}{\text{thermal diffusion rate}} = \frac{\nu}{\alpha}.$$

This means that in fluid flow, if $Pr \ll 1$, it means that thermal diffusivity is dominant, hence heat transfer is mainly by conduction. If $Pr \gg 1$, it means momentum diffusivity dominates.

Boundary layers develop due to the stickness or viscosity of the fluid. A boundary layer maybe laminar or turbulent. The pattern of the fluid flow, whether laminar or turbulent, can be determined efficiently using a dimensionless parameter known as the Reynolds number (Re) named after Obsorne Reynolds who popularized its use in 1883.

$$Re = \frac{\rho U d}{\mu},$$

where ρ is the density of the fluid, U is the velocity of the fluid, d is the diameter of the fluid and μ is the viscosity of the fluid. In a laminar boundary layer, each layer slides past the adjacent layers. Any exchange of mass or momentum occurs between adjacent layers on a microscopic scale. The laminar boundary layers occur when the Reynolds numbers are small. In contrast to laminar boundary layers is the turbulent boundary layer where there is an intense agitation. Turbulent boundary layers are caused by eddy currents which result from differences in the fluid's speed and direction which may sometimes intersect or even counter to the overall direction of fluid flow. The exchange of mass, momentum and energy is now at a much bigger scale than in the laminar boundary layer flow.

A dimensionless parameter of interest in the study of boundary layers is the skin friction drag. Skin friction drag is the frictional shear force exerted on a body aligned parallel to the flow. Since the shear stress is greater in vicinity of the wall or solid surface, the skin friction is greater in the turbulent boundary layer flow than in laminar boundary layer flow. The skin friction C_f is given by:

$$C_f = \frac{\tau_w}{\frac{1}{2}\rho U_\infty^2},$$

where the shear stress is given by

$$\tau_w = \mu \left.\frac{\partial u}{\partial y}\right|_{y=0}.$$

1.1.6 Chemically reacting fluid flow

There are two types of chemical reactions namely homogeneous gas-phase chemistry and heterogeneous surface chemistry. Heterogeneous reactions are of practical interest. A heterogeneous reaction is a chemical reaction where the reactants are components of two or more phases (solid and gas, solid and liquid, two immiscible liquids) or in which one or more reactants undergo chemical change at an interface like what happens on the surface of a solid catalyst. Examples of heterogeneous reactions include those reactions which occur in the phenomena of corrosion and the electrochemical changes that occur in batteries and electrolytic cells. A homogeneous reaction is any chemical reaction that occur in a single phase.

1.2 Literature review on existing numerical methods which have been used to solve fluid flow problems

There has been an increasing interest of scientists and engineers in numerical and analytical techniques for strongly nonlinear fluid flow problems. Analytical methods have significant advantages over numerical methods in providing analytic, verifiable, rapidly convergent approximations. On the other hand, as the degree of nonlinearity of flow problem increases, application of analytic techniques is significantly weakened hence the need to employ numerical techniques.

One of the numerical techniques which has been used to solve problems in non-Newtonian fluid flow is the lattice Boltzmann method (LBM). The LBM has proved to be a powerful numerical technique for the simulation of single and multiphase fluid flows in complex geometries. There are several versions of the lattice Boltzmann method which include: the standard LBM, finite-difference LBM [10], finite-volume LBM, finite-element LBM [11]. Gabbanelli *et al.* [12] presented the lattice-Boltzmann method for non-Newtonian fluids. Wang and Ho [13] studied a new lattice Boltzmann approach for simulating shear-thinning non-Newtonian blood flows described by the power-law, Carreau-Yasuda and Casson rheology models.

The finite element method is another numerical method that has been used to solve fluid flow problem. Omesebi and Akabogu [14] applied Garlekin's finite element method to study the power-law non-Newtonian fluid through the porous media. A weak formulation of the generalized partial differential equations and boundary conditions was obtained. The element matrix in both the spatial and time domains were computed using the Gauss quadrature technique. Chung [15] presented the generalizes multiscale finite element method for non-Newtonian fluid flow in a perforated domain. Tanner [16] used the finite element to study incompressible non-Newtonian fluid flow with free surfaces. Böhme and Rubart [17] used the finite element method to study steady incompressible flow problems of a generalized Newtonian flow. The method is based on the variational formulation of the equations of motion. The continuity is taken into account as a secondary condition by a penalty function method.

The other numerical methods which have used to solve non-Newtonian fluid flow problems are the finite difference method (FDM) and the finite volume method (FVM). The FDM is a method in which the partial derivatives appearing in the governing equations are replaced with algebraic difference quotients yielding a system of algebraic equations which can be solved for the flow-field variables at the specific, discrete grid points in the flow domain. The FVM is a technique by which the integral formulation of the conservation laws are discretized directly in the physical space. One of the most powerful, versatile and accurate finite difference schemes is the Keller box method. Salahuddin *et al.* [18] studied the mixed

convection boundary layer flow of Williamson fluid with slip conditions over a stretching cylinder by using Keller box method.

The homotopy analysis method (HAM) first introduced by Liao [19] is a semi-analytical method that has been used to treat nonlinear partial differential equations that arise from non-Newtonian fluid low. Esmaeilpour *et al.* [20] used the homotopy analysis method to investigate heat transfer of a non-Newtonian fluid flow in an axisymmetric channel with a porous wall. The HAM was employed to obtain the expressions for velocity and temperature fields. Ellahi [21] used the HAM to derive the series solutions for the flow of third grade non-Newtonian fluid variable viscosity. Analytic solution of velocity, temperature and nanoparticle concentration were developed. Rashidi *et al.* [22] presented a theoretical study of thermoconvective boundary layer flow of a generalized third grade viscoelastic power-law non-Newtonian fluid over a porous wedge. The HAM was employed to generate approximate analytical solutions for the transformed nonlinear equations under the prescribed boundary conditions.

The Adomain decomposition method (ADM) is a semi-analytical method for solving ordinary and partial differential equations. The ADM, named after George Adomain [23] is a technique based on the representation of a solution to a functional equation as series of functions. Each term of the series is obtained from a polynomial generated by a power series expansion of an analytic function. Shakeri *et al.* [24] did an investigation on the injective micropolar flow in a porous channel. The model problem was mapped into a system of nonlinear coupled differential equations by using Berman's similarity transformation. The system was solved using ADM. Siddiqui *et al.* [25] discussed the solutions of highly nonlinear differential equations which arise in non-Newtonian fluid dynamics. They solved the basic pipe flow problems of a third grade and 6-constant Oldroyd non-Newtonian fluids. Alarm *et al.* [26] used the Adomain decomposition method to find the solution of the steady thin film flow of non-Newtonian fluid over a vertical cylinder.

The variational iteration method (VIM) was introduced by He [27]. The method has been used by many researchers to solve problems arising in fluid flow problems. Siddiqui *et al.* [28] successfully employed He's variational iteration method to solve a nonlinear boundary value problem arising in the study of thin flow of a third grade fluid down an inclined plane. Farooq *et al.* [29] used the VIM to solve a nonlinear coupled system of ordinary differential equations that arises in the fully developed natural convection flow of a third grade fluid between two vertical parallel walls. Moosavi *et al.* [30] investigated a Sisko fluid on a vertical moving belt and the fluid in a collector.

The SQLM has been used in the numerical study of fluid flow problems. RamReddy and Pradeepa [31] used the SQLM to study homogeneous and heterogeneous reactions on nonlinear convection flow of micropolar fluid saturated porous medium with convective boundary condition. Shateyi and Marewo

[32] used the SQLM to find the numerical solution of mixed convection flow of an MHD Jeffrey fluid over an exponentially stretching sheet in the presence of thermal radiation and chemical. In this study they proved the convergence and stability of the SQLM solution. They concluded that the SQLM is as good as some analytical methods such as the variational iteration method and the homotopy pertubation method. Also, Shateyi *et al.* [33] confirmed the accuracy and validity of the SQLM using `MATLAB`'s `bvp4c` routine method. Motsa [34] used the SQLM to solve the Blasius boundary layer equation and also investigate the unsteady free convective heat and mass transfer on a stretching surface in a porous medium with suction. The SQLM solution was validated by comparing with the numerical solution obtained using `MATLAB` inbuilt routine `bvp4c`. It was shown that the SQLM converges faster than the spectral relaxation method.

The BSQLM was used by Goqo *et al.* [35] to investigate entropy generation in MHD radiative viscous nanofluid over a porous a porous wedge. The numerical solutions obtained were tested for convergence and accuracy using both the convergence error norms and the residual errors. Abbas *et al.* [36] used the BSQLM to analyze heat and mass transfer in an unsteady boundary layer flow of a Casson fluid near a stagnant point over a shrinking/stretching sheet in the presence of thermal radiation. Motsa and Mohammad [37] used the BSQLM to investigate the the boundary layer flow of an Oldroyd-B nanofluid with thermal conductivity.

As reported by Motsa *et al.* [38] , approximate analytical method have some disadvantages. The first drawback is that of slow convergence. Sometimes analytical methods makes it difficult to find closed solutions and also involve a lot of work since they may involve manual integration of approximate series. On the other hand, some numerical methods like the finite difference method achieve good accuracy as the number of grid points is increased. This requires more computer memory and hence increased computational time. Because of these limitations in analytical methods and some numerical methods, we use the spectral quasi-linearization method and the bivariate spectral quasi-linearization method which are computationally efficient.

1.3 Thesis Overview

The work presented in this thesis is on the application of recently introduced numerical methods for solving non differential problems arising in fluid flow. The first two chapters cover the solution of the so-called Bratu problem in one and two dimensions using the spectral quasi-linearization method (SQLM) and the bivariate spectral quasi-linearization method (BSQLM) respectively. This work produced two research papers which have been published. Chapters 3 and 4 mainly focus on the numerical solution of

the boundary layer flow of a non-Newtonian fluid model. The work from the two produced two research papers which have been submitted for possible publication.

This thesis is organized as follows:

- Chapter 2 - This chapter presents the numerical solution of the Bratu problem in one dimension. Since the problem is one dimension, the numerical solution is obtained using the SQLM which is best applicable for problems in one space variable. An outline of the SQLM for a general non-linear differential equation is given. The highly nonlinear Bratu problem is first linearized using a Newton-Raphson method. A system of linear differential equations obtained is solved using the spectral collocation method. A `MATLAB` code is written to produce the numerical solution. The results obtained are compared against those from the B-spline method and the iterative finite difference method in literature.

- Chapter 3 - The work in this chapter is an extension of the work in Chapter 2. The Bratu problem is presented in its two-dimensional form. The method of solution applicable now is the BSQLM. The procedures of getting the numerical solution are almost the same as those discussed in Chapter 2. Results obtained are presented in graphical and tabular form. The results are verified by comparison with those from published literature.

- Chapter 4 - This chapter investigates the boundary layer flow of a non-Newtonian fluid past a vertical porous plate. A system of coupled nonlinear equations that describes the model is given. Suitable transformations are used to transform the model into a system of linear coupled partial differential equations. An outline of the BSQLM for solving a general coupled system is given. The physical non-dimensional parameters which are discussed include the Nusselt number, the Prandtl number, the Sherwood number and the skin friction coefficient. The effects of these thermophysical quantities on fluid velocity, fluid temperature and fluid concentration profiles are investigated. The results are compared against those in literature.

- Chapter 5 - The work in this chapter is basically an extension of the Jeffrey model discussed in Chapter 4. The effects of thermal radiation and chemical reaction in the model are taken into consideration. The BSQLM is used to investigate the effects of some physical dimensionless parameters (discussed in Chapter 4) on the velocity, temperature and concentration profiles.

- Chapter 6- We conclude the thesis by a summary.

Chapter 2

A SPECTRAL QUASI-LINEARIZATION METHOD FOR SOLVING THE ONE DIMENSIONAL BRATU PROBLEM

2.1 Introduction

The Bratu problem which was set by Bratu [39] in 1914 comes in different forms. The most generalized Bratu's problem is the so-called Liouville-Bratu-Gelfand equation which as given by Mounim and Dormale [40] has the form

$$\begin{aligned} \Delta y(\mathbf{x}) &= -\lambda e^{y(\mathbf{x})},\ \mathbf{x} \in \Omega \subset \mathbb{R}^n, \\ y &= 0,\ \mathbf{x} \in \partial\Omega, \end{aligned} \tag{2.1.1}$$

where the constant $\lambda > 0$ is a physical parameter and $\partial\Omega$ is the boundary of Ω. According to Jacobsen and Schmitt [41], Eqn (2.1.1) arises via the study of the quasilinear parabolic problem

$$\begin{aligned} \nu_t &= \Delta\nu + \lambda(1-\varepsilon\nu)^m e^{\nu(1+\varepsilon\nu)},\ \mathbf{x} \in \Omega, \\ \nu &= 0, \quad \mathbf{x} \in \partial\Omega, \end{aligned}$$

which is known as the solid fuel ignition model. This is derived as a model for thermal reaction process in a combustible, nondeformable material of a constant density during the ignition period. The parameter λ is known as the Frank-Kamenetskii parameter given in Luo *et al.* [42], ν is a dimensionless temperature and $1/\varepsilon$ is the activation energy. In this work, we restrict ourselves to the Bratu problem in the one-dimension given by

$$y''(x) = -\lambda e^{y(x)},\ 0 \leq x \leq 1, x \in \mathbb{R}. \tag{2.1.2}$$

From Mohsen [43], Adesanya *et al.* [44], Kafri and Khuri [45], the analytical solution of Eq.(2.1.2) is given by

$$y(x) = -2\ln\left[\frac{\cosh((x-\frac{1}{2})\frac{\omega}{2})}{\cosh(\frac{\omega}{4})}\right], \tag{2.1.3}$$

where ω is the solution of the equation $\omega = \sqrt{2\lambda}\cosh\left(\frac{\omega}{4}\right)$. The Bratu problem has zero, one or two solutions when $\lambda > \lambda_c$, $\lambda = \lambda_c$ and $\lambda < \lambda_c$, respectively, where the critical value λ_c, satisfies the equation

$$1 = \frac{1}{4}\sqrt{2\lambda_c}\sinh\left(\frac{1}{4}\omega\right).$$

According to Boyd [46], $\lambda_c = 3.513830719$.

The Bratu problem is worth investigating due to its several applications in both science and engineering. Some of the applications of the two-point boundary value problem for Bratu's equation as in Liao and Tan [47], include the Chandrasekhar model of the expansion of the universe. The Bratu problem arises in the electrospinning process for the production of ultra-fine polymer fibers, Wan *et al.* [48]. Apart from these physical applications, the Bratu problem has been used as a benchmark for non-linear solvers. In particular, Motsa and Sibanda [49] tested and proved the accuracy and validity of the modified quasilinearization method using the Bratu problem. Also Semary and Hassan [50] proposed a numerical approach based on the variational iteration method with an auxiliary parameter to predict the multiplicity of the solutions of homogeneous nonlinear ordinary differential equations. The method was tested successfully using the Bratu problem.

A lot of work has been done by researchers to find the numerical solution of the Bratu problem in one dimension. Temimi and Romdhane [51] proposed a new iterative finite difference scheme based on the Newton-Raphson-Kantrovich approximation method to solve the classical Bratu problem. Hassan and Semary [52] used the optimal homotopy analysis method to solve the Bratu problem. With this method,

they successfully obtained the two branches of the Bratu problem for different values of the parameter λ. Mohsen [43] used the non-standard finite difference method to treat the one-dimensional Bratu problem. Other numerical techniques which were used to solve the Bratu problem include the shooting method, Abbasbandy *et al.* [53], finite element method, Buckmire [54], homotopy analysis method, Hassan and El-Tawil [55] and the Laplace Adomain decomposition method, Syam and Hamdan [56]. The SQLM was first successfully used by Motsa *et al* [57] to solve non-linear partial differential equations modelling unsteady boundary-layer flows. Shateyi *et al.* [33] also used the method to solve a system of differential equations arising from a problem of MHD micropolar fluid flow, heat and mass transfer over unsteady stretching sheet through porous media in the presence of a heat source/sink and chemical reaction.

In this present work, we employ the SQLM for the first time (to the best of our knowledge) to solve the Bratu problem in one dimension. The SQLM which is a combination of a non-pertubation technique and the Chebyshev spectral collocation method gives an algorithm with accelerated and assured convergence. We choose the SQLM as a method of solution because it is known to produce very accurate results. We will investigate the applicability of this recently introduced numerical method in solving highly non-linear differential equations with the the Bratu problem as a typical example. The Bratu problem is known for the difficulty to obtain its numerical solution for the eigenvalues near the critical point ($\lambda_c = 3.513830719$). Some existing state-of-the-art numerical methods fail to compute the solution at the critical point or give non-accurate results. It is shown in this paper that the SQLM produces results (at $\lambda_c = 3.513830719$) that are correct up to 10 decimal places of the exact solution. The SQLM gives a solution of the desired accuracy within only 4 iterations. The SQLM is a powerful tool which, with some modifications, can be used solve two-dimensional highly non-linear partial differential equations where explicit solutions are unlikely to be found.

2.2 Method of solution

The SQLM is a combination of two numerical methods, Quasi-linearization method (QLM) and the Chebyshev spectral collocation method (CSCM). The QLM which is Newton-Raphson based, was originally proposed by Bellman and Kalaba [58]. It is used to linearize the non-linear differential equation into an iterative sequence of linear differential equations. The resulting system of equations is integrated using the CSCM.

2.2.1 Main idea

2.2.1.1 Quasi-linearization

Consider an n^{th}-order nonlinear differential equation of the form

$$\mathcal{G}\left(\mathbf{y}(x)\right) = 0, \quad x \in [a, b], \tag{2.2.4}$$

subject to given boundary conditions. If we expand Eq.(2.2.4) in Taylor series about

$$\mathbf{z}(x) = \left(z(x), \frac{dz(x)}{dx}, \cdots, \frac{d^{n-1}z(x)}{dx^{n-1}}, \frac{d^n z(x)}{dx^n}\right),$$

and re-arrange terms upon neglecting higher order terms in the resulting equation we get

$$\nabla\mathcal{G}(\mathbf{z}) \cdot \mathbf{y} = \nabla\mathcal{G}(\mathbf{z}) \cdot \mathbf{z} - \mathcal{G}(\mathbf{z}), \tag{2.2.5}$$

which is a linear differential equation in $\mathbf{y}$. If we replace $\mathbf{z}$ and $\mathbf{y}$ with approximations $\mathbf{y}_s$ and $\mathbf{y}_{s+1}$ of $\mathbf{y}$ at s and $s+1$ iteration levels, respectively, we get

$$\nabla\mathcal{G}(\mathbf{y}_s(x)) \cdot \mathbf{y}_{s+1}(x) = \nabla\mathcal{G}(\mathbf{y}_s(x)) \cdot \mathbf{y}_s(x) - G(\mathbf{y}_s(x)), \tag{2.2.6}$$

which expands to

$$\sum_{k=0}^{n} \frac{d^k y_{s+1}}{dx^k} \frac{\partial\mathcal{G}(y_s)}{\partial y_s^{(k)}} = \sum_{k=0}^{n} \frac{d^k y_s}{dx^k} \frac{\partial\mathcal{G}(y_s)}{\partial y_s^{(k)}} - \mathcal{G}(y_s), \ s = 0, 1, 2, \cdots. \tag{2.2.7}$$

Provided $y_0(s)$ is known, solving Eq. (2.2.7) for each $s = 0, 1, 2, \cdots$ yields a sequence

$$\{y_1(x), y_2(x), y_3(x), \cdots\},$$

of approximations to actual solution $y(x)$ of differential Eq. (2.2.4). We expect that $y_s(x) \to y(x)$ as $s \to \infty$ at each $x \in [a, b]$.

2.2.1.2 Chebyshev differentiation

It is convenient to use the linear transformation

$$x(\eta) = \frac{1-\eta}{2}a + \frac{1+\eta}{2}b, -1 \leq \eta \leq 1,$$

to migrate from the physical domain $[a,b]$ on the x-axis to the computational domain $[-1,1]$ on the η-axis. Consequently, Eq. (2.2.7) becomes

$$\begin{aligned}\sum_{k=0}^{n}\frac{\partial G(y_s)}{\partial y_s^{(k)}}\left(\frac{2}{b-a}\right)^k\frac{d^k y_{s+1}(\eta)}{d\eta^k} &= \sum_{k=0}^{n}\frac{\partial G(y_s)}{\partial y_s^{(k)}}\left(\frac{2}{b-a}\right)^k\frac{d^k y_s(\eta)}{d\eta^k}-\mathcal{G}(\mathbf{y}_s(\eta)), \qquad (2.2.8)\\ s &= 0,1,2,\cdots.\end{aligned}$$

Let

$$-1=\eta_E<\eta_{E-1}<\cdots<\eta_1<\eta_0=1,$$

where $\eta_i=\cos\left(\frac{\pi i}{E}\right)$ with $i=0,1,2,\cdots,E$ are Gauss -Lobatto collocation points. We approximate the derivatives of the unknown $y(\eta)$ at the collocation points using the formula

$$\frac{d^m}{d\eta^m}y_s(\eta_i)=\sum_{j=0}^{E}[D^m]_{ij}y_s(\eta_j),\quad i=0,1,2,\cdots,E, \qquad (2.2.9)$$

where the $(E+1)\times(E+1)$ matrix D is called the Chebyshev differentiation matrix given by the following theorem, Trefethen [59]:

Theorem 2.1. *For each $E\geq 1$, let the rows and columns of each $(E+1)\times(E+1)$ Chebyshev spectral differentiation matrix D_E be indexed from 0 to E. The entries of the matrix are:*

$$\begin{aligned}(D_{EE})_{00} &= \frac{2E^2+1}{6},\quad (D_E)_{EE}=-\frac{2E^2+1}{6},\\ (D_E)_{ij} &= \frac{-x_j}{2(1-x_j^2)},\quad j=1,2,\cdots,E-1,\\ (D_E)_{ij} &= \frac{c_i(-1)^{i+j}}{c_j(x_i-x_j)},\quad i\neq j,\quad i,j=1,2,\cdots,E-1,\end{aligned}$$

where

$$c_i=\begin{cases}2, & i=0 \text{ or } E\\ 1, & \text{Otherwise.}\end{cases}$$

This process is called Chebyshev differentiation. Evaluating Eqn. (2.2.8) at $\eta=\eta_i,(i=0,1,2,\cdots,E)$ and applying formula (2.2.9) gives linear system

$$\left[\mathbf{b_{n,s}}\widehat{D}^n+\mathbf{b_{n-1,s}}\widehat{D}^{n-1}+\cdots+\mathbf{b_1,s}\widehat{D}+\mathbf{b_{0,s}}\right]\mathbf{y}_{s+1}=\mathbf{f}_s, \qquad (2.2.10)$$

where

$$\begin{aligned}\mathbf{b_{n,s}} &= \text{diag}\{b_{n,s}(\eta_0), b_{n,s}(\eta_1), \cdots, b_{n,s}(\eta_E)\},\\ &= \begin{pmatrix} b_{n,s}(\eta_0) & & & \\ & b_{n,s}(\eta_1) & & \\ & & \ddots & \\ & & & b_{n,s}(\eta_E) \end{pmatrix},\end{aligned}$$

is an $(E+1)\times(E+1)$ diagonal matrix, $\widehat{D}^n = \left(\frac{2}{b-a}\right)^n D^n$,

$$\mathbf{y}_{s+1}(\eta) = \left[y_{s+1}(\eta_0), y_{s+1}(\eta_1), \cdots, y_{s+1}(\eta_E)\right]^T,$$

and

$$\mathbf{f}_s = \left[\mathbf{b_{n,s}}\widehat{D}^n + \mathbf{b_{n-1,s}}\widehat{D}^{n-1} + \cdots + \mathbf{b_1, s}\widehat{D} + \mathbf{b_{0,s}}\right]\mathbf{y}_s - F(\mathbf{y}_s).$$

In short, Eq.(2.2.10) can be written as

$$A\mathbf{y}_{s+1} = \mathbf{f}_s, \tag{2.2.11}$$

where

$$A = \mathbf{b_{n,s}}\widehat{D}^n + \mathbf{b_{n-1,s}}\widehat{D}^{n-1} + \cdots + \mathbf{b_1, s}\widehat{D} + \mathbf{b_{0,s}}.$$

Suppose Eq.(2.2.4) is subject to boundary conditions $y(a) = \lambda$ and $y(b) = \beta$, then Eq.(2.2.11) is subject to boundary conditions $y_{s+1}(-1) = \lambda$ and $y_{s+1}(1) = \beta$. We include these boundary conditions in Eq. (2.2.11) as follows

$$\left(\begin{array}{c|ccc} 1 & 0 & \cdots & 0 \\ \hline & & A & \\ & & & \\ \hline 0 & \cdots & 0 & 1 \end{array}\right)\left(\begin{array}{c} y_{s+1}(\eta_0) \\ \hline \\ \mathbf{y}_{s+1} \\ \\ \hline y_{s+1}(\eta_E) \end{array}\right) = \left(\begin{array}{c} \beta \\ \hline \\ \mathbf{f}_s \\ \\ \hline \lambda \end{array}\right);\ s = 0, 1, 2, \cdots. \tag{2.2.12}$$

Before we solve linear system (2.2.12), we need to specify initial approximation $y_0(\eta)$. We choose it so that it satisfies the prescribed boundary conditions.

2.2.2 Application to the current problem

The equivalent form of Eq.(2.1.2), on the η axis is

$$\frac{d^2y(\eta)}{d\eta^2} + \lambda\frac{e^{y(\eta)}}{4} = 0, \quad -1 \leq \eta \leq 1 \tag{2.2.13}$$

$$y(-1) = y(1) = 0. \tag{2.2.14}$$

Applying Eq.(2.2.8) to Eq.(2.2.13) we get

$$\frac{d^2y_{s+1}(\eta)}{d\eta^2} + \frac{\lambda}{4}e^{y_s(\eta)}y_{s+1}(\eta) = \frac{\lambda}{4}e^{y_s(\eta)}[y_s(\eta) - 1], s = 0, 1, 2, \cdots, \tag{2.2.15}$$

and Eq.(2.2.14) is replaced by boundary conditions

$$y_{s+1}(-1) = y_{s+1}(1) = 0.$$

Chebyshev differentiation replaces Eq.(2.2.15) with

$$A\mathbf{y}_{s+1} = \mathbf{r}_s, \ s = 0, 1, 2, \cdots \tag{2.2.16}$$

where $A = \widehat{D}^2 + \text{diag}\left\{\frac{\lambda}{4}e^{\mathbf{y_s}}\right\}$, $\mathbf{r}_s = \frac{\lambda}{4}e^{\mathbf{y_s}} \circ [\mathbf{y_s} - \mathbf{i}]$, $\mathbf{i} = [1\ 1\ \cdots\ 1]^T$ and the so-called Hadarmard product $M \circ N$ is the element-wise multiplication of matrices M and N. In order to generate approximations $\mathbf{y}_{s+1}$, $s = 1, 2, \cdots, E$, we choose the initial approximation $y_0(x) = x(1-x)$ so that boundary conditions (2.2.14) are satisfied. After applying the boundary conditions, we use MATLAB 2016 to solve the system

$$\left(\begin{array}{c|ccc|c} 1 & 0 & \cdots & 0 & \\ \hline & & & & \\ & & A & & \\ & & & & \\ \hline 0 & \cdots & 0 & 1 & \end{array}\right)\left(\begin{array}{c} y_{s+1}(1) \\ \hline \\ \mathbf{y}_{s+1} \\ \\ \hline y_{s+1}(-1) \end{array}\right) = \left(\begin{array}{c} 0 \\ \hline \\ \mathbf{r}_s \\ \\ \hline 0 \end{array}\right); \ s = 0, 1, 2, \cdots.$$

2.3 Results and discussion

In this section, we present the numerical solution of the Bratu problem using the SQLM. As in Calgar [60], we consider the three cases where the physical parameter λ assumes values $\lambda = 1$, $\lambda = 2$ and $\lambda = 3.51$, which guarantee the existence of locally unique solutions, in turn. The results from the SQLM

are compared against the exact solution and those from the B-spline method, Caglar [60] and the iterative finite difference (IFD) method, Temimi and Ben-Romdhane [51]. In all the numerical experiments in this paper, 20 collocations points are used and the tolerance level was set to be $\delta = 10^{-12}$.

Fig 2.1 shows the nature of the exact solution of the Bratu problem by plotting $\|u(x)\|_\infty$ against λ. The figure shows that the Bratu problem has two solutions for $\lambda < \lambda_c$ leading to two branches (the lower branch and the upper branch). There is a single solution at $\lambda = \lambda_c$ and no solution for $\lambda > \lambda_c$. In this study it is noted that the SQLM solution to the Bratu problem converges only to the lower branch solution. The difficulty for the upper branch solution is attributed to the effects of the square root singularity at the limit point where the two branches meet, Boyd [61].

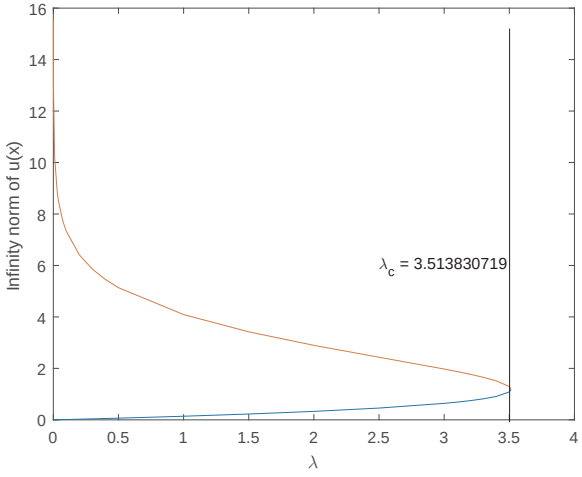

Figure 2.1: The maximum value of $u(x)$ versus λ.

Tables 5.1 presents the solution to the Bratu problem using the SQLM compared against the exact solution and the results from the Picard's Green's Embedded Method (PGEM), Kafri and Khuri [45] for the value $\lambda = 0.001$. The results show that SQLM solution is correct up to 12 decimal places of the exact solution. The treatment of the Bratu problem using the SQLM for the value $\lambda = 0.0001$ is done in Table 2.2. The results show that the SQLM is very accurate with an absolute error of order 10^{-15}.

Table 2.1: The numerical solution using SQLM for $\lambda = 0.001$

x	Exact solution $(\times 10^{-3})$	SQLM $(\times 10^{-3})$	PGEM [45]
0.1	0.045004088117135	0.045004088117288	0.0450040881172878
0.2	0.080007734516151	0.080007734516306	0.0800077345163063
0.3	0.105010589140030	0.105010589139878	0.1050105891398780
0.4	0.120012401937081	0.120012401937160	0.1200124019371595
0.5	0.125013022873429	0.125013022873643	0.1250130228736431
0.6	0.120012401937081	0.120012401937160	0.1200124019371595
0.7	0.105010589140030	0.105010589139878	0.1050105891398781
0.8	0.080007734516151	0.080007734516306	0.0800077345163063
0.9	0.045004088117135	0.045004088117288	0.0450040881172879

Table 2.2: The numerical solution using SQLM for $\lambda = 0.0001$

x	Exact solution $(\times 10^{-4})$	SQLM $(\times 10^{-4})$	Absolute error $(\times 10^{-15})$
0.1	0.045000408759033	0.045000408756172	0.286146364307342
0.2	0.080000773347890	0.080000773345161	0.272934344396070
0.3	0.105001058767209	0.105001058766396	0.081272811289050
0.4	0.120001240019569	0.120001240019368	0.020139055353918
0.5	0.125001302105152	0.125001302103733	0.141952557564454
0.6	0.120001240019569	0.120001240019368	0.020135667222129
0.7	0.105001058767209	0.105001058766396	0.081267729091367
0.8	0.080000773347890	0.080000773345161	0.272941120659648
0.9	0.045000408759033	0.045000408756172	0.286139588043764

Table 2.3 shows the numerical solution of the Bratu problem compared against the exact solution, the B-spline and IFD methods when $\lambda = 1$. The results show that the SQLM agrees with the exact solution up to 10 decimal places and hence it is the most accurate method. The B-spline and the IFD methods are correct to 5 and 9 decimal places respectively.

Table 2.3: The numerical solution using SQLM for $\lambda = 1$

x	Exact solution	SQLM	B-spline [60]	IFD [51]
0.1	0.0498467912	0.0498467912	0.0498438103	0.0498467914
0.2	0.0891899346	0.0891899346	0.0891844690	0.0891899350
0.3	0.1176090958	0.1176090958	0.1176017599	0.1176090962
0.4	0.1347902539	0.1347902539	0.1347817559	0.1347902544
0.5	0.1405392144	0.1405392144	0.1405303221	0.1405392150
0.6	0.1347902539	0.1347902539	0.1347817559	0.1347902544
0.7	0.1176090958	0.1176090958	0.1176017599	0.1176090962
0.8	0.0891899346	0.0891899346	0.0891844690	0.0891899350
0.9	0.0498467912	0.0498467912	0.0498438103	0.0498467914

As done earlier, we compare the SQLM solution of the Bratu problem against the exact solution, the B-spline and the IFD methods for the value $\lambda = 2$. Results from Table 2.4 show that the SQLM is the most accurate numerical method with the solution correct to 10 decimal places of the exact solution. The accuracy of the B-spline method and the IFD method for $\lambda = 2$ drops to 3 and 9 decimal places, respectively, when compared to the case when $\lambda = 1$. In Table 2.6 we calculated the absolute error of the SQLM compared with the exact solution and show absolute errors of other methods in literature. It is shown that the SQLM produces very accurate results.

Table 2.4: The numerical solution using SQLM for $\lambda = 2$

x	Exact solution	SQLM	B-spline [60]	IFD [51]
0.1	0.1144107433	0.1144107433	0.1143935651	0.1144107440
0.2	0.2064191165	0.2064191165	0.2063865190	0.2064191178
0.3	0.2738793118	0.2738793118	0.2738344125	0.2738793135
0.4	0.3150893642	0.3150893642	0.3150365062	0.3150893662
0.5	0.3289524213	0.3289524213	0.3288968072	0.3289524234
0.6	0.3150893642	0.3150893642	0.3150365062	0.3150893662
0.7	0.2738793118	0.2738793118	0.2738344125	0.2738793136
0.8	0.2064191165	0.2064191165	0.2063865190	0.2064191178
0.9	0.1144107433	0.1144107433	0.1143935651	0.1144107440

Table 2.5: The solution of the Bratu problem for $\lambda = 3.51$

x	Exact solution	SQLM	B-spline [60]	IFD [51]
0.1	0.3643358036	0.3643358036	0.357388461	0.3643358036
0.2	0.6778697057	0.6778697057	0.664283874	0.6778697057
0.3	0.9222141971	0.9222141971	0.902930838	0.9222141971
0.4	1.0786342408	1.0786342408	1.055419782	1.0786342408
0.5	1.1326179783	1.1326179783	1.107989815	1.1326179783
0.6	1.0786342408	1.0786342408	1.055419782	1.0786342408
0.7	0.9222141971	0.9222141971	0.902930838	0.9222141971
0.8	0.6778697057	0.6778697057	0.664283874	0.6778697057
0.9	0.3643358036	0.3643358036	0.357388461	0.3643358036

Figures 5.4.25, 2.3, 2.4, 2.5 and 2.6 are the graphical representations of the spectral quasi-linearization solutions of the Bratu problem compared against the exact solution for the values of $\lambda(= 0.001, 0.0001, 1, 2, 3.51)$, respectively. In all the figures, it is shown that the numerical solutions are in excellent agreement with the exact solution.

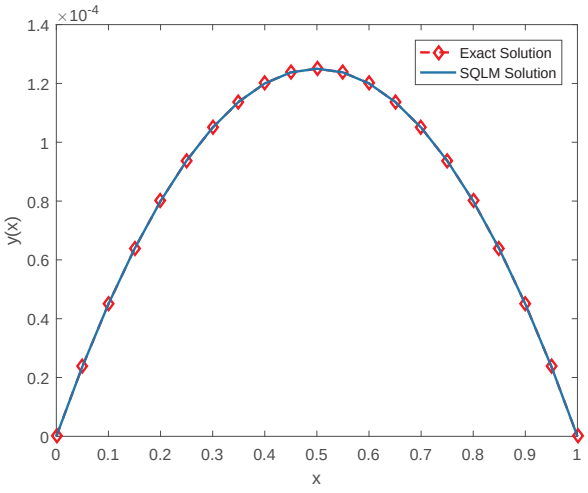

Figure 2.2: The approximate solution for the Bratu problem when $\lambda = 0.001$.

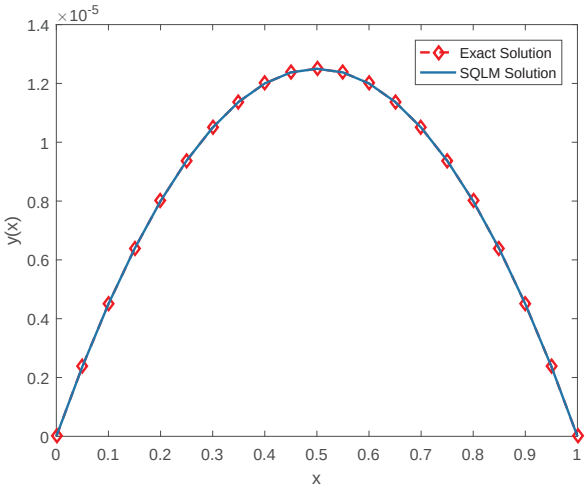

Figure 2.3: The approximate solution for the Bratu problem when $\lambda = 0.0001$.

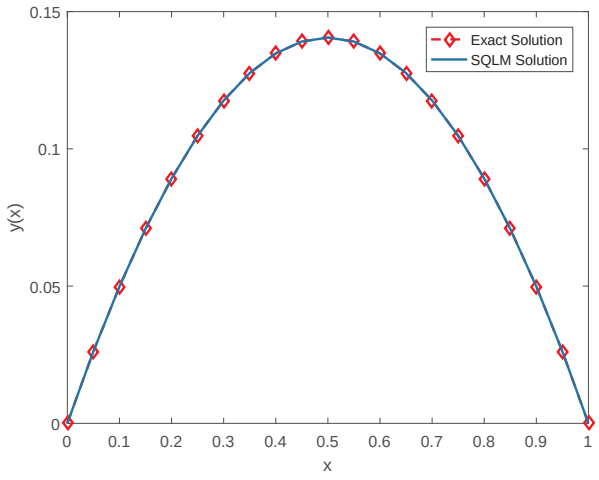

Figure 2.4: The approximate solution for the Bratu problem when $\lambda = 1$.

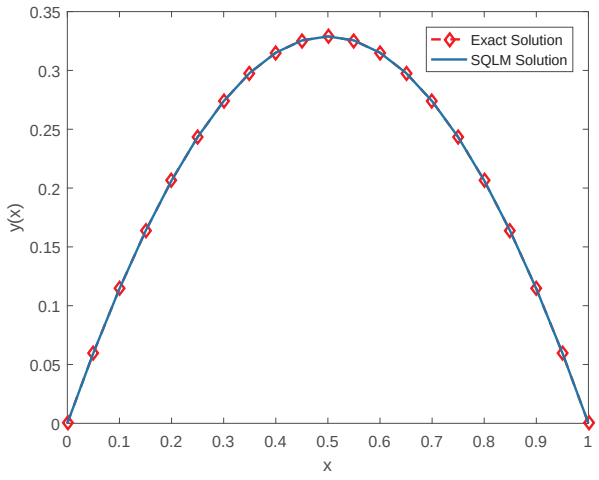

Figure 2.5: The approximate solution for the Bratu problem when $\lambda = 2$.

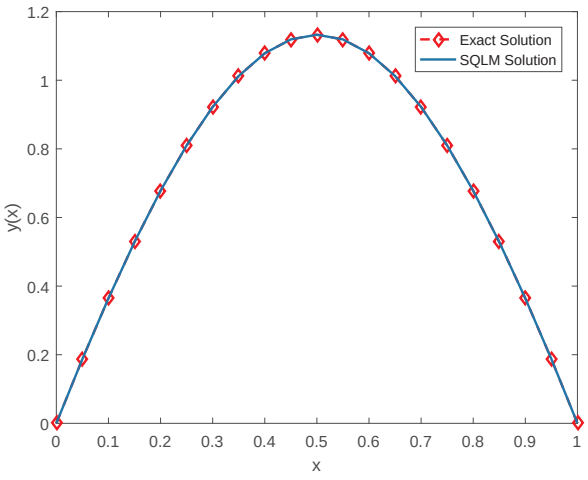

Figure 2.6: The approximate solution for the Bratu problem when $\lambda = 3.51$.

Table 2.6: The absolute errors of the SQLM for $\lambda = 3.51$

x		$\mathcal{E}$	
	SQLM	B-spline method [60]	IFD method [51]
0.1	$0.7905898158 \times 10^{-11}$	$3.8417236955 \times 10^{-2}$	$1.8158929693 \times 10^{-7}$
0.2	$3.4995673026 \times 10^{-11}$	$7.4813536778 \times 10^{-2}$	$3.5108052465 \times 10^{-7}$
0.3	$5.4936721838 \times 10^{-11}$	$1.0582742282 \times 10^{-1}$	$4.9369527244 \times 10^{-7}$
0.4	$3.1665337019 \times 10^{-11}$	$1.2711688086 \times 10^{-1}$	$5.9071346326 \times 10^{-7}$
0.5	$5.2795767758 \times 10^{-11}$	$1.3475287761 \times 10^{-1}$	$6.2535001444 \times 10^{-7}$
0.6	$3.1663560662 \times 10^{-11}$	$1.2711688086 \times 10^{-1}$	$5.9071862424 \times 10^{-7}$
0.7	$5.4934057303 \times 10^{-11}$	$1.0582742282 \times 10^{-1}$	$4.9370493804 \times 10^{-7}$
0.8	$3.4991787246 \times 10^{-11}$	$7.4813536776 \times 10^{-2}$	$3.5109296703 \times 10^{-7}$
0.9	$0.7904454868 \times 10^{-11}$	$3.8417236953 \times 10^{-2}$	$1.8160371318 \times 10^{-7}$

Table 2.7 shows the effects of increasing the number $E + 1$ of collocation points used on the accuracy of the SQLM. The results shown are for $E = 20$, $E = 30$ and $E = 70$. It is noted that increasing the collocation points also increases the accuracy of the results and it increases in the computer time.

Table 2.7: Numerical values for different values of E for $\lambda = 2$

x	Exact solution	E =20	E=30	E=70
0.1	0.114410743267746	0.114410743262896	0.114410743262897	0.114410743267192
0.2	0.206419116487609	0.206419116478316	0.206419116478319	0.206419116478331
0.3	0.273879311825552	0.273879311812661	0.273879311812666	0.273879311812685
0.4	0.315089364225670	0.315089364210426	0.315089364210432	0.315089364210454
0.5	0.328952421341113	0.328952421325051	0.328952421325056	0.328952421325081
0.6	0.315089364225670	0.315089364210425	0.315089364210429	0.315089364210456
0.7	0.273879311825552	0.273879311812660	0.273879311812663	0.273879311812688
0.8	0.206419116487609	0.206419116478316	0.206419116478318	0.206419116478342
0.9	0.114410743267746	0.114410743262895	0.114410743262897	0.114410743250821
Run time(s)		0.056094	0.085169	0.375401
No. of iter		4	4	4

A graphical illustration of the solution of the Bratu problem using the SQLM for different values of the physical parameter λ is done in Figure 2.7. It is noted in Fig 2.7 that the SQLM solutions for the three values $(\lambda = 1, \lambda = 2, \lambda = 3.51)$ satisfy the boundary conditions. Increasing the parameter λ results in an increase in the solution profile.

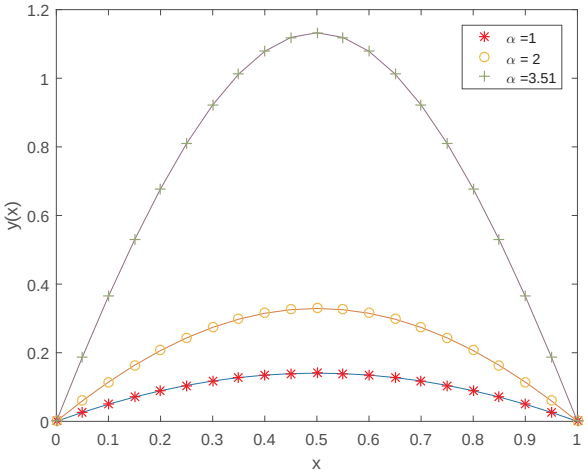

Figure 2.7: The approximate solutions for the Bratu problem $\lambda = 1, 2$ and 3.51.

2.4 Conclusion

In this study, the Spectral quasi-linearization method was used to seek a numerical solution for the one-dimensional Bratu problem. The numerical results presented in this study were for the five chosen values of the parameter λ. The SQLM gave results which agreed with the exact solution to 10 decimal places. From the study we can conclude that the SQLM is more accurate than the B-spline method and the iterative finite difference method. Increasing the number of computational grid points makes the results better but requires more run time.

Chapter 3

ON THE BIVARIATE SPECTRAL QUASI-LINEARIZATION METHOD FOR SOLVING THE TWO DIMENSIONAL BRATU PROBLEM

3.1 Introduction

Most real life phenomenon are modeled by partial differential equations (PDEs). According to Boyd [62] and Slunyaev and Shrira [63], most phenomenon in science, engineering, biological sciences and fluid mechanics are described by PDEs which are usually non-linear. Due to the complexity of the domains in which they are defined, it is usually very difficult or even impossible, except for a few special cases, to find exact solutions to the defining PDEs. This motivated researchers to develop numerical and analytical methods to approximate solutions to these non-linear PDEs. Some of the well known analytical methods that have been used to solve non-linear PDEs include homotopy pertubation method by He [64], Adomain decomposition method by Adomain [65] , power series expansions by Mohan and Al-Bayaty [66], the artificial small parameter method by Lyapunov [67] and the δ-pertubation expansion

method by Ji-huan [68]. Although these methods help us to understand many non-linear phenomena, they have their own disadvantage in that the convergence of the solution series is not guaranteed due to their dependence on small or large physical parameters. Some examples of numerical methods that have been used to solve non-linear phenomena include finite element methods by Argyris and Haase [69], finite difference methods by Vliegenthart [70], quasi-linearization technique by Motsa and Sibanda [49], iterative finite difference method by Temimi [71] and the B-spline method by Caglar [72].

An example of a highly non-linear differential equation is the so-called Bratu problem, first set up by Bratu [39] and named after him . The simplest form of the Bratu problem in one dimension is:

$$\frac{d^2u}{dx^2} + \lambda e^{u(x)} = 0, \; x \in [0,1] \tag{3.1.1}$$

subject to boundary conditions $u(0) = u(1) = 0$. The exact solution of Eq (3.1.1) is given by

$$u(x) = -2\ln\left[\frac{\cosh((x-\frac{1}{2})\frac{\omega}{2})}{\cosh(\frac{\omega}{4})}\right],$$

where ω is the solution of the equation $\omega = 2\sqrt{2\lambda}\cosh\left(\frac{\omega}{4}\right)$, Jacobsen and Schmitt [41]. The Bratu problem has no, unique, or two solutions if $\lambda > \lambda_c$, $\lambda = \lambda_c$ or $\lambda < \lambda_c$ respectively, where the critical value is given by Mohsen [73] as $\lambda_c = 3.51382$. Jacobsen and Schmitt [41] also gave the generalization of the Bratu problem as the Liouville-Bratu-Gelfand problem which in the n-dimensional coordinate system takes the form

$$\Delta u(\mathbf{x}) + \lambda e^{u(\mathbf{x})} = 0, \; \mathbf{x} \in \Omega, \tag{3.1.2}$$

where the square domain Ω is bounded in $\mathbb{R}^n$ together with homogeneous Dirichlet boundary conditions $u(\mathbf{x}) = 0$, $\mathbf{x} \in \partial\Omega$, where $\partial\Omega$ is the boundary of Ω.

In this study, we consider the two dimensional Bratu problem which has the form

$$\frac{\partial^2 u}{\partial x^2} + \frac{\partial^2 u}{\partial y^2} + \lambda e^u = 0, \; (x,y) \in [0,1] \times [0,1], \tag{3.1.3}$$

subject to boundary conditions

$$u(0,y) = u(1,y) = u(x,0) = u(x,1) = 0, \tag{3.1.4}$$

where λ is a positive number. Similar to the 1D case, depending on the value of the parameter λ, Eq

(3.1.3) has no, one, or two solutions if $\lambda > \lambda_c$, $\lambda = \lambda_c$ or $\lambda < \lambda_c$, respectively, where the critical value $\lambda_c = 6.808124423$, Chang and Chien [74]. The two dimensional Bratu problem has no exact solution as is the case with the one dimensional Bratu problem. However, Odejide and Aregbesola [75] presented a near exact solution that satisfy Eq (3.1.3) at just one collocation point $(x_c, y_c) = \left(\frac{1}{2}, \frac{1}{2}\right)$ as well as the boundary conditions. The analytical solution is given by Odejide and Aregbesola [75] as

$$u(x,y) = 2\ln\left[\frac{\cosh(\frac{\omega}{4})\cosh[(x-\frac{1}{2})(y-\frac{1}{2})\omega]}{\cosh((x-\frac{1}{2})\frac{\omega}{2})\cosh(y-\frac{1}{2})\frac{\omega}{2}}\right], \tag{3.1.5}$$

where ω is a solution of the equation

$$\omega^2 = \lambda\cosh^2\left(\frac{\omega}{4}\right).$$

.

The two dimensional Bratu problem has attracted the attention of so many researchers because of its wide range of physical, chemical and engineering applications. It is reported in Jacobsen and Schmitt [41] that the Bratu problem is used to model the thermal reaction process in a combustible non-deformable material. The Bratu problem also appears in the Chandrasekhar model of the expansion of the universe, chemical reactor theory and nanotechnology, Mohnsen [43]. Recently, the Bratu problem has found applications in engineering such as electro-spinning process for the fabrication of nano-fibers, Wan *et al.* [48]. Apart from the physical applications, Yang and Liao [76] reported that the Bratu problem is also used as a benchmark for newly developed numerical and analytical methods.

Some numerical methods that have been used to treat the Bratu problem in two dimensions. Raja *et al* [77] solved the two-dimensional Bratu problem using neural network, swarm intelligence and sequential quadratic programming. Yang and Liao [76] presented a new analytic approach, the wavelet homotopy analysis method and applied it on the two-dimensional Bratu problem. The Finite Difference and the Weighted Residual Method (WRM) were used by Odejide and Aregbesola [75] to solve the Bratu problem. Boyd [46] used Chebyshev pseudospectral method using Gegenbauer polynomialsby. Mohsen [43] used the iterative finite difference method to solve the two-dimensional Bratu problem. Syam and Hamdan [56] used a numerical technique based on the Laplace Adomain decomposition method to find an approximate solution of the Bratu problem.

The main objective of this work is to solve (for the first time), the so-called Bratu problem in two dimensions using the Bivariate Spectral Quasi-Linearization Method (BSQLM). The BSQLM introduced by Motsa *et al.* [38], is a modification of the Spectral Quasi-linearization Method by Motsa *et al.* [57] to solve non-linear PDEs in two dimensions. Some of the problems successfully solved using

the BSQLM include the modified Kdv equation, Burger equation, the Cahn-Hillard equation and the Fitzhugh-Nagumo equations [78]. It is in this work that researchers concluded that the method is accurate, reliable and applicable to nonlinear evolution equations. The results obtained also showed that the method achieves high accuracy with relatively fewer spatial grid points and converges fast to the exact solution. Also, Motsa and Ansari [37] solved non-dimensionalized PDEs describing a time dependent boundary layer flow and heat transfer of an incompressible Oldroyd-B nanofluid past an impulsively stretching sheet using the BSQLM. The results obtained converged rapidly.

3.2 Methods of solution

3.2.1 Bivariate spectral quasi-linearization

In this section, we briefly describe the BSQLM. The BSQLM uses quasi-linearization, Chebyshev collocation and bivariate Lagrange interpolation.

3.2.1.1 Quasi-linearization

The quasi-linearization method (QLM) which is based on Newton-Raphson method was introduced by Bellman and Kalaba [58]. It is a technique for simplifying non-linear PDEs using the linear terms of the Taylor series expansion about an initial approximation. Let us consider a general second order non-linear differential equation

$$F(\mathbf{u}) = R(\mathbf{x}),\ \mathbf{x} = (x, y) \in [a, b] \times [c, d], \tag{3.2.6}$$

subject to given boundary conditions. The unknown function

$$\mathbf{u} = \left(u, \frac{\partial u}{\partial x}, \frac{\partial^2 u}{\partial x^2}, \frac{\partial^2 u}{\partial x \partial y}, \frac{\partial u}{\partial y}, \frac{\partial^2 u}{\partial y^2}\right),$$

and F is a non-linear operator. Expanding F using linear Taylor series expansion about $\mathbf{v}$ we get

$$F(\mathbf{v}) + \nabla F(\mathbf{v}) \cdot (\mathbf{u} - \mathbf{v}) \approx R(\mathbf{x}), \tag{3.2.7}$$

Assuming that $\mathbf{v}$ is an approximate solution sufficiently close to $\mathbf{u}$ and adopting the notation $\mathbf{u}_r$ and $\mathbf{u}_{r+1}$ for $\mathbf{v}$ and $\mathbf{u}$ respectively, we have

$$\nabla F(\mathbf{u}_r)\cdot\mathbf{u}_{r+1} = \nabla F(\mathbf{u}_r)\cdot\mathbf{u}_r - F(\mathbf{u}_r) + R(\mathbf{x}),\ r = 0, 1, 2, \cdots, \tag{3.2.8}$$

Solving Eq (3.2.8) generates a sequence $\{\mathbf{u}_r\}$ and hence u_r such that $u_r \to u$ as $r \to \infty$.

3.2.1.2 Bivariate Lagrange interpolation and Chebyshev differentiation

We seek the solution u of Eq (3.1.3) of the form

$$u(x,y) \approx \sum_{j=0}^{N}\sum_{i=0}^{M} u(x_j, y_i)L_{ji}(x,y),$$

where the functions $L_{ji}(x,y) = L_j(x)L_i(y)$ are bivariate Lagrange polynomials defined as

$$L_j(x) = \prod_{\substack{k=0\\k\neq j}}^{N}\frac{x-x_k}{x_j-x_k},\quad L_i(y) = \prod_{\substack{k=0\\k\neq i}}^{M}\frac{y-y_k}{y_i-x_k}$$

The functions $L_j(x)$ and $L_i(y)$ both obey the Kronecker delta equation, that is,

$$L_{ji}(x_n, y_m) = \begin{cases} 1, & \text{if } j = n,\ i = m \\ 0, & \text{otherwise} \end{cases}$$

Before applying the spectral method, it is convenient to transform the physical domain $[a,b]\times[c,d]$ in the x-y axis to the computational domain $[-1,1]\times[-1,1]$ in the ξ-η axis using linear transformations $x(\xi) = \frac{a+b}{2} + \frac{b-a}{2}\xi$ and $y(\eta) = \frac{c+d}{2} + \frac{d-c}{2}\eta$. Approximating the partial derivatives of u at Chebyshev-Gauss-Lobatto collocation points

$$\{x_j\}_{j=0}^{N} = \cos\left(\frac{\pi j}{N}\right),\quad \{y_i\}_{i=0}^{M} = \cos\left(\frac{\pi i}{M}\right),$$

we have

$$\begin{aligned}\left.\frac{\partial u}{\partial x}\right|_{x=x_j,y=y_i} &\approx \sum_{p=0}^{N}\sum_{q=0}^{M} u(x_p,y_q)\frac{dL_p(x_j)}{dx}L_q(y_i)\\ &= \sum_{p=0}^{N} D_{jp}u(x_p,y_i) = \mathbf{D}\mathbf{U}_i.\end{aligned}$$

$$\left.\frac{\partial u}{\partial y}\right|_{x=x_j,y=y_i} \approx \sum_{q=0}^{M} d_{iq}u(x_j,y_q) = \sum_{q=0}^{M} d_{iq}\mathbf{U}_q,$$

and

$$\begin{aligned}\left.\frac{\partial^2 u}{\partial x\partial y}\right|_{x=x_j,y=y_i} &\approx \sum_{p=0}^{N}\sum_{q=0}^{M} u(x_p,y_q)\frac{dL_p(x_j)}{dx}\frac{dL_q(y_i)}{dy} \\ &= \sum_{q=0}^{M} d_{iq}\Big(\mathbf{D}\mathbf{U}_q\Big),\end{aligned}$$

where $\widehat{\mathbf{D}} = \big(\frac{b-a}{2}\big)\mathbf{D}$ and $\widehat{\mathbf{d}}_{iq} = \big(\frac{d-c}{2}\big)d_{iq}$ are the standard Chebyshev differentiation matrices, Trefethen [59] of orders $(N+1)\times(N+1)$ and $(M+1)\times(M+1)$, respectively, and

$$\mathbf{U}_i = \Big(u(x_0,y_i), u(x_1,y_i), \cdots, u(x_{N-1},y_i), u(x_N,y_i)\Big)^T,$$

for $i = 0,1,2,\cdots,N$. The superscript T denotes matrix transpose. Higher order derivatives of u are defined as follows:

$$\left.\frac{\partial^n u}{\partial x^n}\right|_{x=x_j,y=y_i} \approx \mathbf{D}^n\mathbf{U}_i, \ \left.\frac{\partial^n u}{\partial y^n}\right|_{x=x_j,y=y_i} \approx \sum_{q=0}^{M} d_{iq}^n\mathbf{U}_q, \ n = 2,3,\cdots,$$

and

$$\frac{\partial^{n+m}u}{\partial x^n\partial y^m} = \sum_{q=0}^{M} d_{iq}^m\Big(\mathbf{D}^n\mathbf{U}_q\Big), \ n,m = 1,2,\cdots.$$

Expanding Eq (3.2.8) we get

$$\alpha_{5,r}\frac{\partial^2 u_{r+1}}{\partial x^2} + \alpha_{4,r}\frac{\partial^2 u_{r+1}}{\partial y^2} + \alpha_{3,r}\frac{\partial^2 u_{r+1}}{\partial x\partial y} + \alpha_{2,r}\frac{\partial u_{r+1}}{\partial x} + \alpha_{1,r}\frac{\partial u_{r+1}}{\partial y} + \alpha_{0,r}u_{r+1} = K_r, \qquad (3.2.9)$$

where

$$\begin{aligned}\alpha_{5,r} &= \frac{\partial F(u_r)}{\partial u_{xx}}, \ \alpha_{4,r} = \frac{\partial F(u_r)}{\partial u_{yy}}, \ \alpha_{3,r} = \frac{\partial F(u_r)}{\partial u_{xy}}, \ \alpha_{2,r} = \frac{\partial F(u_r)}{\partial u_x}, \ \alpha_{1,r} = \frac{\partial F(u_r)}{\partial u_y}, \ \alpha_{0,r} = \frac{\partial F(u_r)}{\partial u} \\ K_r &= \alpha_{5,r}\frac{\partial^2 u_r}{\partial x^2} + \alpha_{4,r}\frac{\partial^2 u_r}{\partial y^2} + \alpha_{3,r}\frac{\partial^2 u_r}{\partial x\partial y} + \alpha_{2,r}\frac{\partial u_r}{\partial x} + \alpha_{1,r}\frac{\partial u_r}{\partial y} + \alpha_{0,r}u_r - F(\mathbf{u}_r) + R(\mathbf{x}).\end{aligned}$$

Approximating the function u and its derivatives in Eq (3.2.9) at collocation points (x_j, y_i) we get

$$\alpha_{5,r}(\mathbf{x},y_i)\widehat{\mathbf{D}}^2\mathbf{U}_{r+1,i}+\alpha_{4,r}(\mathbf{x},y_i)\sum_{q=0}^{M}\widehat{d}^2_{jq}\mathbf{U}_{r+1,q}+\alpha_{3,r}(\mathbf{x},y_i)\sum_{q=0}^{M}\widehat{d}^2_{iq}\left(\widehat{\mathbf{D}}^2\mathbf{U}_{r+1,q}\right) \tag{3.2.10}$$

$$+\quad \alpha_{2,r}(\mathbf{x},y_i)\widehat{\mathbf{D}}\mathbf{U}_{r+1,i}+\alpha_{1,r}(\mathbf{x},y_i)\sum_{q=0}^{M}\widehat{d}_{iq}\left(\widehat{\mathbf{D}}\mathbf{U}_{r+1,q}\right)+\alpha_{0,i}(\mathbf{x},y_i)\mathbf{U}_{r+1,i}=\mathbf{K}_{r,i},\quad j=0,1,\cdots,N.$$

where

$$\alpha_{a,r}(\mathbf{x},y_i)=\begin{bmatrix}\alpha_{a,r}(x_0,y_i) & & & \\ & \alpha_{a,r}(x_1,y_i) & & \\ & & \ddots & \\ & & & \alpha_{a,r}(x_N,y_i)\end{bmatrix},\quad a=0,1,\cdots,5,$$

and

$$K_{r,i} = \alpha_{5,r}(\mathbf{x},y_i)\widehat{\mathbf{D}}^2\mathbf{U}_{r,i}+\alpha_{4,r}(\mathbf{x},y_i)\sum_{q=0}^{M}\widehat{d}^2_{jq}\mathbf{U}_{r,q}+\alpha_{3,r}(\mathbf{x},y_i)\sum_{q=0}^{M}\widehat{d}^2_{iq}\left(\widehat{\mathbf{D}}^2\mathbf{U}_{r,q}\right)+\alpha_{2,r}(\mathbf{x},y_i)\widehat{\mathbf{D}}\mathbf{U}_{r,i}$$

$$+\quad \alpha_{1,r}(\mathbf{x},y_i)\sum_{q=0}^{M}\widehat{d}_{iq}\left(\widehat{\mathbf{D}}\mathbf{U}_{r,q}\right)+\alpha_{0,i}(\mathbf{x},y_i)\mathbf{U}_{r,i}-F(u_r(\mathbf{x},y_i))+R(\mathbf{x},y_i).$$

In compact form, Eq (3.2.10) can be written as:

$$\begin{bmatrix}A_{0,0} & A_{0,1} & A_{0,2} & \cdots & A_{0,M}\\ A_{1,0} & A_{1,1} & A_{1,2} & \cdots & A_{1,M}\\ \vdots & \vdots & \vdots & \ddots & \vdots\\ A_{N-1,0} & A_{N-1,1} & A_{N-1,2} & \cdots & A_{N-1,M}\\ A_{N,0} & A_{N,1} & A_{N,2} & \cdots & A_{N,M}\end{bmatrix}\begin{bmatrix}\mathbf{U}_{r+1,0}\\ \mathbf{U}_{r+1,1}\\ \vdots\\ \mathbf{U}_{r+1,N-1}\\ \mathbf{U}_{r+1,N}\end{bmatrix}=\begin{bmatrix}\mathbf{K}_0\\ \mathbf{K}_1\\ \vdots\\ \mathbf{K}_{M-1}\\ \mathbf{K}_M\end{bmatrix}, \tag{3.2.11}$$

where

$$A_{ii} = \alpha_{5,r}(\mathbf{x},y_i)\widehat{\mathbf{D}}^2+\alpha_{4,r}(\mathbf{x},y_i)\widehat{d}_{ii}\mathbf{I}+\alpha_{3,r}(\mathbf{x},y_i)\widehat{d}^2_{ii}\widehat{\mathbf{D}}^2+\alpha_{2,r}\mathbf{x},y_i\widehat{\mathbf{D}}+\alpha_{1,r}(\mathbf{x},y_i)\widehat{d}_{ii}\widehat{\mathbf{D}}+\alpha_{0,r}(\mathbf{x},y_i),$$

and

$$A_{ij} = \widehat{d}_{ij}\mathbf{I},\quad \text{when}\quad i\neq j.$$

3.2.2 Application to the current problem

The equivalent form of Eq (3.1.3) in the ξ-η axis is

$$\frac{\partial^2 u}{\partial \xi^2} + \frac{\partial^2 u}{\partial \eta^2} + \frac{\lambda}{4} e^{u(\xi,\eta)} = 0, \ (\xi, \eta) \in [-1, 1] \times [-1, 1], \tag{3.2.12}$$

subject to boundary conditions

$$u(-1, \eta) = u(1, \eta) = u(\xi, -1) = u(\xi, 1) = 0. \tag{3.2.13}$$

Applying formula Eq (3.2.8) on Eq (3.2.12) we get its linear counterpart

$$\frac{\partial^2 u_{r+1}}{\partial \xi^2} + \frac{\partial^2 u_{r+1}}{\partial \eta^2} + \frac{\lambda}{4} e^{u_r(\xi,\eta)} u_{r+1} = \frac{\lambda}{4} e^{u_r}[u_r - 1], \tag{3.2.14}$$

$$u_{r+1}(-1, \eta) = u_{r+1}(1, \eta) = u_{r+1}(\xi, -1) = u_{r+1}(\xi, 1) = 0, \tag{3.2.15}$$

for $r = 0, 1, 2, \cdots$ and $(u_{r+1} = u_{r+1}(\xi, \eta))$. Applying the spectral collocation method we get

$$\sum_{p=0}^{N} \widehat{D}^2_{jp} U_{r+1}(\xi_p, \eta_i) + \sum_{q=0}^{M} \widehat{d}^2_{iq} U_{r+1}(\xi_j, \eta_q) + \frac{\lambda}{4} e^{U_r(\xi_i,\eta_i)} U_{r+1}(\xi_j, \eta_i) = K_i, \tag{3.2.16}$$

subject to boundary conditions

$$U_{r+1}(\xi_N, \eta_j) = U_{r+1}(\xi_0, \eta_j) = U_{r+1}(\xi_i, \eta_M) = U_{r+1}(\xi_i, \eta_0) = 0. \tag{3.2.17}$$

Substituting Eq (3.2.17) into Eq (3.2.16) we get

$$\sum_{p=1}^{N-1} \widehat{D}^2_{jp} U_{r+1}(\xi_p, \eta_i) + \sum_{q=1}^{M-1} \widehat{d}^2_{iq} U_{r+1}(\xi_j, \eta_q) + \frac{\lambda}{4} e^{U_r(\xi_j,\eta_i)} U_{r+1}(\xi_j, \eta_i) = K_i, \tag{3.2.18}$$

$$\Rightarrow \mathbf{A}\mathbf{U}_{r+1} = \mathbf{K}_i. \tag{3.2.19}$$

Eq (3.2.19) can be written in matrix form as

$$\begin{bmatrix} A_{0,0} & A_{0,1} & \cdots & A_{0,M-1} & A_{0,M} \\ A_{1,0} & A_{1,2} & \cdots & A_{1,M-1} & A_{1,M} \\ \vdots & \vdots & \ddots & \vdots & \vdots \\ A_{N-1,0} & A_{N-1,1} & \cdots & A_{N-1,M-1} & A_{N-1,M} \\ A_{N,0} & A_{N,1} & \cdots & A_{N,M-1} & A_{N,M} \end{bmatrix} \begin{bmatrix} \mathbf{U}_{r+1,0} \\ \mathbf{U}_{r+1,1} \\ \vdots \\ \mathbf{U}_{r+1,N-1} \\ \mathbf{U}_{r+1,N} \end{bmatrix} = \begin{bmatrix} \mathbf{K}_0 \\ \mathbf{K}_1 \\ \vdots \\ \mathbf{K}_{M-1} \\ \mathbf{K}_M \end{bmatrix}, \tag{3.2.20}$$

where

$$\begin{aligned} A_{ii} &= \widehat{\mathbf{D}}^2 + \hat{d}_{ii} I + \text{diag}\left[\frac{\lambda}{4} e^{\mathbf{U}_{r,i}}\right], \\ A_{ij} &= \hat{d}_{ij}^2 \mathbf{I}, \\ \mathbf{K}_i &= \frac{\lambda}{4} e^{\mathbf{U}_{r,i}} \circ \left[\mathbf{U}_{r,i} - \mathbf{i}\right]. \end{aligned}$$

The column vector $\mathbf{i} = \left[11 \cdots 1\right]^T$ and the Hamadard product $A \circ B$ is the element-wise multiplication of matrices A and B of the same order. Boundary conditions are applied to the system (3.2.20) as follows:

$$\begin{bmatrix} \mathbf{I} & \mathbf{0} & \mathbf{0} & \cdots & \mathbf{0} & \mathbf{0} \\ \mathbf{0} & \widehat{\mathbf{A}}_{1,1} & \widehat{\mathbf{A}}_{1,2} & \cdots & \widehat{\mathbf{A}}_{1,M-1} & \mathbf{0} \\ \vdots & \vdots & \vdots & \ddots & \vdots & \vdots \\ \mathbf{0} & \widehat{\mathbf{A}}_{N-1,1} & \widehat{\mathbf{A}}_{N-1,2} & \cdots & \widehat{\mathbf{A}}_{N-1,M-1} & \mathbf{0} \\ \mathbf{0} & \mathbf{0} & \mathbf{0} & \cdots & \mathbf{0} & \mathbf{I} \end{bmatrix} \begin{bmatrix} \widehat{\mathbf{U}}_{r+1,0} \\ \widehat{\mathbf{U}}_{r+1,1} \\ \vdots \\ \widehat{\mathbf{U}}_{r+1,N-1} \\ \widehat{\mathbf{U}}_{r+1,N} \end{bmatrix} = \begin{bmatrix} \mathbf{0} \\ \widehat{\mathbf{K}}_1 \\ \vdots \\ \widehat{\mathbf{K}}_{M-1} \\ \mathbf{0} \end{bmatrix}, \tag{3.2.21}$$

where $\mathbf{I}$ and $\mathbf{0}$ are identity and zero matrices, respectively, of order $N \times M$ and

$$\widehat{\mathbf{A}}_{ij} = \left(\begin{array}{ccccc} 1 & 0 & \cdots & 0 & 0 \\ \hline & & A_{ij} & & \\ \hline 0 & 0 & \cdots & 0 & 1 \end{array}\right) \quad \text{and} \quad \widehat{\mathbf{K}}_i = \left(\begin{array}{c} 0 \\ \hline \mathbf{K}_i \\ \hline 0 \end{array}\right).$$

3.2.3 Chebyshev spectral collocation method

As mentioned before, the exact solution of the two dimensional Bratu problem is unknown. As a basis of comparison, we will use the Chebyshev spectral collocation method which uses Kronecker multiplication, abbreviated CSCM-K in this work, to solve the transformed Eq (3.2.12) subject to boundary conditions Eq (3.2.13). We intend to use the CSCM-K because of its known high order accuracy, Raja *et al.* [79]. In multi-dimensional problems, the spectral collocation methods make use of Kronecker products to discretize the differential operators. It is worth noting that though the BSQLM uses spectral collocation, its main difference with the CSCM-K is the manner in which the two methods treat non-linearity.

Definition 3.1. If A and B are of dimensions $p \times q$ and $r \times s$, respectively, then the Kronecker product $A \otimes B$ is the matrix of dimension $pr \times qs$ with $p \times q$ block form where the i, j block is $a_{i,j}B$, that is

$$A \otimes B = \begin{bmatrix} a_{1,1}B & a_{1,2}B & \cdots & a_{1,q-1}B & a_{1,q}B \\ a_{2,1}B & a_{2,2}B & \cdots & a_{2,q-1}B & a_{1,q}B \\ \vdots & \vdots & \ddots & \vdots & \vdots \\ a_{p-1,1}B & a_{p-1,2}B & \cdots & a_{p-1,q-1}B & a_{p-1,q}B \\ a_{p,1}B & a_{p,2}B & \cdots & a_{p,q-1}B & a_{p,q}B \end{bmatrix}.$$

The matrix $A \otimes B$ is not dense, at the same time not as sparse as matrices from traditional methods like the finite element or finite difference methods. Since Eq (3.2.12) is highly non-linear, its solution is computed iteratively using the linear system

$$M\mathbf{u}_{s+1} = \mathbf{f}_s, \quad s = 0, 1, 2, \cdots, \tag{3.2.22}$$

where $M = I \otimes \widehat{D}^2 + \widehat{D}^2 \otimes I$, $\mathbf{f}_s = -\exp(\mathbf{u}_s)$ and $\mathbf{u}_s$ is the current iteration. $I \otimes \widehat{D}^2$ and $\widehat{D}^2 \otimes I$ denote second order spectral differentiation in the x and y directions respectively. $A \otimes B$ can be easily computed using the MATLAB command `kron(A,B)`. The homogeneous boundary conditions Eq (3.2.13) are implemented by deleting the first and last rows and columns of the spectral differentiation matrix.

3.3 Results and discussion

Solving Eq (3.1.6) for different values of the parameter λ (shown in Table 3.1), we obtain two values of ω labeled ω_1 and ω_2. Substituting the values of ω_1 and ω_2 into Eq (3.1.5) and take the maximum of $u(x, y)$(denoted u_{max1} and u_{max2}) we get results are shown in Table 3.1. We consider the values of λ as done in [75].

Table 3.1: The maximum values of $u(x, y)$ for different values of λ and ω

	ω		u_{max}	
λ	ω_1	ω_2	u_{max1}	u_{max2}
0.1	0.317222727	19.19637291	0.006282809236	8.212027794
0.5	0.718546417	14.98479987	0.03209723648	6.107219872
1.0	1.033569462	13.03823930	0.06603661666	5.135773050
2.0	1.517164599	10.93870277	0.1405392141	4.091467246
3.0	1.939726525	9.581699793	0.2264817040	3.421097726
4.0	2.357551054	8.507199571	0.3289524214	2.895531266
5.0	2.811554938	7.548098106	0.4580374660	2.433153338
6.0	3.373507764	6.576569259	0.6401466966	1.975266972
6.4	3.674358094	6.131465409	0.7464589086	1.770569562
6.8	4.108395792	5.56288431	0.9091426554	1.515096612
7.0	4.551853663	5.054342699	1.085158948	1.515096612
7.02	4.667812741	4.932041041	1.132617977	1.294585480
7.027661438	4.798690688	4.798714561	1.186832218	1.242742595

A graphical representation of the results in Table 3.1 is done in Fig 3.1

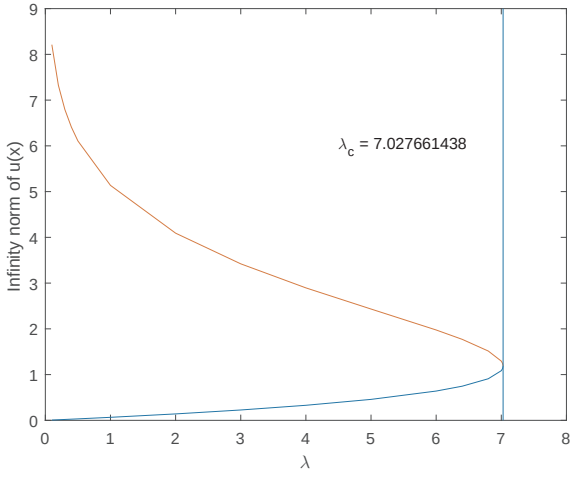

Figure 3.1: The maximum values of $u(x, y)$ versus λ.

Fig 3.1 shows that the analytical solution has two branches (lower and upper branches). It is also clear that the Bratu problem has two solutions for $0 < \lambda < \lambda_c$, one solution for $\lambda = \lambda_c$ and no solution for $\lambda > \lambda_c$. The mesh plots of the lower branch ($\lambda = 5$, $\omega_1 = 2.811554938$) and upper branch ($\lambda = 5$, $\omega_2 = 7.548098106$) are shown in Fig 3.2.

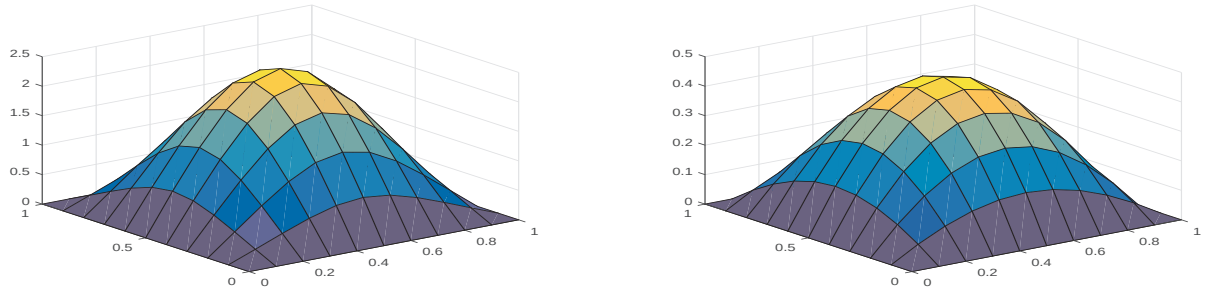

(a) Upper branch solution $\lambda = 5$ and $\omega_2 = 7.548098106$

(b) Lower branch solution $\lambda = 5$ and $\omega_1 = 2.811554938$

Figure 3.2: Mesh plots of the upper and lower solutions for selected values of λ and ω

In Table 5.1, we compare the values of u_{max} of the three methods, WRM, CSCM-K and BSQLM. We consider the values of the parameter λ as done in [75]. We also consider the solution in the domain subdivided into equal 4×4 sub-regions. Since the exact solution of the two dimensional Bratu problem is not known in literature, we use the results from WRM and CSCM-K as our basis of comparison to the BSQLM results. The results in Table (5.1) show that the BSQLM solution agree to 5 decimal places with the results from CSCM-K which is known to be highly accurate method.

Table 3.2: The maximum values of the solution $u(x, y)$ by the WRM, CSCM-K and BSQLM for different values of λ

λ	WRM [75]	CSCM-K	BSQLM
0.1	0.00739148232	0.007427053468645	0.007427132966698
0.5	0.03781451306	0.037984412494968	0.037985298386246
1.0	0.0779460505	0.078104419480805	0.078103863139426
2.0	0.1665928797	0.166902012852600	0.166900505362755
3.0	0.2698543078	0.270370407490254	0.270374143745502
4.0	0.3945269608	0.395540911835512	0.395540918829025
5.0	0.554387275	0.556970351040996	0.556971761314595
6.0	0.7871142546	0.796804803376730	0.796803797175867
6.4	0.9292292746	1.003321398467646	1.003326671983020
6.8	1.169825663	0.968377381095159	0.968377828328672
6.939571828	1.453226755	1.099599554422270	1.099599287729232

Rounding off the results in Table 5.1 to the nearest 5 decimal places for $\lambda(= 1, 2, 3, 4, 5, 6)$ we get the results in Table 3.3. These results compare very well with the results obtained by [76] after solving the two dimensional Bratu problem using the optimal homotopy analysis (oHAM) and wavelet homotopy analysis (wHAM) and the iterative wHAM.

Table 3.3: The maximum values of $u(x, y)$ for various values of λ

λ	WRM [75]	oHAM [76]	wHAM [76]	iterative wHAM [76]	CSCM-K	BSQLM
1.0	0.07795	0.07810	0.07810	0.07810	0.07810	0.07810
2.0	0.16659	0.16689	0.16690	0.16690	0.16690	0.16690
3.0	0.26985	0.27036	0.27037	0.27037	0.27037	0.27037
4.0	0.39453	0.39552	0.39554	0.39554	0.39554	0.39554
5.0	0.55439	0.55696	0.55697	0.55697	0.55697	0.55697
6.0	0.78711	0.79711	0.79680	0.79710	0.79680	0.79710

We solve the two dimensional Bratu problem using BSQLM for $\lambda = 1$ and 10×10 sub-regions of the problem domain $[0, 1] \times [0, 1]$. A graphical representation of the solution is a mesh plot in Fig (3.3) which agrees with the

solution plot in [76]. With the fuel ignition model as one of the physical applications of the Bratu problem, taking $u(x, y)$ to represent temperature, the results in Fig (3.3) show that there is a continuous decrease of temperature from the midpoint towards the boundary.

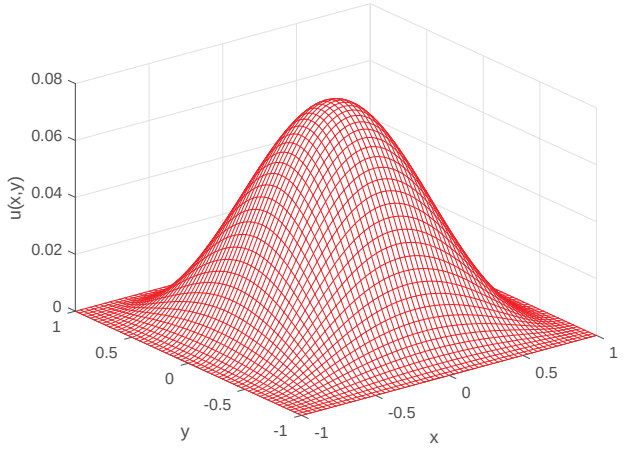

Figure 3.3: Solution of the Bratu problem using BSQLM for $\lambda = 1$.

Table 3.4 compares u_{max} from BSQLM, CSCM-K and FDM for different values of the λ_c as done in [75]. For all the cases, we consider equal sub-regions and a tolerance level of 10^{-6}. The results show that the BSQLM produces results in good agreement with CSCM-K.

Table 3.4: The maximum values of $u(x, y)$ for various values of λ_c and $N \times N$.

$N \times N$	λ_c	WRM [75]	CSCM-K	BSQLM
5×5	6.739545	1.2295280	0.9396735	0.9396720
10×10	6.792610	1.3835357	1.2979979	1.2979965
20×20	6.80497	1.3911583	1.3488587	1.3488579
40×40	6.81565	1.3881487	1.2560298	1.2560290
100×100	7.12222	1.3565527	1.1507510	1.1507509

Due to lack of an exact solution, it is impossible to directly compute the accuracy of the BSQLM in solving the two dimensional Bratu problem. We now compare the two methods, BSQLM and CSCM-K in terms of speed of convergence and computational efficiency.

Table 3.5: Runtime and the number of iterations

$N \times N$	BSQLM		CSCM-K	
	Runtime(s)	No. of iterations	Runtime(s)	No. of iterations
5×5	0.035430	6	0.020919	12
10×10	0.039587	5	0.035721	12
20×20	0.132422	4	0.532621	12
40×40	0.497956	4	4.559524	12
60×60	7.462640	3	21.314275	12
80×80	31.353469	3	144.779811	12
100×100	126.152106	3	577.760840	12

Table 3.5 shows a comparison between BSQLM and CSCM-K in terms of runtime in seconds and number of iterations for the solutions to converge within a tolerance level of 10^{-15} for different values of equal sub-regions $N \times N$. In all the cases, we consider the constant parameter $\lambda = 1$. It is worth noting that after the 10×10 sub-region, the BSQLM solution takes less time to converge than the CSCM-K solution. This shows that the BSQLM is more computationally efficient than CSCM-K. Moreover, as the subdivisions are made finer, the BSQLM needs less iterations to converge than the CSCM-K which needs a constant 12 iterations to converge. This proves that the BSQLM is faster than CSCM-K.

3.4 Conclusion

We solved the two dimensional Bratu problem using the bivariate spectral collocation method (BSQLM) and the Chebyshev spectral collocation method that uses Kronecker multiplication (CSCM-K). Both methods produced solutions which converge to the lower solution. We compared the results with those from finite difference method (FDM) and weighted residual method (WRM) in literature. We observed that results from BSQLM and CSCM-K are inclose agreement from the results in Table 5.1. Rounding-off the results in Table 5.1 to 5 decimal places for selected values of λ we get results in Table 3.3 which are in excellent agreement with the results obtained using the oHAM, wHAM and iterative HAM. This proves that the BSQLM is capable of producing reliable results as it compares well with the wHAM which is known to have a high computational efficiency. From the results in Table 3.5, we conclude that BSQLM is faster and more computationally efficient than CSCM-K.

Chapter 4

A NUMERICAL STUDY OF LAMINAR BOUNDARY LAYER FLOW, HEAT AND MASS TRANSFER OF A NON-NEWTONIAN FLUID PAST A VERTICAL POROUS PLATE

4.1 Introduction

According to Sochi [80], a Newtonian fluid is one which satisfies the relation

$$\tau = \mu\dot{\gamma},$$

where τ is the amount of stress, $\dot{\gamma}$ is the rate of strain and the constant of proportionality μ is the viscosity of the fluid. In contrast, a non-Newtonian fluid is one which does not obey Newton's law of viscosity, that is, shows non-linearity between the stress and rate of strain. In a non-Newtonian fluid, the relationship between the shear stress and rate of strain is non-linear through the origin at a given temperature and pressure and hence can not be

described using the classical Navier-Stokes equations. Unlike Newtonian fluids, non-Newtonian fluids are more complicated because there does not exist a single constitutive relation that can be used to explain all of them, Hussanan *et al.* [81]. Some of the typical examples of fluids which exhibit non-Newtonian behavior include: salt solutions, blood, paint, shampoo, toothpaste, starch suspensions, cosmetics, pharmaceuticals, jellies, polymeric liquids, tomato sauce, drilling mud, clay coating, soaps, ketchup.

In recent years, researchers have devoted considerable attention to the study of the behavior of non-Newtonian fluids in motion. This is due to the fact that the flow of non-Newtonian fluids has numerous applications in manufacturing and processing industry. Fluid flow phenomena in porous media has industrial applications in: filtration, catalysis, petroleum exploration and recovery and chromatography. In nature, this fluid flow occurs in water transportation by living plants and movement of soil waters. There is some work which has been done on the flow of non-Newtonian fluids in porous media. Yilmaz *et al.* [82] did an experimental investigation of Newtonian and non-Newtonian fluid flows in porous media, Kozicki and Tiu [83] did a unified model for non-Newtonian flow in packed beds and porous media, and some studies in Pearson and Tardy [84], Sadowski and Bird [85] and Liu and Masliyah [86]. Heat and mass transfer of non-Newtonian fluids in porous media arise in an extensive array of applications in modern nuclear engineering, mineral and chemical processing. Some of the applications of heat transfer problem of non-Newtonian fluids are in hot rolling, lubrication, cooling problems and drag reduction, Hosseini *et al.* [87]. Deburge and Han [88] studied heat transfer in a channel with porous wall for turbine cooling application, Chhabra [1] reported on the fluid flow, heat and mass transfer in non-Newtonian fluid.

There are different types of non-Newtonian models which include power Jeffrey model in Qasim [89], Oldroyd-B in Khan *et al.* [90], Maxwell models [91] and the second grade [92]. A lot of work has been on the Jeffrey fluid. Shateyi and Marewo [32] investigated the mixed convection flow of an MHD Jeffrey fluid flow over an exponentially stretching sheet. Turkyilmazoglu and Pop [93] investigated the flow and heat transfer of a Jeffrey fluid near the stagnation point on a stretching/shrinking sheet. Ellahi *et al.* [94] discussed the effects of nanoparticles to analyze Jeffrey fluid along a catheter. Some notable work where the Jeffrey fluid model has been applied include: peristaltic flow of Jeffrey fluid with variable-viscosity through a porous medium in an asymmetric channel [95], peristaltic transport of Jeffrey fluid under the effect of magnetohydrodynamic [96], radiative flow of Jeffrey fluid in a porous medium with power law heat flux and heat source [97].

The main objective of this study is to use (for the first time) the bivariate-spectral quasi-linearization method (BSQLM) to numerically study the laminar boundary layer flow, heat and mass transfer of a Jeffrey fluid past a vertical porous plate. The governing equations for the existing non-Newtonian fluid model are highly nonlinear. The BSQLM was introduced by Motsa *et al.* [98] as a numerical method to solve nonlinear evolution PDEs. They proved the applicability, accuracy and reliability of the BSQLM algorithm by solving equations which include the Kdv-Burger equation [99], Cahn-Hillard equation [100] and Burgers-Fisher equation [101]. The BSQLM was successfully used by Motsa and Mohammad [37] to investigate the the boundary layer flow of an Oldroyd-B nanofluid with thermal conductivity. It is in this work that the authors concluded that the BSQLM gives accurate results which converge rapidly when applied on a system of partial differential equations. Muzara *et al.* [102]

successfully used the bivariate spectral quasi-linearization to solve the highly non-linear two dimensional Bratu problem.

4.2 Problem statement and mathematical formulation

The constitutive equations for a Jeffrey fluid are given by Nadeem and Akbar [103] as

$$\begin{aligned} \tau &= -p\mathbf{I} + \mathbf{S}, \\ S &= \frac{\mu}{1+\lambda_1}\left[\mathbf{R}_1 + \lambda_2\left(\frac{\partial \mathbf{R}_1}{\partial t} + \mathbf{v}\cdot\nabla\right)\mathbf{R}_1\right], \end{aligned}$$

where τ is the Cauchy stress tensor, $\mathbf{S}$ is the extra stress tensor, μ is the dynamic viscosity, λ_1 and λ_2 are the thermal parameters of Jeffrey fluid and $\mathbf{R}_1$ is the Rivlin-Ericksen tensor defined by
$\mathbf{R}_1 = (\nabla V) + (\nabla V)'$. We consider the laminar boundary layer flow with heat and mass transfer of a Jeffrey fluid past a vertical porous plate. The non-Newtonian Jeffrey fluid and the vertical plate are maintained at a constant temperature and concentration. The vertical plate and the fluid are maintained at a constant temperature T_w and concentration C_w, higher than the ambient temperature T_∞ and concentration C_∞, respectively. The x-coordinate is measured from the leading edge of the plate and the y-coordinate is measured normal to the plate. The gravitational acceleration g acts vertically downwards. Under the Boussinesq and boundary layer approximations, the governing equations for this problem can be written as Prasad *et al.* [104],

$$\frac{\partial u}{\partial x} + \frac{\partial v}{\partial y} = 0, \tag{4.2.1}$$

$$\begin{aligned} u\frac{\partial u}{\partial x} + v\frac{\partial u}{\partial y} &= \frac{\nu}{1+\lambda_1}\left[\frac{\partial^2 u}{\partial y^2}\right] + \frac{\nu\lambda_2}{1+\lambda_1}\left(u\frac{\partial^3 u}{\partial x \partial y^2} - \frac{\partial u}{\partial x}\frac{\partial^2 u}{\partial y^2} + \frac{\partial u}{\partial y}\frac{\partial^2 u}{\partial x \partial y} + v\frac{\partial^3 u}{\partial y^3}\right) \\ &+ g\beta_T(T - T_\infty) + g\beta_C(C - C_\infty), \end{aligned} \tag{4.2.2}$$

$$u\frac{\partial T}{\partial x} + v\frac{\partial T}{\partial y} = \alpha\frac{\partial^2 T}{\partial y^2}, \tag{4.2.3}$$

$$u\frac{\partial C}{\partial x} + v\frac{\partial C}{\partial y} = D_m\frac{\partial^2 C}{\partial y^2}, \tag{4.2.4}$$

where u and v are velocities in the x and y directions, respectively. The appropriate boundary conditions for the velocity components are given by:

$$u = 0, \;\; v = 0, \quad \text{at } y = 0 \;\text{ and }\; u \to 0, \;\; \frac{\partial u}{\partial y} \to 0, \;\; \text{as } \; y \to \infty. \tag{4.2.5}$$

Also, the surface mass concentration and surface temperature boundary conditions are given by:

$$C = C_w, \;\; T = T_w, \quad \text{at } y = 0, \;\; \text{and} \quad C \to C_\infty, \;\; T \to T_\infty \;\; \text{as} \;\; y \to \infty. \tag{4.2.6}$$

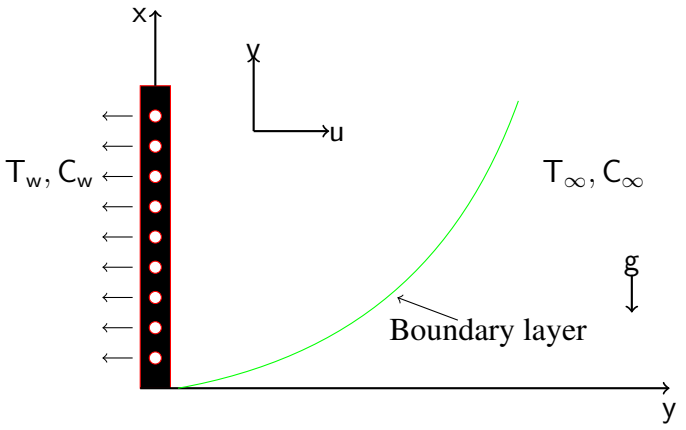

Figure 4.1: Flow configuration and coordinate system

4.3 Similarity transformation

To obtain solutions of the Eqs (4.2.2)-(4.2.4), we transform the equations into dimensionless form using the following transformations [105]:

$$\xi = x^{\frac{1}{2}} a^{-\frac{1}{2}}, \; \eta = \frac{By}{x^{\frac{1}{4}}}, \; f(\xi,\eta) = \frac{\Psi}{4\nu B x^{\frac{3}{4}}}, \; \theta(\xi,\eta) = \frac{T - T_\infty}{T_w - T_\infty}, \; \Phi(\xi,\eta) = \frac{C - C_\infty}{C_w - C_\infty},$$
$$Pr = \frac{\nu}{\alpha}, \; Sc = \frac{\nu}{D_m}, \; B = \left(\frac{g\beta(T_w - T_\infty)}{4\nu^2}\right)^{\frac{1}{4}}, \; De = \frac{\lambda_1 \nu B^2}{x^{\frac{1}{2}}}, \; Gr_x = \frac{g\beta(T_w - T_\infty)a^3}{\nu^2} \tag{4.3.7}$$

where ξ is the non-dimensional tangential coordinate, η is the non-dimensional radial coordinate, f is the dimensionless stream function, Pr is the Prandtl number, Sc is the Schmidt number, Gr_x is the Grashof number, and De is the Deborah number characterizing the fluidity of the material (viscoelasticity). The resulting momentum, energy, and concentration boundary layer equations take the form:

$$\begin{aligned} \frac{1}{1+\lambda} f''' \;\; &+ \;\; 3ff'' - 2(f')^2 + \frac{De}{1+\lambda}(f''^2 - 2f'f''' - 3ff^{iv}) + \theta + K\phi \\ &= \;\; 2\xi\left[f'\frac{\partial f'}{\partial \xi} - f''\frac{\partial f}{\partial \xi} - \frac{De}{1+\lambda}\left(f'\frac{\partial f'''}{\partial \xi} + f''\frac{\partial f''}{\partial \xi} - f'''\frac{\partial f'}{\partial \xi} - f^{iv}\frac{\partial f}{\partial \xi}\right)\right], \end{aligned} \tag{4.3.8}$$

$$\frac{\theta''}{Pr} + 3f\theta' = 2\xi\left(f'\frac{\partial\theta}{\partial\xi} - \theta'\frac{\partial f}{\partial\xi}\right), \tag{4.3.9}$$

$$\frac{\phi''}{Sc} + 3f\phi' = 2\xi\left(f'\frac{\partial\phi}{\partial\xi} - \phi'\frac{\partial f}{\partial\xi}\right). \tag{4.3.10}$$

The prime denotes differentiation with respect to the similarity variable η. We introduce a stream function ψ which is related to the velocities u and v according to the Cauchy-Riemann equations $u = \dfrac{\partial\psi}{\partial y}$ and $v = -\dfrac{\partial\psi}{\partial x}$.

$$\begin{gathered}\text{At } \eta = 0,\ \ f(0,\xi) = 0,\ \ \frac{\partial f(0,\xi)}{\partial\eta} = 0,\ \ \theta(0,\xi) = 1,\ \ \phi(0,\xi) = 1.\\ \text{As } \eta\to\infty,\ \ \frac{\partial f(\infty,\xi)}{\partial\eta}\to 0,\ \ \frac{\partial^2 f(\infty,\xi)}{\partial\eta^2}\to 0,\ \ \theta(\infty,\xi)\to 0,\ \ \phi(\infty,\xi)\to 0.\end{gathered} \tag{4.3.11}$$

Here primes denote the differentiation with respect to η. The skin friction ($f''(\xi,0)$), Nusselt number ($-\theta'(\xi,0)$) and Sherwood number ($-\phi'(\xi,0)$) can be defined using the transformations described by Eqs (4.3.7) to get the following expressions:

$$\frac{C_f}{{Gr_x}^{\frac{3}{4}}} = f''(\xi,0),\ \ \frac{Nu_x}{\sqrt[4]{Gr}} = -\theta'(\xi,0),\ \ \frac{Sh_x}{\sqrt[4]{Gr}} = -\phi'(\xi,0), \tag{4.3.12}$$

respectively.

4.4 Method of solution

4.4.1 Quasi-linearization

The quasi-linearization technique which was originally developed by Bellman and Kalaba [58] provides an explicit approach of obtaining approximate solutions to nonlinear differential equations. The sequence of approximate solutions from QLM are known to converge monotonically and quadratically, Ahmad *et al.* [106]. With reference to nonlinear PDEs (4.3.8) - (4.3.10), we consider the coupled system

$$\Lambda_r[\mathcal{M},\mathcal{N},\mathcal{O}] = 0,\ \ \text{for } r = 1,2,3, \tag{4.4.13}$$

where the nonlinear operators Λ_1, Λ_2 and Λ_3 denote Eq (4.3.8), Eq (4.3.9) and Eq (4.3.10) respectively. We also define

$$\mathcal{M} = \left\{f, \frac{\partial f}{\partial\eta}, \frac{\partial^2 f}{\partial\eta^2}, \frac{\partial^3 f}{\partial\eta^3}, \frac{\partial^4 f}{\partial\eta^4}, \frac{\partial f}{\partial\xi}, \frac{\partial^2 f}{\partial\xi\partial\eta}, \frac{\partial^3 f}{\partial\xi\partial\eta^2}, \frac{\partial^4 f}{\partial\xi\partial\eta^3}\right\},$$

$$\mathcal{N} = \left\{\theta, \frac{\partial\theta}{\partial\eta}, \frac{\partial^2\theta}{\partial\eta^2}, \frac{\partial\theta}{\partial\xi}\right\} \text{ and } \mathcal{O} = \left\{\phi, \frac{\partial\phi}{\partial\eta}, \frac{\partial^2\phi}{\partial\eta^2}, \frac{\partial\phi}{\partial\xi}\right\}.$$

We now adopt the subscripts s and $s+1$ for the previous and current iteration levels respectively. Assuming that the difference between to two consecutive iterations is small, the linear multi-dimensional Taylor series expansion of Eq (4.4.13) about the previous approximation, after re-arranging terms, gives the quasi-linearization formula

$$\begin{aligned} & \mathcal{M}_{s+1}\cdot\nabla_{\mathcal{M}}\Lambda_r[\mathcal{M}_s,\mathcal{N}_s,\mathcal{O}_s] + \mathcal{N}_{s+1}\cdot\nabla_{\mathcal{N}}\Lambda_r[\mathcal{M}_s,\mathcal{N}_s,\mathcal{O}_s] + \mathcal{O}_{s+1}\cdot\nabla_{\mathcal{O}}\Lambda_r[\mathcal{M}_s,\mathcal{N}_s,\mathcal{O}_s] \\ = \; & \mathcal{M}_s\cdot\nabla_{\mathcal{M}}\Lambda_r[\mathcal{M}_s,\mathcal{N}_s,\mathcal{O}_s] + \mathcal{N}_s\cdot\nabla_{\mathcal{N}}\Lambda_r[\mathcal{M}_s,\mathcal{N}_s,\mathcal{O}_s] + \mathcal{O}_s\cdot\nabla_{\mathcal{O}}\Lambda_r[\mathcal{M}_s,\mathcal{N}_s,\mathcal{O}_s] \\ - \; & \Lambda_r[\mathcal{M}_s,\mathcal{N}_s,\mathcal{O}_s], \quad s=0,1,2,\cdots, \end{aligned} \tag{4.4.14}$$

where the differential operators are defined as:

$$\nabla_{\mathcal{M}} = \left\{\frac{\partial}{\partial f}, \frac{\partial}{\partial f'}, \frac{\partial}{\partial f''}, \frac{\partial}{\partial f'''}, \frac{\partial}{\partial f_\xi}, \frac{\partial}{\partial f'_\xi}, \frac{\partial}{\partial f''_\xi}, \frac{\partial}{\partial f'''_\xi}\right\},$$

$$\nabla_{\mathcal{N}} = \left\{\frac{\partial}{\partial\theta}, \frac{\partial}{\partial\theta'}, \frac{\partial}{\partial\theta''}, \frac{\partial}{\partial\theta_\xi}\right\} \text{ and } \nabla_{\mathcal{O}} = \left\{\frac{\partial}{\partial\phi}, \frac{\partial}{\partial\phi'}, \frac{\partial}{\partial\phi''}, \frac{\partial}{\partial\phi_\xi}\right\}.$$

Applying the quasi-linearization formula (4.4.14) on the Eqs (4.3.8) - (4.3.10) we get

$$\begin{aligned} a_{0,s}f^{iv}_{s+1} + a_{1,s}f'''_{s+1} + a_{2,s}f''_{s+1} + a_{3,s}f'_{s+1} + a_{4,s}f_{s+1} + a_{5,s}\theta_{s+1} + a_{6,s}\phi_{s+1} & \\ + a_{7,s}\frac{\partial f'''_{s+1}}{\partial\xi} + a_{8,s}\frac{\partial f''_{s+1}}{\partial\xi} + a_{9,s}\frac{\partial f'_{s+1}}{\partial\xi} + a_{10,s}\frac{\partial f_{s+1}}{\partial\xi} & = B_{1,s}, \end{aligned} \tag{4.4.15}$$

$$b_{0,s}\theta''_{s+1} + b_{1,s}\theta'_{s+1} + b_{2,s}f'_{s+1} + b_{3,s}f_{s+1} + b_{4,s}\frac{\partial f_{s+1}}{\partial\xi} + b_{5,s}\frac{\partial\theta_{s+1}}{\partial\xi} = B_{2,s}, \tag{4.4.16}$$

$$c_{0,s}\phi''_{s+1} + c_{1,s}\phi'_{s+1} + c_{2,s}f'_{s+1} + c_{3,s}f_{s+1} + c_{4,s}\frac{\partial f_{s+1}}{\partial\xi} + c_{5,s}\frac{\partial\phi_{s+1}}{\partial\xi} = B_{2,s}, \tag{4.4.17}$$

where the variable coefficients are defined as follows:

$$
\begin{aligned}
a_{0,s} &= -3\frac{De}{1+\lambda}f_s - 2\xi\frac{\partial f_s}{\partial \xi},\ a_{1,s} = \frac{1}{1+\lambda}\left(1 - 2De f_s' - 2\xi De\frac{\partial f_s'}{\partial \xi}\right),\\
a_{2,s} &= 2\frac{De}{1+\lambda}(f_s'' + \xi\frac{\partial f_s''}{\partial \xi}) + 2\xi\frac{\partial f_s}{\partial \xi} + 3f_s,\\
a_{3,s} &= -4f_s' - 2\xi\frac{\partial f_s'}{\partial \xi} - 2\frac{De}{1+\lambda}f_s''' + 2\xi\frac{De}{1+\lambda}\frac{\partial f_s''}{\partial \xi},\ a_{4,s} = 3f_s'' - 3\frac{De}{1+\lambda}f_s^{iv},\ a_{5,s} = 1,\ a_{6,s} = K,\\
a_{7,s} &= 2\xi\frac{De}{1+\lambda}f_s',\ a_{8,s} = 2\xi\frac{De}{1+\lambda}f_s'',\ a_{9,s} = -2\xi\left(f_s' + \frac{De}{1+\lambda}f_s'''\right),\ a_{10,s} = 2\xi f_s'' - 2\xi f_s^{iv},\\
b_{0,s} &= \frac{1}{Pr}, b_{1,s} = 3f_s + 2\xi\frac{\partial f_s}{\partial \xi},\ b_{2,s} = -2\xi\frac{\partial \theta_s}{\partial \xi},\ b_{3,s} = 3\theta_s',\ b_{4,s} = 2\xi\theta_s',\ b_{5,s} = -2\xi f_s',\ c_{0,s} = \frac{1}{Sc},\\
c_{1,s} &= 3f_s + 2\xi\frac{\partial f_s}{\partial \xi},\ c_{2,s} = -2\xi\frac{\partial \phi_s}{\partial \xi},\ c_{3,s} = 3\phi_s',\ c_{4,s} = 2\xi\phi_s',\ c_{5,s} = -2\xi f_s',\\
B_{1,s} &= \frac{De}{1+\lambda}\left(2\xi f_s''\frac{\partial f_s''}{\partial \xi} - 2\xi f_s'''\frac{\partial f_s'}{\partial \xi} + (f_s'')^2 - 2f_s'f_s''' - 3f_s f_s^{iv} - 2\xi f_s^{iv}\frac{\partial f_s}{\partial \xi}\right) + 3f_s f_s'' - 2(f_s')^2,\\
B_{2,s} &= 3f_s\theta_s' - 2\xi f_s'\frac{\partial \theta_s}{\partial \xi} + 2\xi\theta_s'\frac{\partial f_s}{\partial \xi},\ B_{3,s} = 3f_s\phi_s' - 2\xi f_s'\frac{\partial \phi_s}{\partial \xi} + 2\xi\phi_s'\frac{\partial f_s}{\partial \xi}.
\end{aligned}
$$

The Eqns (4.4.15), (4.4.16) and (4.4.17) are subject to boundary conditions

$$
\begin{aligned}
f_{s+1}(0,\xi) &= 0,\ \frac{\partial f_{s+1}}{\partial \eta}(0,\xi) = 1,\ \frac{\partial f_{s+1}}{\partial \eta}(\infty,\xi) = 0,\ \frac{\partial^2 f_{s+1}}{\partial \eta^2}(\infty,\xi) = 0,\\
\theta_{s+1}(0,\xi) &= 1,\ \theta_{s+1}(\infty,\xi) = 0,\\
\phi_{s+1}(0,\xi) &= 1,\ \phi_{s+1}(\infty,\xi) = 0,
\end{aligned}
\tag{4.4.18}
$$

respectively.

4.4.2 Chebyshev differentiation and bivariate Lagrange interpolation

In this work, we consider approximating functions of the form

$$
\begin{aligned}
f(\eta,\xi) &\approx \sum_{j=0}^{N}\sum_{i=0}^{M} f(\eta_j,\xi_i)L_j(\eta)L_i(\xi),\\
\theta(\eta,\xi) &\approx \sum_{j=0}^{N}\sum_{i=0}^{M} \theta(\eta_j,\xi_i)L_j(\eta)L_i(\xi),\\
\phi(\eta,\xi) &\approx \sum_{j=0}^{N}\sum_{i=0}^{M} \phi(\eta_j,\xi_i)L_j(\eta)L_i(\xi),
\end{aligned}
$$

where the characteristic Lagrange polynomials are defined as

$$L_j(\eta) = \prod_{\substack{k=0 \\ k\neq j}}^{N} \frac{\eta - \eta_k}{\eta_j - \eta_k}, \quad L_i(\xi) = \prod_{\substack{k=0 \\ k\neq i}}^{M} \frac{\xi - \xi_k}{\xi_i - \xi_k},$$

so that they both obey the Kronecker delta equation, that is,

$$L_{ji}(\eta_n, \xi_m) = \begin{cases} 1, & \text{if } j = n,\ i = m \\ 0, & \text{otherwise.} \end{cases} \tag{4.4.19}$$

To apply Chebyshev differentiation, it is convenient to transform the physical domains $[0, \eta_\infty]$(η_∞ is a number large enough for boundary conditions at the end point to still apply) in the η direction and $[0, 1]$ in the ξ direction to the computational domain $[-1, 1]$ using the Chebyshev-Gauss-Lobatto collocation points, Shamsi and Dehghan [107],

$$\eta_j = \cos\left(\frac{\pi_j}{N}\right), \quad \xi_i = \cos\left(\frac{\pi_i}{M}\right), \quad j = 0, 1, \cdots, N, \quad i = 0, 1, \cdots, M, \tag{4.4.20}$$

and set

$$\begin{aligned} \left.\frac{\partial f_{s+1}}{\partial \eta}\right|_{\substack{\eta=\eta_j \\ \xi=\xi_i}} &\approx \sum_{p=0}^{N}\sum_{q=0}^{M} f_{s+1}(\eta_p, \xi_q)\frac{dL_p(\eta_j)}{d\eta}L_q(\xi_i) \\ &= \sum_{p=0}^{N} D_{jp} f_{s+1}(\eta_p, \xi_i) = \mathbf{DF}_{s+1,i}, \end{aligned} \tag{4.4.21}$$

$$\left.\frac{\partial f_{s+1}}{\partial \xi}\right|_{\substack{\eta=\eta_j \\ \xi=\xi_i}} \approx \sum_{q=0}^{M} d_{iq} f_{s+1}(\eta_j, \xi_q) = \sum_{q=0}^{M} d_{iq}\mathbf{F}_{s+1,q}, \tag{4.4.22}$$

and

$$\begin{aligned} \left.\frac{\partial^2 f_{s+1}}{\partial \xi \partial \eta}\right|_{\substack{\eta=\eta_j \\ \xi=\xi_i}} &\approx \sum_{p=0}^{N}\sum_{q=0}^{M} f_{s+1}(\eta_p, \xi_q)\frac{dL_p(\eta_j)}{d\eta}\frac{dL_q(\xi_i)}{d\xi} \\ &= \sum_{q=0}^{M} d_{iq}\Big(\mathbf{DF}_{s+1,q}\Big). \end{aligned} \tag{4.4.23}$$

Similarly, the derivatives of θ and ϕ with respect to η and ξ are defined as

$$\left.\frac{\partial \theta_{s+1}}{\partial \eta}\right|_{\substack{\eta=\eta_j \\ \xi=\xi_i}} \approx \mathbf{D}\theta_{s+1,i}, \quad \left.\frac{\partial \theta_{s+1}}{\partial \xi}\right|_{\substack{\eta=\eta_j \\ \xi=\xi_i}} \approx \sum_{q=0}^{M} d_{iq}\theta_{s+1,q}, \tag{4.4.24}$$

and

$$\left.\frac{\partial \phi_{s+1}}{\partial \eta}\right|_{\substack{\eta=\eta_j \\ \xi=\xi_i}} \approx \mathbf{D}\phi_{s+1,i}, \quad \left.\frac{\partial \phi_{s+1}}{\partial \xi}\right|_{\substack{\eta=\eta_j \\ \xi=\xi_i}} \approx \sum_{q=0}^{M} d_{iq}\phi_{s+1,q}, \tag{4.4.25}$$

respectively. We define the column vectors

$$\begin{aligned}
\mathbf{F}_{s+1,i} &= [f_{s+1}(\eta_0,\xi_i), f_{s+1}(\eta_1,\xi_i), \cdots, f_{s+1}(\eta_{N-1},\xi_i), f_{s+1}(\eta_N,\xi_i)]^T, \\
\boldsymbol{\theta}_{s+1,i} &= [\theta_{s+1}(\eta_0,\xi_i), \theta_{s+1}(\eta_1,\xi_i), \cdots, \theta_{s+1}(\eta_{N-1},\xi_i), \theta_{s+1}(\eta_N,\xi_i)]^T, \\
\boldsymbol{\phi}_{s+1,i} &= [\phi_{s+1}(\eta_0,\xi_i), \phi_{s+1}(\eta_1,\xi_i), \cdots, \phi_{s+1}(\eta_{N-1},\xi_i), \phi_{s+1}(\eta_N,\xi_i)]^T,
\end{aligned}$$

where the superscript T denotes matrix transpose. $\mathbf{D}$ and $\mathbf{d}_{iq}$ are the standard first order Chebyshev differentiation, Trefethen [59] matrices of size $(N+1)\times(N+1)$ and $(M+1)\times(M+1)$ respectively. Applying spectral collocation on Eqns (4.4.15) - (4.4.17) we get

$$\begin{aligned}
&\mathbf{A}_{1,1}\mathbf{F}_{s+1,i} + \mathbf{A}_{1,2}\theta_{s+1,i} + \mathbf{A}_{1,3}\phi_{s+1,i} \\
&+\sum_{q=0}^{M}\left(\mathbf{a}_{7,i}D^3 + \mathbf{a}_{8,i}D^2 + \mathbf{a}_{9,i}D + \mathbf{a}_{10,r}\right)d_{iq}\mathbf{F}_{s+1,q} \quad = \quad \mathbf{B}_{1,i},
\end{aligned} \tag{4.4.26}$$

$$\mathbf{A}_{2,1}\mathbf{F}_{s+1,i} + \mathbf{A}_{2,2}\theta_{s+1,i} + \mathbf{b}_{4,i}\sum_{q=0}^{M} d_{iq}\mathbf{F}_{s+1,q} + \mathbf{b}_{5,i}\sum_{q=0}^{M} d_{iq}\theta_{s+1,q} \quad = \quad \mathbf{B}_{2,i}, \tag{4.4.27}$$

$$\mathbf{A}_{3,1}\mathbf{F}_{s+1,i} + \mathbf{A}_{3,3}\phi_{s+1,i} + \mathbf{c}_{4,i}\sum_{q=0}^{M} d_{iq}\mathbf{F}_{s+1,q} + \mathbf{c}_{5,i}\sum_{q=0}^{M} d_{iq}\phi_{s+1,q} \quad = \quad \mathbf{B}_{3,i}. \tag{4.4.28}$$

The coupled-system Eqns (4.4.26) - (4.4.28) can be written in matrix form as

$$\begin{bmatrix}
\mathbf{A}_{1,1}^{(i,j)} & \mathbf{A}_{1,2}^{(i,j)} & \mathbf{A}_{1,3}^{(i,j)} \\
\mathbf{A}_{2,1}^{(i,j)} & \mathbf{A}_{2,2}^{(i,j)} & \mathbf{A}_{2,3}^{(i,j)} \\
\mathbf{A}_{3,1}^{(i,j)} & \mathbf{A}_{3,2}^{(i,j)} & \mathbf{A}_{3,3}^{(i,j)}
\end{bmatrix}
\begin{bmatrix}
\mathbf{F}_{s+1,i} \\ \theta_{s+1,i} \\ \phi_{s+1,i}
\end{bmatrix} =
\begin{bmatrix}
\mathbf{B}_{1,s} \\ \mathbf{B}_{2,s} \\ \mathbf{B}_{3,s}
\end{bmatrix}, \tag{4.4.29}$$

where, when $i = j$,

$$\begin{aligned}
\mathbf{A}_{1,1}^{(i,i)} &= \text{diag}\{\mathbf{a}_{0,i}\}D^4 + \text{diag}\{\mathbf{a}_{1,i}\}D^3 + \text{diag}\{\mathbf{a}_{2,i}\}D^2 + \text{diag}\{\mathbf{a}_{3,i}D + \text{diag}\{\mathbf{a}_{4,i}\} \\
&+ \Big(\text{diag}\{\mathbf{a}_{7,i}\}D^3 + \text{diag}\{\mathbf{a}_{8,i}\}D^2 + \text{diag}\{\mathbf{a}_{9,i}\}D + \text{diag}\{\mathbf{a}_{10,i}\}\Big)d_{i,i}, \\
\mathbf{A}_{1,2}^{(i,i)} &= \text{diag}\{\mathbf{a}_{4,s}\},\ \mathbf{A}_{1,3}^{(i,i)} = \text{diag}\{\mathbf{a}_{5,s}\},\ \mathbf{A}_{2,1}^{(i,i)} = \text{diag}\{\mathbf{b}_{2,i}\}D + \text{diag}\{\mathbf{b}_{3,i}\} + \text{diag}\{\mathbf{b}_{4,i}\}d_{i,i} \\
\mathbf{A}_{2,2}^{(i,i)} &= \text{diag}\{\mathbf{b}_{0,s}\}D^2 + \text{diag}\{\mathbf{b}_{1,s}\}D + \text{diag}\{b_{5,i}\}d_{i,i},\ A_{2,3}^{(i,i)} = \mathbf{0}, \\
\mathbf{A}_{3,1}^{(i,i)} &= \text{diag}\{\mathbf{c}_{2,i}\}D + \text{diag}\{\mathbf{c}_{3,i}\} + \text{diag}\{\mathbf{c}_{4,i}\}d_{i,i}, A_{3,2}^{(i,i)} = \mathbf{0}, \\
\mathbf{A}_{3,3}^{(i,i)} &= \text{diag}\{\mathbf{c}_{0,i}\}D^2 + \text{diag}\{\mathbf{c}_{1,i}\}D + \text{diag}\{\mathbf{c}_{5,i}\}d_{i,i},
\end{aligned}$$

and when $i \neq j$,

$$\begin{aligned}
A_{1,1}^{(i,j)} &= \Big(\text{diag}\{\mathbf{a}_{6,i}\}D^2 + \text{diag}\{\mathbf{a}_{7,i}\}D + \text{diag}\{\mathbf{a}_{8,i}\}\Big)d_{i,j},\ A_{1,2}^{(i,j)} = \mathbf{0},\ A_{1,3}^{(i,j)} = \mathbf{0},\ A_{2,1}^{(i,j)} = \text{diag}\{\mathbf{b}_{4,i}\}d_{i,j}, \\
A_{2,2}^{(i,j)} &= \text{diag}\{\mathbf{b}_{5,i}\}d_{i,j},\ A_{2,3}^{(i,j)} = \mathbf{0},\ A_{3,1}^{(i,j)} = \text{diag}\{\mathbf{c}_{4,i}\}d_{i,j},\ A_{3,2}^{(i,j)} = \mathbf{0},\ A_{3,3}^{(i,j)} = \text{diag}\{\mathbf{c}_{5,i}\}d_{i,j}, \\
\mathbf{B}_{1,s} &= \frac{De}{1+\lambda}\Big(2\xi\mathbf{F}_s'' \circ \frac{\partial \mathbf{F}_s''}{\partial \xi} - 2\xi\mathbf{F}_s''' \circ \frac{\partial \mathbf{F}_s'}{\partial \xi} - \mathbf{F}_s'' \circ \mathbf{F}_s'' - 2\mathbf{F}_s \circ \mathbf{F}_s''' - 3\mathbf{F}_s \circ \mathbf{F}_s^{iv} - 2\xi\mathbf{F}_s^{iv} \circ \frac{\partial \mathbf{F}_s}{\partial \xi}\Big) \\
&+ 3\mathbf{F}_s \circ \mathbf{F}_s'' - 2\mathbf{F}_s' \circ \mathbf{F}_s',\ \mathbf{B}_{2,s} = 3\mathbf{F}_s \circ \theta_s' - 2\xi\mathbf{F}_s' \circ \frac{\partial \theta_s}{\partial \xi} + 2\xi\theta_s' \circ \frac{\partial \mathbf{F}_s}{\partial \xi}, \\
\mathbf{B}_{3,s} &= 3\mathbf{F}_s \circ \phi_s' - 2\xi\mathbf{F}_s' \circ \frac{\partial \phi_s}{\partial \xi} + 2\xi\phi_s' \circ \frac{\partial \mathbf{F}_s}{\partial \xi}.
\end{aligned}$$

The boundary conditions (4.4.18) are transformed to

$$\begin{aligned}
f_{s+1}(0,\xi_i) &= 0,\ \sum_{p=0}^{N} D_{Np} f_{s+1}(\eta_p,\xi_i) = 1,\ \sum_{p=0}^{N} D_{0p} f_{s+1}(\eta_p,\xi_i) = 0,\ \sum_{p=0}^{N} D_{0p}^2 f_{s+1}(\eta_p,\xi_i) = 0, \\
\theta_{s+1}(N,\xi_i) &= 1,\ \theta_{s+1}(0,\xi_i) = 0, \\
\phi_{s+1}(N,\xi_i) &= 1,\ \phi_{s+1}(0,\xi_i) = 0,\ i = 0,1,\cdots N.
\end{aligned} \tag{4.4.30}$$

4.5 Results and discussions

The bivariate spectral quasi-linearization method was used to solve a system of coupled non-linear partial differential equations (4.2.1)-(4.2.4). It is remarked that the BSQLM results presented in this work were obtained using $N = 60$ and $M = 10$ collocation points in the η and ξ directions respectively. All the values were obtained using MATLAB 2016. To validate our results, we use solution based errors as in Motsa and Ansari [108]. This is achieved by computing the differences between approximate solutions at the current and the previous iteration levels, denoted s and $s+1$, respectively. The error norms in approximating $f(\eta,\xi)$, $\theta(\eta,\xi)$ and $\phi(\eta,\xi)$ are defined

as follows:

$$\text{Error}_f = \max_{0\leqslant i\leqslant N} ||\mathbf{F}_{s+1,i} - \mathbf{F}_{s,i}||_\infty, \ \text{Error}_\theta = \max_{0\leqslant i\leqslant N} ||\theta_{s+1,i} - \theta_{s,i}||_\infty, \ \text{Error}_\phi = \max_{0\leqslant i\leqslant N} ||\phi_{s+1,i} - \phi_{s,i}||_\infty$$

Fig 4.2 shows that the bi-variate spectral quasi-linearization solution for f, θ and ϕ converge to the exact solution after 5 iterations.

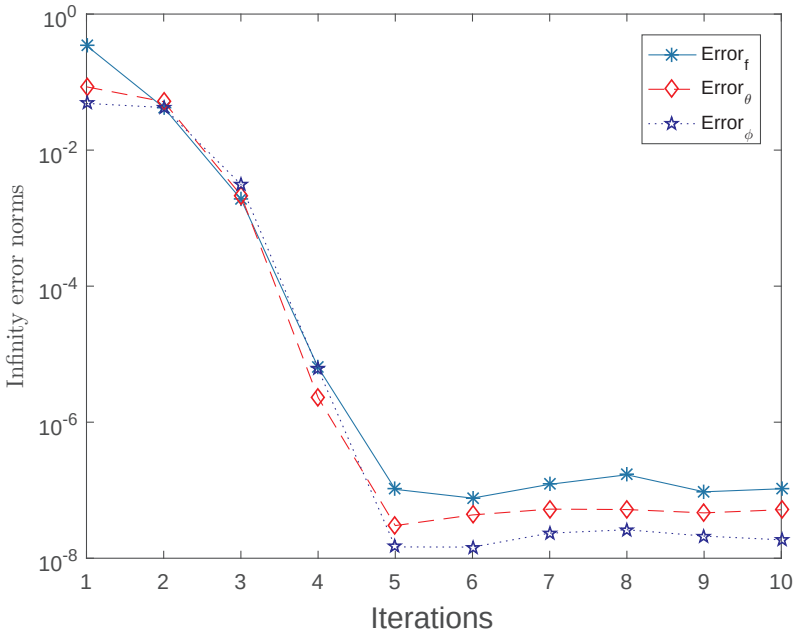

Figure 4.2: Convergence graphs of the solutions $f(\eta,\xi)$, $\theta(\eta,\xi)$ and $\phi(\eta,\xi)$.

Table 4.1 displays the numerical results obtained by the bivariate spectral collocation method for the main parameters, namely the skin friction $(f''(\xi,0))$, Nusselt number $(-\theta'(\xi,0))$ and the Sherwood number $(-\phi'(\xi,0))$ when we vary λ, Sc and Pr. The values were compared with those obtained using the finite difference algorithm based on the Keller's box method, Prasad [104]. The results were found to be in good agreement. We observe that increasing the ratio relaxation to retardation times increases the skin friction, heat transfer rate and mass transfer rate. Increasing the Schmidt number has the effect of increasing the skin friction, heat transfer rate and mass transfer rate. The fluid particles need much more time to come back from a perturbed system to an equilibrium system, thus increasing frictional force on the surface at the same time reducing the rates of heat and mass transfer on the wall surface. The skin friction and heat transfer rate are decreased with increasing Prandtl number whilst the mass transfer rate is enhanced.

Table 4.1: The values of $f''(\xi,0)$, $-\theta'(\xi,0)$ and $-\phi'(\xi,0)$ for various values of λ, Sc and Pr for $De = 0.1$ and $\xi = 1$.

			Results from (104)			Results from present study		
λ	S_c	Pr	$f''(\xi,0)$	$-\theta'(\xi,0)$	$-\phi'(\xi,0)$	$f''(\xi,0)$	$-\theta'(\xi,0)$	$-\phi'(\xi,0)$
0.2	1.2	0.71	0.8289	0.5225	0.6757	0.8289	0.5224	0.6757
	1.5		0.8264	0.5214	0.7471	0.8265	0.5214	0.7471
	2.0		0.8233	0.5202	0.5465	0.8233	0.5202	0.5464
1.0	0.6	0.71	1.1625	0.5606	0.5112	1.1630	0.5606	0.5113
1.5			1.3386	0.5742	0.5228	1.3387	0.5742	0.5230
2.0			1.5003	0.5849	0.5317	1.5003	0.5850	0.5317
0.1	0.6	1.0	0.7973	0.5997	0.4593	0.7973	0.5998	0.4593
		2.0	0.7185	0.7702	0.4151	0.7185	0.7702	0.4150
		3.0	0.6740	0.8854	0.3926	0.6741	0.8854	0.3926

Figs (4.3), (4.4) and (4.5) show the influence of the ratio of relaxation to retardation times parameter (λ) on the velocity, temperature and concentration profiles. The prescribed default parameter values are $Pr = 0.71$, $Sc = 0.6$, $De = 0.1$ and $K = 0.5$. The values of λ considered are $0, 1, 3, 7$. The results obtained show that the velocity of the Jeffrey fluid past a vertical porous plate is significantly increased with an increase in λ. Physically, an increase in λ_1 means increasing the relaxation time which then accelerates the fluids. On the other hand, the temperature and concentration are depressed slightly with an increase in λ.

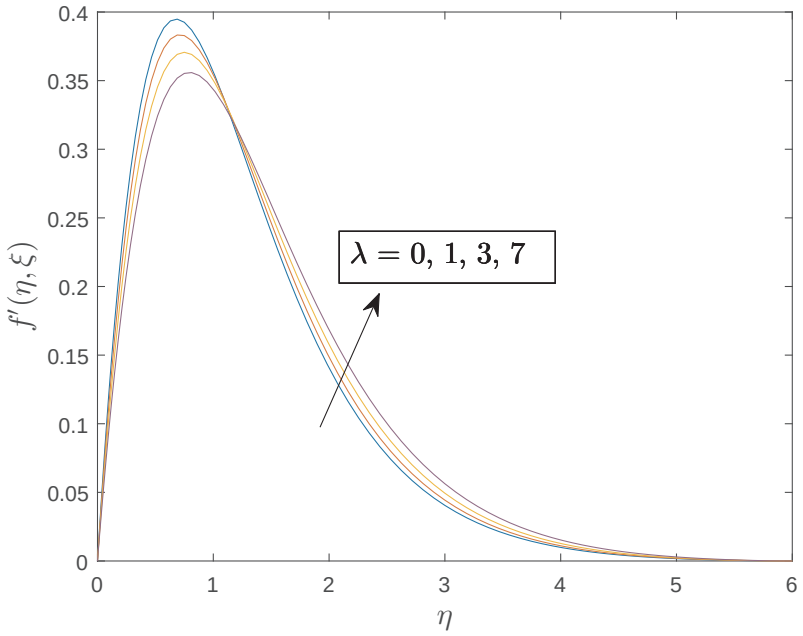

Figure 4.3: The influence of λ on the velocity profiles.

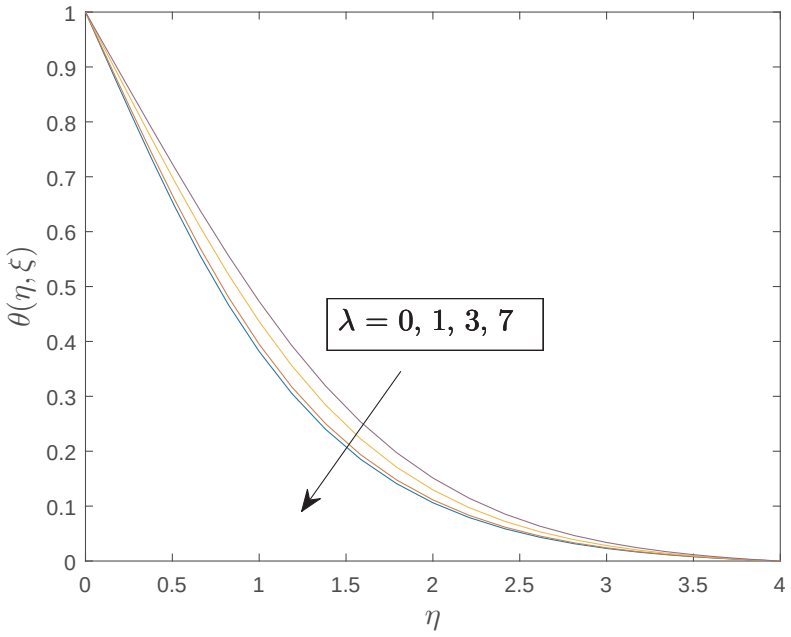

Figure 4.4: The influence of λ on the temperature profiles.

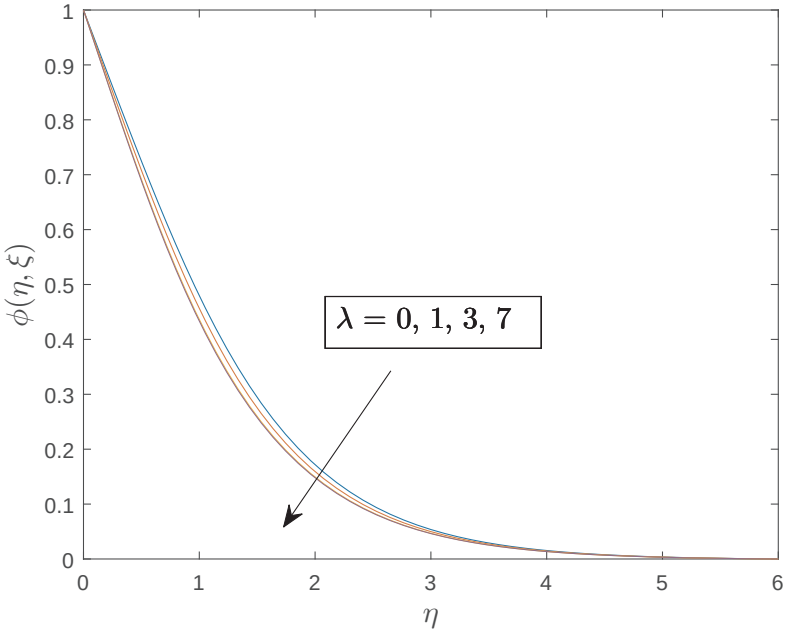

Figure 4.5: The influence of λ on the concentration profiles.

Figs (4.6), (4.7) and (4.8) show the variations of the fluid velocity, temperature and concentration with the increase in the Prandtl number. The prescribed default parameter values are $Sc = 0.6$, $De = 0.1$, $\lambda = 0.2$ and $K = 0.5$. The parameter values considered are $Pr(= 0.71, 1, 1.5, 2.5)$. From the graphical results it is observed that the flow velocity of the fluid is decreases with an increase in the Pr parameter value. Also, the increase in Pr parameter values effects a substantial decrease in the fluid temperature. However, an increase in Pr causes an increase in the fluid concentration. With the increase in Pr , the thermal diffusion decreases and therefore the thermal boundary layer becomes thinner. This in turn reduces the dimensionless temperature.

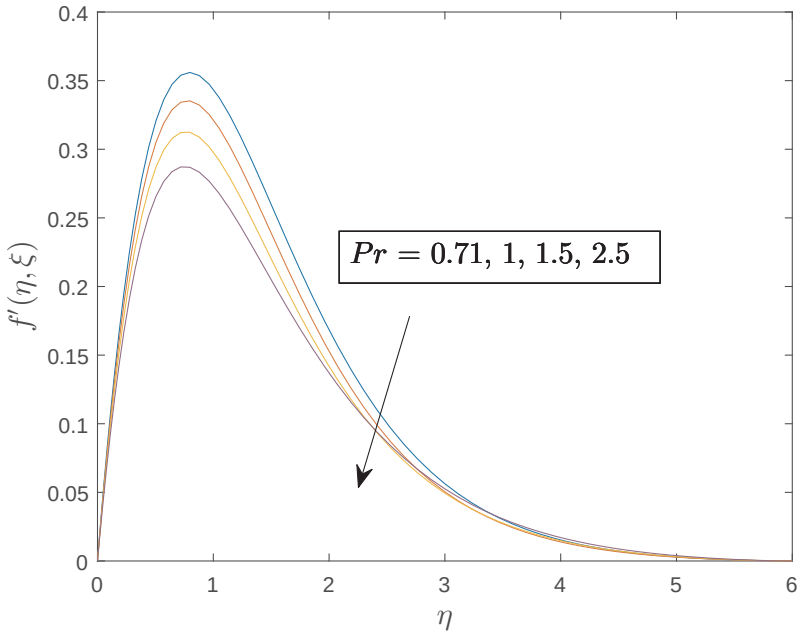

Figure 4.6: The influence of Pr on the velocity profiles.

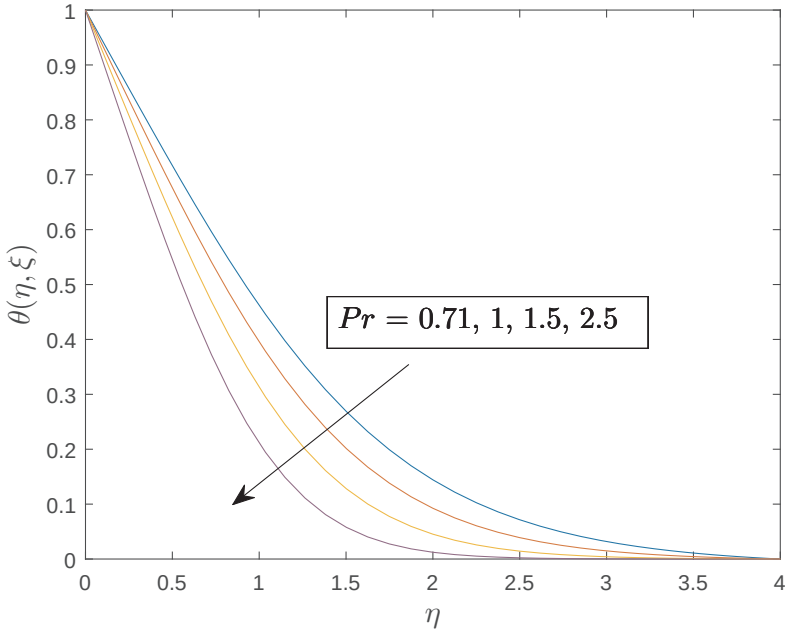

Figure 4.7: The influence of Pr on the temperature profiles.

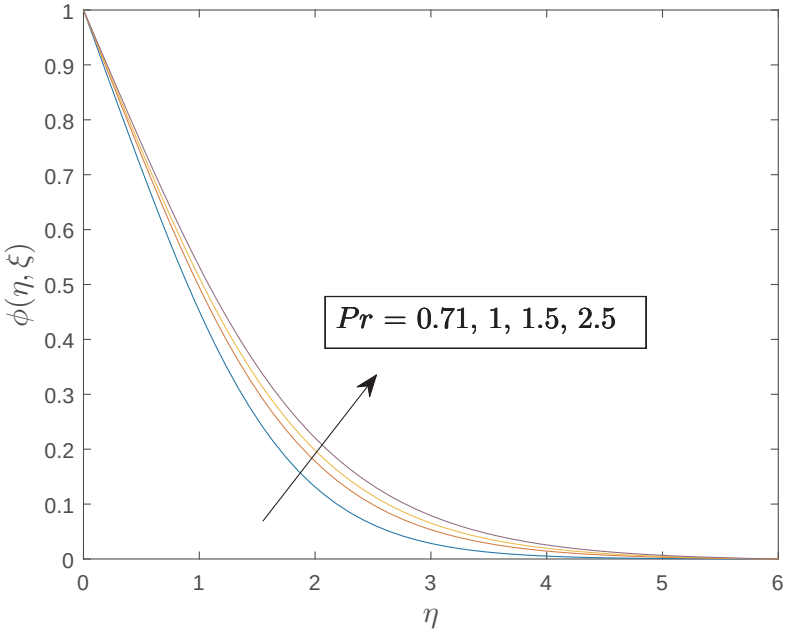

Figure 4.8: The influence of Pr on the concentration profiles.

Figs (4.9), (4.10) and (4.11) show the effects of Schmidt number parameter on the fluid flow velocity, temperature and concentration. The prescribed default parameter values are $Pr = 0.71$, $De = 0.1$, $\lambda = 0.2$ and $K = 0.5$. The parameter values considered are $Sc(= 0.2, 0.4, 0.6, 1)$. Increasing Sc values reduces the fluid flow velocity. There is a slight increase in fluid temperature. Fluid concentration is reduced strongly with an increase in the Sc values. Physically, as Sc increases, the molecular diffusion decreases and this lead to a decrease in the concentration boundary thickness, and hence the concentration profile.

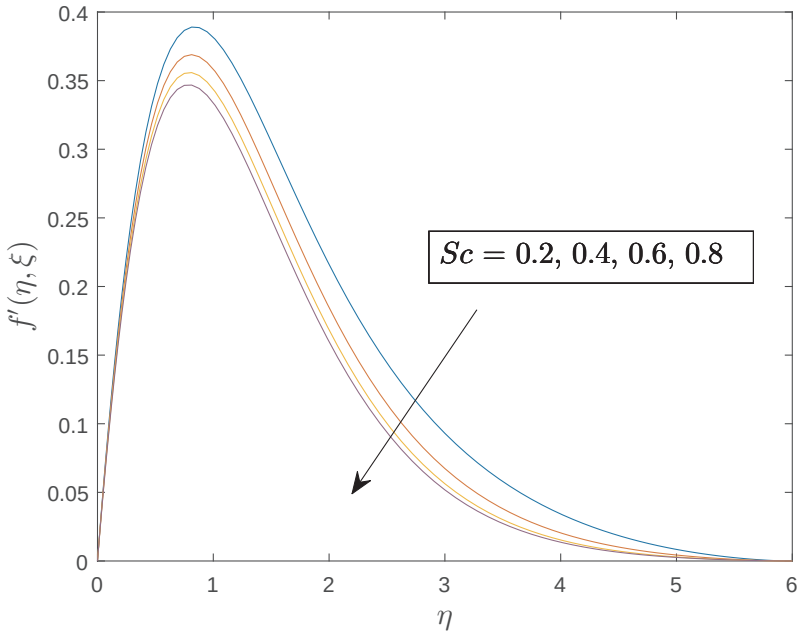

Figure 4.9: The influence of Sc on the velocity profiles.

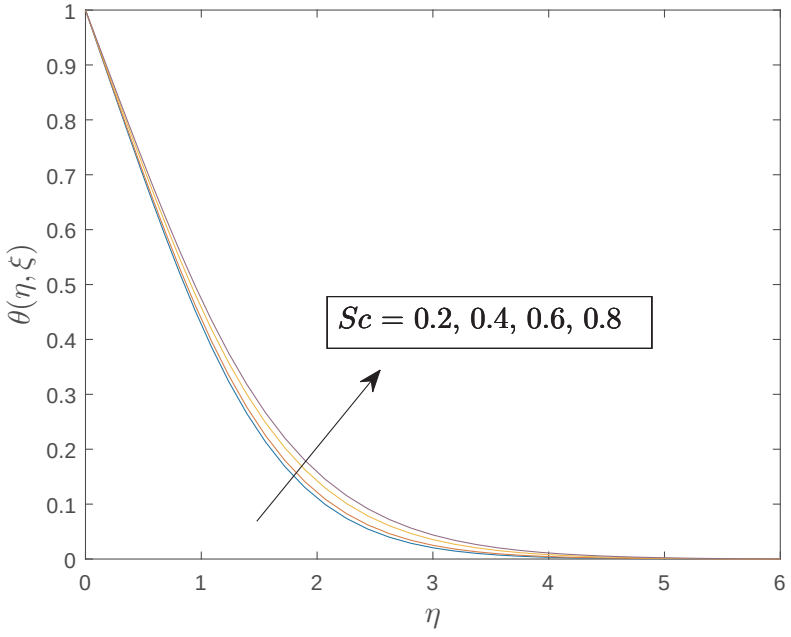

Figure 4.10: The influence of Sc on the temperature profiles.

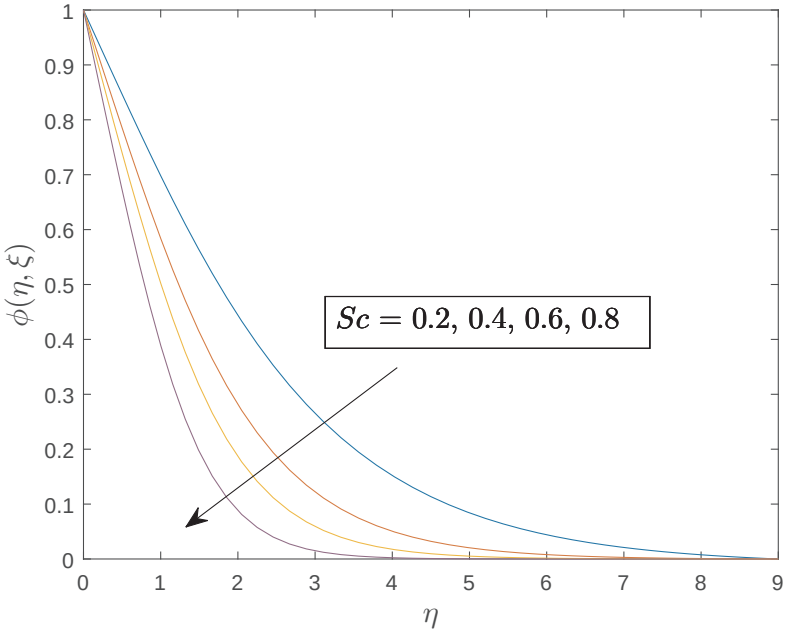

Figure 4.11: The influence of Sc on the concentration profiles.

Conclusion

The bi-variate spectral quasi-linearization method was used to solve a system of transformed partial differential equations that model the flow of a Jeffrey fluid through a vertical porous plate. Results were displayed in tabular form to show the effects of varying the ratio of relaxation to retardation times (λ), Schmidt number (Sc) and the Prandtl number (Pr) on the skin friction, heat and mass transfer rates. Graphs were plotted to show the influence λ, Sc and Pr on the velocity, temperature and concentration profiles of the Jeffrey fluid. Solution based errors were computed. Results were displayed in a table and graphs plotted to show the convergence of the method. From the results we can conclude that the method converges to the exact solution. The following are the significant observations from the study:

1. Increasing the Schmidt number decelerates the Jeffrey fluid flow, reduces the skin friction, heat and mass transfer rates and strongly depresses the concentration whilst the temperature is increased.

2. Increasing the parameter ratio of relaxation and retardation times (λ), increases the fluid velocity, the skin friction, heat and mass transfer rates whilst it reduces temperature and concentration.

3. Increasing the Prandtl number decreases the fluid velocity, the fluid temperature, skin friction, mass transfer rate whilst heat transfer rate and the concentration are increased.

Chapter 5

A NUMERICAL ANALYSIS OF LAMINAR BOUNDARY LAYER FLOW OF A JEFFREY FLUID PAST A VERTICAL POROUS PLATE IN THE PRESENCE OF THERMAL RADIATION AND CHEMICAL REACTION

5.1 Introduction

Basically, there are three modes of heat transfer namely, conduction, convection and radiation. In this study we mainly focus on thermal radiation in non-Newtonian fluid flow. Thermal radiation is energy emitted by matter at a finite temperature with no medium of propagation required. The effects of thermal radiation on the flow field in the case of force and natural convection are important in the context of space technology and processes involving high temperatures, Khan *et al.* [109]. Many processes of industrial areas occur at high temperatures and the study of radiative heat transfer becomes very important for the design of the equipments. Examples of applications of thermal radiation effects in fluid flow are found in nuclear power plants, gas turbines and the various propulsion devices for aircraft. The research on combined heat and mass transfer with chemical reaction and thermophoresis

effect can help in food processing, cooling towers, chemically reactive vapor deposition boundary layers in optical materials processing, catalytic combustion boundary layers, chemical diffusion in disk electrode modeling and carbon monoxide reactions in metallurgical mass transfer and kinetics [110].

There is a lot of work that has been done on simultaneous heat and mass transfer with chemical reaction in non-Newtonian fluid flow. Ganapathirao *et al.* [111] studied the effects of chemical reaction, heat and mass transfer on an unsteady mixed convection, boundary layer flow over a wedge with heat generation in the presence of suction or injection. Vajravelu *et al.* [112] studied the diffusion of a chemically reactive species of a power-law fluid past a stretching surface. Postelnicu [113] presented influence of chemical reaction on heat and mass transfer by natural convection from vertical surfaces in porous media considering Soret and Dufour effects.

The combined heat and mass transfer problems with chemical reaction in non-Newtonian fluids are of importance in many processes and have, therefore, received a considerable amount of attention in recent years. The effects of heat and mass transfer on non-Newtonian fluid flow with chemical reactions are of significant in chemical technology and hydrometallurgical industries. There are two types chemical reactions namely homogeneous gas-phase chemistry and heterogeneous surface chemistry. Chhabra [1] studied the heat and mass transfer in non-Newtonian fluid. EI-Sayed *et al.* [114] investigated the effects of chemical reaction, heat, and mass transfer of non-Newtonian fluid flow through porous medium in a vertical peristaltic tube. Srinivasacharya and Reddy [115] did a study on the effects of chemical reaction and radiation on the mixed convection heat and mass transfer over a vertical plate in power-law fluid saturated porous medium. Some of the work which has been done on heat and mass transfer in non-Newtonian fluids include the work by Gorla *et al.* [116], Xie *et al.* [117] and Sojoudi *et al.* [118].

The main objective of this work is to investigate the simultaneous heat and mass transfer in a non-Newtonian fluid past a vertical porous plate in the presence of thermal radiation and chemical reaction using the bivariate spectral quasi-linearization method. The main difference between this current study and the other previous study on the flow of the Jeffrey fluid, Prasad *et al.* [104] is the inclusion of both thermal radiation and chemical reaction terms in the model. Due to the flow behavior of non-Newtonian fluids, our current model constitutes some coupled highly non-linear partial differential equations which are complex to handle. In this work, we choose the bivariate spectral quasi-linearization method which is a powerful and accurate numerical method in solving non-linear partial differential equations. The BSQLM was originally developed by Motsa *et al.* [38] as a method of solving higher order non-linear evolution partial differential equations. They used the method to solve several non-linear equations such as the Fisher's equation, Burgers-Huxley equation and the Fitzhug-Nagumo equation. The results obtained were compared with respective known analytical solutions and confirmed that the BSQLM is highly accurate, convergent and effective. Oyelakin *et al.* [119] used the BSQLM to investigate unsteady mixed convection in nanofluid flow through a porous medium with thermal radiation. Also, Muzara *et al.* [120] successfully solved the highly non-liner two-dimensional Bratu problem using the BSQLM.

5.2 Problem statement and mathematical formulation

In this study, we consider the laminar boundary layer flow of a Jeffrey fluid past a vertical porous plate in the presence of thermal radiation and chemical reaction. The x^*-axis is measured along the plate in the upward direction and the y^*-axis is measured normal to the plate in the outward direction. Initially, the surface of the plate and the Jeffrey fluid are at rest at a uniform temperature T^*_∞ and concentration C^*_∞, respectively. Instantaneously, the temperature and the concentration are raised to values $T^*_w(> T^*_\infty)$ and $C^*_w(> C^*_\infty)$, respectively. The geometry of the problem is shown in Figure (4.1). The stress tensor for the Jeffrey fluid is given by Devakar *et al.* [121]

$$\tau = -p\mathbf{I} + \frac{\mu}{1+\lambda_1}\left[\nabla V + (\nabla V)^T + \lambda_2 \frac{d}{dt}(\nabla V + (\nabla V)^T)\right],$$

where p is the pressure, $\mathbf{I}$ is the identity matrix and V is the velocity vector.

After incorporating the Jeffrey fluid stress tensor in the momentum equation, the model is given by

$$\frac{\partial u^*}{\partial x^*} + \frac{\partial v^*}{\partial y^*} = 0, \tag{5.2.1}$$

$$u^*\frac{\partial u^*}{\partial x^*} + v^*\frac{\partial u^*}{\partial y^*} = \frac{\nu}{1+\lambda_1}\left[\frac{\partial^2 u^*}{\partial y^{*2}}\right] + g\beta_T(T^* - T^*_\infty) + g\beta_c(C^* - C^*_\infty) \\ \frac{\nu\lambda_2}{1+\lambda_1}\left(u^*\frac{\partial^3 u^*}{\partial x^*\partial y^{*2}} + \frac{\partial u^*}{\partial y^*}\frac{\partial^2 u^*}{\partial x^*\partial y^*} - \frac{\partial u^*}{\partial x^*}\frac{\partial^2 u^*}{\partial y^{*2}} + v^*\frac{\partial^3 u^*}{\partial y^{*3}}\right), \tag{5.2.2}$$

$$u^*\frac{\partial T^*}{\partial x^*} + v^*\frac{\partial T^*}{\partial y^*} = \alpha\frac{\partial^2 T^*}{\partial y^{*2}} - \frac{\partial q_r}{\partial y^*}, \tag{5.2.3}$$

$$u^*\frac{\partial C^*}{\partial x^*} + v^*\frac{\partial C^*}{\partial y^*} = D_m\frac{\partial^2 C^*}{\partial y^{*2}} - k_r(C^* - C^*_\infty), \tag{5.2.4}$$

where (u^*, v^*) are the velocities along (x^*, y^*) directions respectively. λ_1 is the ratio of relaxation to retardation times, λ_2 is the retardation time, T^* is the fluid temperature, C^* is the fluid concentration, D_m is mass diffusivity, k_r is the chemical reaction rate constant, ν is kinematic viscosity, q_r is the radiative heat flux, ρ is fluid density. Also g, β_T, β_C, α are gravitational acceleration, thermal expansion coefficient, solutal expansion coefficient, and thermal diffusivity, respectively. Under the Rosseland approximation, the radiative heat flux q_r has the form, El-Aziz and Yahya [122]

$$q^*_r = -\frac{4\sigma^*}{3k^*}\frac{\partial T^{*4}}{\partial y^*}, \tag{5.2.5}$$

where σ^* is the Stefan-Boltzmann constant and k^* is the mean absorption coefficient. Assuming that the temperature differences within the Jeffrey fluid flow are sufficiently small, applying linear Taylor's series expansion of T^{*4} about T^*_∞ gives

$$T^{*4} \simeq 4T^{*3}_\infty T^* - 3T^{*4}_\infty. \tag{5.2.6}$$

From Eqn (5.2.6), we have

$$\frac{\partial q_r^*}{\partial y^*} = -\frac{16\sigma^* T_\infty^{*3}}{3k^*}\frac{\partial^2 T^*}{\partial y^{*2}}, \tag{5.2.7}$$

which reduces Eqn (5.2.4) to the form

$$u^*\frac{\partial T^*}{\partial x^*} + v^*\frac{\partial T^*}{\partial y^*} = \alpha\frac{\partial^2 T^*}{\partial y^{*2}} + \frac{16\sigma^* T_\infty^{*3}}{3k^*}\frac{\partial^2 T^*}{\partial y^{*2}}. \tag{5.2.8}$$

The boundary conditions for the temperature, concentration and velocity are given by:

$$u^* = 0,\ v^* = 0,\ T^* = T_w^*,\ C^* = C_w^* \quad at\ y^* = 0, \tag{5.2.9}$$

$$u^* \to 0,\ \frac{\partial u^*}{\partial y^*} \to 0,\ C^* \to C_\infty^*,\ T^* \to T_\infty^* \text{ as } y^* \to \infty. \tag{5.2.10}$$

5.3 Similarity transformations

To transform the system of Eqns (5.2.1)- (5.2.4) into a dimensionless one, we introduce a stream function ψ such that $u^* = \frac{\partial \psi}{\partial y}$ and $v^* = -\frac{\partial \psi}{\partial x}$. The continuity Eqn (5.2.1) is automatically satisfied. Now, we define the following dimensionless variables [123]:

$$\begin{aligned} \xi &= \left(\frac{x^*}{L}\right)^{1/2},\ \eta = C_1 y x^{*-1/4},\ C_1 = \frac{g\beta(T_w^* - T_\infty^*)}{4\nu^2},\ \psi = 4\nu C_1 x^{*3/4} f,\ Pr = \frac{\nu}{\alpha},\ Sc = \frac{\nu}{D_m}, \\ \theta(\xi,\eta) &= \frac{T^* - T_\infty^*}{T_w^* - T_\infty^*},\ \phi(\xi,\eta) = \frac{C^* - C_\infty^*}{C_w^* - C_\infty^*},\ Gr_x = \frac{g\beta(T_w^* - T_\infty^*)L^3}{\nu^2},\ De = \frac{\lambda_1 \nu C_1^2}{x^{*1/2}}. \end{aligned} \tag{5.3.11}$$

The similarity transformations defined in Eqn (5.3.11) when applied to the momentum, energy and concentration equations yield

$$\begin{aligned} &\frac{1}{1+\lambda}\frac{\partial^3 f}{\partial \eta^3} + 3f\frac{\partial^2 f}{\partial \eta^2} - 2\left(\frac{\partial f}{\partial \eta}\right)^2 + \frac{De}{1+\lambda}\left[\left(\frac{\partial^2 f}{\partial \eta^2}\right)^2 - 2\frac{\partial f}{\partial \eta}\frac{\partial^3 f}{\partial \eta^3} - 3f\frac{\partial^4 f}{\partial \eta^4}\right] + \theta + K\phi \\ &= 2\xi\left[\frac{\partial f}{\partial \eta}\frac{\partial^2 f}{\partial \eta \partial \xi} - \frac{\partial^2 f}{\partial \eta^2}\frac{\partial f}{\partial \xi} - \frac{De}{1+\lambda}\left(\frac{\partial f}{\partial \eta}\frac{\partial^4 f}{\partial \eta^3 \partial \xi} + \frac{\partial^2 f}{\partial \eta^2}\frac{\partial^3 f}{\partial \eta^2 \partial \xi} - \frac{\partial^3 f}{\partial \eta^3}\frac{\partial^2 f}{\partial \eta \partial \xi} - \frac{\partial^4 f}{\partial \eta^4}\frac{\partial f}{\partial \xi}\right)\right], \end{aligned} \tag{5.3.12}$$

$$\left(\frac{1}{Pr} + \frac{4}{3Q}\right)\frac{\partial^2 \theta}{\partial \eta^2} + 3f\frac{\partial \theta}{\partial \eta} = 2\xi\left(\frac{\partial f}{\partial \eta}\frac{\partial \theta}{\partial \xi} - \frac{\partial \theta}{\partial \eta}\frac{\partial f}{\partial \xi}\right), \tag{5.3.13}$$

$$\frac{1}{Sc}\frac{\partial^2 \phi}{\partial \eta^2} + 3f\frac{\partial \phi}{\partial \eta} - \Delta\phi = 2\xi\left(\frac{\partial f}{\partial \eta}\frac{\partial \phi}{\partial \xi} - \frac{\partial \phi}{\partial \eta}\frac{\partial f}{\partial \xi}\right). \tag{5.3.14}$$

The dimensionless boundary conditions takes the form

$$f(0,\xi)=0,\ \ \frac{\partial f}{\partial \eta}(0,\xi)=0,\ \ \theta(0,\xi)=1,\ \ \phi(0,\xi)=1 \tag{5.3.15}$$

$$\frac{\partial f}{\partial \eta}(\infty,\xi)\to 0,\ \ \frac{\partial^2 f}{\partial \eta^2}(\infty,\xi)\to 0,\ \ \theta(\infty,\xi)\to 0,\ \ \phi(\infty,\xi)\to 0, \tag{5.3.16}$$

where $\Delta=\dfrac{k_r x^{\frac{1}{2}}}{\nu B^2}$ is a chemical reaction parameter, $Q=\dfrac{\nu k^*}{4T_\infty^3\sigma^*}$ is the radiation parameter and $K=\dfrac{\beta^*(C_w^*-C_\infty^*)}{\beta(T_w^*-T_\infty^*)}$ is the concentration to thermal buoyancy ratio parameter.

The engineering design quantities of physical interest to be discussed in this work are the skin-friction coeeffi-cient (C_f) which is a measure of shear stress at the plate, the Nusselt number (Nu) which is a measure of the rate of heat transfer and the Sherwood number (Sh) which measures the rate of mass transfer at the plate. These quantities are given by:

$$\begin{aligned} C_f &= \left(\frac{\partial u}{\partial y}\right)_{y=0} = 4\nu\mu C_1^3 x^{\frac{1}{4}} f''(\xi,0),\\ Nu &= -\frac{k\Delta T}{(T_w-T_\infty)}\left(\frac{\partial T}{\partial y}\right)_{y=0} = -k\Delta T C_1 x^{-\frac{1}{4}}\theta'(\xi,0),\\ Sh &= -\frac{D_m\Delta C}{(C_w-C_\infty)}\left(\frac{\partial C}{\partial y}\right)_{y=0} = -D_m\Delta C C_1 x^{-\frac{1}{4}}\phi'(\xi,0). \end{aligned}$$

5.4 Method of solution

5.4.1 Quasi-linearization

Eqns (5.3.12)- (5.3.14) form a coupled system of non-linear partial differential equations which we denote by

$$\Gamma_s[\varsigma^1,\varsigma^2,\varsigma^3]=0,\ \ s=1,2,3, \tag{5.4.17}$$

where the non-linear operators Γ_1, Γ_2 and Γ_3 denote Eqns (5.3.12), (5.3.13) and (5.3.14), respectively. We also define

$$\varsigma^1=\left[f,\frac{\partial f}{\partial\eta},\frac{\partial^2 f}{\partial\eta^2},\frac{\partial^3 f}{\partial\eta^3},\frac{\partial^4 f}{\partial\eta^4},\frac{\partial f}{\partial\xi},\frac{\partial^2 f}{\partial\eta\partial\xi},\frac{\partial^3 f}{\partial\eta^2\partial\xi},\frac{\partial^4 f}{\partial\eta^3\partial\eta}\right],$$

$$\varsigma^2=\left[\theta,\frac{\partial\theta}{\partial\eta},\frac{\partial^2\theta}{\partial\eta^2},\frac{\partial\theta}{\partial\xi}\right]\ \text{and}\ \varsigma^3=\left[\phi,\frac{\partial\phi}{\partial\eta},\frac{\partial^2\phi}{\partial\eta^2},\frac{\partial\phi}{\partial\xi}\right].$$

Let us assume that the difference between the solution of Eqn (5.4.17) at the current iteration level $\Gamma_s[\varsigma_{r+1}^1, \varsigma_{r+1}^2, \varsigma_{r+1}^3]$ and some previous level $\Gamma_s[\varsigma_r^1, \varsigma_r^2, \varsigma_r^3]$ is sufficiently small. Expanding Eqn (5.4.17) in Taylor series, upon ignoring higher order terms gives

$$\Gamma_s[\varsigma^1, \varsigma^2, \varsigma^3] \approx \Gamma_s[\varsigma_r^1, \varsigma_r^2, \varsigma_r^3] + (\varsigma_{r+1}^1 - \varsigma_r^1, \varsigma_{r+1}^2 - \varsigma_r^2, \varsigma_{r+1}^3 - \varsigma_r^3) \cdot \nabla\Gamma_s[\varsigma_r^1, \varsigma_r^2, \varsigma_r^3], \tag{5.4.18}$$

where $\nabla = (\nabla_{\varsigma^1}, \nabla_{\varsigma^2}, \nabla_{\varsigma^1})$ is a vector of partial differential operators defined by

$$\begin{aligned}
\nabla_{\varsigma^1} &= \left[\frac{\partial}{\partial f}, \frac{\partial}{\partial f'}, \frac{\partial}{\partial f''}, \frac{\partial}{\partial f'''}, \frac{\partial}{\partial f^{iv}}, \frac{\partial}{\partial f_\xi}, \frac{\partial}{\partial f'_\xi}, \frac{\partial}{\partial f''_\xi}, \frac{\partial}{\partial f'''_\xi}\right], \\
\nabla_{\varsigma^2} &= \left[\frac{\partial}{\partial \theta}, \frac{\partial}{\partial \theta'}, \frac{\partial}{\partial \theta''}, \frac{\partial}{\partial \theta_\xi}\right], \\
\nabla_{\varsigma^3} &= \left[\frac{\partial}{\partial \phi}, \frac{\partial}{\partial \phi'}, \frac{\partial}{\partial \phi''}, \frac{\partial}{\partial \phi_\xi}\right].
\end{aligned}$$

Also, expanding Eqn (5.4.18) and re-arranging terms yields the quasi-linearization formula

$$\begin{aligned}
&\varsigma_{r+1}^1 \cdot \nabla\Gamma_s[\varsigma_r^1, \varsigma_r^2, \varsigma_r^3] + \varsigma_{r+1}^2 \cdot \nabla\Gamma_s[\varsigma_r^1, \varsigma_r^2, \varsigma_r^3] + \varsigma_{r+1}^3 \cdot \nabla\Gamma_s[\varsigma_r^1, \varsigma_r^2, \varsigma_r^3] \\
= \;& \varsigma_r^1 \cdot \nabla\Gamma_s[\varsigma_r^1, \varsigma_r^2, \varsigma_r^3] - \varsigma_r^1 \cdot \nabla\Gamma_s[\varsigma_r^1, \varsigma_r^2, \varsigma_r^3] - \varsigma_r^1 \cdot \nabla\Gamma_s[\varsigma_r^1, \varsigma_r^2, \varsigma_r^3] - \Gamma_s[\varsigma_r^1, \varsigma_r^2, \varsigma_r^3].
\end{aligned} \tag{5.4.19}$$

Applying the quasi-linearization formula (5.4.19) onto the coupled system Eqns (5.3.12)-(5.3.14) gives:

$$\begin{aligned}
a_{0,r}\frac{\partial^4 f_{r+1}}{\partial \eta^4} &+ a_{1,r}\frac{\partial^3 f_{r+1}}{\partial \eta^3} + a_{2,r}\frac{\partial^2 f_{r+1}}{\partial \eta^2} + a_{3,r}\frac{\partial f_{r+1}}{\partial \eta} + a_{4,r} f_{r+1} + a_{5,r}\theta_{r+1} + a_{6,r}\phi_{r+1} \\
&+ a_{7,r}\frac{\partial^4 f_{r+1}}{\partial \eta^3 \partial \xi} + a_{8,r}\frac{\partial^3 f_{r+1}}{\partial \eta^2 \partial \xi} + a_{9,r}\frac{\partial^2 f_{r+1}}{\partial \eta \partial \xi} + a_{10,r}\frac{\partial f_{r+1}}{\partial \xi} = R_{1,r},
\end{aligned} \tag{5.4.20}$$

$$b_{0,r}\frac{\partial^2 \theta_{r+1}}{\partial \eta^2} + b_{1,r}\frac{\partial \theta_{r+1}}{\partial \eta} + b_{2,r}\frac{\partial f_{r+1}}{\partial \eta} + b_{3,r} f_{r+1} + b_{4,r}\frac{\partial f_{r+1}}{\partial \xi} + b_{5,r}\frac{\partial \theta_{r+1}}{\partial \xi} = R_{2,r}, \tag{5.4.21}$$

$$c_{0,r}\frac{\partial^2 \phi_{r+1}}{\partial \eta^2} + c_{1,r}\frac{\partial \phi_{r+1}}{\partial \eta} + c_{2,r}\phi_{r+1} + c_{3,r}\frac{\partial f_{r+1}}{\partial \eta} + c_{4,r} f_{r+1} + c_{5,r}\frac{\partial f_{r+1}}{\partial \xi} + c_{6,r}\frac{\partial \phi_{r+1}}{\partial \xi} = R_{3,r}, \tag{5.4.22}$$

where the variable coefficients obtained from the previous iteration are given by

$$\begin{aligned}
a_{0,r} &= -3\frac{De}{1+\lambda}f_r - 2\xi\frac{\partial f_r}{\partial \xi},\ a_{1,r} = \frac{1}{1+\lambda}\left(1 - 2De\frac{\partial f_r}{\partial \eta} - 2\xi De\frac{\partial^2 f_r}{\partial \eta \partial \xi}\right),\\
a_{2,r} &= 2\frac{De}{1+\lambda}\left(\frac{\partial^2 f}{\partial \eta^2} + \xi\frac{\partial^3 f_r}{\partial \eta^2 \partial \xi}\right) + 2\xi\frac{\partial f_r}{\partial \xi} + 3f_r,\\
a_{3,r} &= -4\frac{\partial f_r}{\partial \eta} - 2\xi\frac{\partial^2 f_r}{\partial \eta \partial \xi} - 2\frac{De}{1+\lambda}\frac{\partial^3 f_r}{\partial \eta^3} + 2\xi\frac{De}{1+\lambda}\frac{\partial^3 f_r}{\partial \eta^2 \partial \xi},\ a_{4,r} = 3\frac{\partial^2 f_r}{\partial \eta^2} - 3\frac{De}{1+\lambda}\frac{\partial^4 f_r}{\partial \eta^4},\\
a_{5,r} &= 1,\ a_{6,r} = K,\ a_{7,r} = 2\xi\frac{De}{1+\lambda}\frac{\partial f_r}{\partial \eta},\ a_{8,r} = 2\xi\frac{De}{1+\lambda}\frac{\partial^2 f_r}{\partial \eta^2},\ a_{9,r} = -2\xi\left(\frac{\partial f_r}{\partial \eta} + \frac{De}{1+\lambda}\frac{\partial^3 f_r}{\partial \eta^3}\right),\\
a_{10,r} &= 2\xi\frac{\partial^2 f_r}{\partial \eta^2} - 2\xi\frac{\partial^4 f_r}{\partial \eta^4},\ b_{0,r} = \frac{1}{Pr} + \frac{4}{3F},\ b_{1,r} = 3f_r + 2\xi\frac{\partial f_r}{\partial \xi},\ b_{2,r} = -2\xi\frac{\partial \theta_r}{\partial \xi},\ b_{3,r} = 3\frac{\partial \theta_r}{\partial \eta},\\
b_{4,r} &= 2\xi\frac{\partial \theta_r}{\partial \eta},\ b_{5,r} = -2\xi\frac{\partial f_r}{\partial \eta},\ c_{0,r} = \frac{1}{Sc},\ c_{1,r} = 3f_r + 2\xi\frac{\partial f_r}{\partial \xi},\ c_{2,r} = -\Delta,\ c_{3,r} = -2\xi\frac{\partial \phi_r}{\partial \xi},\\
c_{4,r} &= 3\frac{\partial \phi}{\partial \eta},\ c_{5,r} = 2\xi\frac{\partial \phi_r}{\partial \eta},\ c_{6,r} = -2\xi\frac{\partial f_r}{\partial \eta}.
\end{aligned}$$

The terms on the right side, also calculated from the previous iteration, are given by

$$\begin{aligned}
R_{1,r} &= \frac{De}{1+\lambda}\left(2\xi\frac{\partial^2 f_r}{\partial \eta^2}\frac{\partial^3 f_r}{\partial \eta^2 \partial \xi} - 2\xi\frac{\partial^3 f_r}{\partial \eta^3}\frac{\partial^2 f_r}{\partial \eta \partial \xi} + \left(\frac{\partial f_r}{\partial \eta}\right)^2 - 2\frac{\partial f_r}{\partial \eta}\frac{\partial^3 f_r}{\partial \eta^3} - 3f_r\frac{\partial^4 f_r}{\partial \eta^4} - 2\xi\frac{\partial^4 f_r}{\partial \eta^4}\frac{\partial f_r}{\partial \xi}\right)\\
&+ 3f_r\frac{\partial^2 f_r}{\partial \eta^2} - 2\left(\frac{\partial f_r}{\partial \eta}\right)^2,\\
R_{2,r} &= 3f_r\frac{\partial \theta_r}{\partial \eta} - 2\xi\frac{\partial f_r}{\partial \eta}\frac{\partial \theta_r}{\partial \xi} + 2\xi\frac{\partial \theta_r}{\partial \eta}\frac{\partial f_r}{\partial \xi},\\
R_{3,r} &= 3f_r\frac{\partial \phi_r}{\partial \eta} - 2\xi\frac{\partial f_r}{\partial \eta}\frac{\partial \phi_r}{\partial \xi} + 2\xi\frac{\partial \phi_r}{\partial \eta}\frac{\partial f_r}{\partial \xi}.
\end{aligned}$$

5.4.2 Chebyshev differentiation and bivariate interpolation

In this article, we consider approximating functions of the form

$$\begin{aligned}
f(\eta,\xi) &\approx \sum_{j=0}^{N_\eta}\sum_{i=0}^{N_\xi} f(x_j,y_i)\mathcal{L}_j(x)\mathcal{L}_i(y),\\
\theta(\eta,\xi) &\approx \sum_{j=0}^{N_\eta}\sum_{i=0}^{N_\xi} \theta(x_j,y_i)\mathcal{L}_j(x)\mathcal{L}_i(y),\\
\phi(\eta,\xi) &\approx \sum_{j=0}^{N_\eta}\sum_{i=0}^{N_\xi} \phi(x_j,y_i)\mathcal{L}_j(x)\mathcal{L}_i(y),
\end{aligned}$$

where the usual characteristic Lagrange polynomials are defined as

$$\mathcal{L}_j(\eta) = \prod_{\substack{k=0 \\ k\neq j}}^{N_\eta} \frac{\eta - \eta_k}{\eta_j - \eta_k}, \quad \mathcal{L}_i(\xi) = \prod_{\substack{k=0 \\ k\neq i}}^{N_\xi} \frac{\xi - \xi_k}{\xi_i - \xi_k}. \tag{5.4.23}$$

In order to apply the spectral collocation method, it is convenient to transform the physical domains $[0, L_\infty]$ and $[0, 1]$ in the η and ξ directions to the computational domain $[-1, 1]$ using the linear transformations $\eta = \frac{L_\infty}{2}(1+x)$ and $\xi = \frac{1}{2}(1 + y)$, respectively. Approximating the derivatives of the approximating functions at the Chebyshev-Gauss-Lobatto collocation points [124],

$$\{x_j\} = \left\{ \cos\left(\frac{\pi j}{N_\eta}\right) \right\}_{j=0}^{N_\eta}, \quad \{y_i\} = \left\{ \cos\left(\frac{\pi i}{N_\xi}\right) \right\}_{i=0}^{N_\xi}, \quad j = 0, 1, \cdots, N_\eta, \quad i = 0, 1, \cdots, N_\xi, \tag{5.4.24}$$

gives

$$\begin{aligned} \left.\frac{\partial f}{\partial \eta}\right|_{(x_j, y_i)} &\approx \sum_{p=0}^{N_\eta} \sum_{q=0}^{N_\xi} f(x_p, y_q) \frac{d\mathcal{L}_p(x_j)}{d\eta} \mathcal{L}_q(y_i) = \frac{2}{L_\infty} \sum_{p=0}^{N_\eta} f(x_p, y_i) \frac{d\mathcal{L}_p(x_j)}{dx} \\ &= \frac{2}{L_\infty} \sum_{p=0}^{N_\eta} D_{jp} f(x_p, y_i) = \mathbf{DF}_i, \quad i = 0, 1, 2, \cdots, N_\eta, \end{aligned}$$

where $\mathbf{D} = (\frac{2}{L_\infty})D$, D is the Chebyshev differentiation matrix of order $(N_\eta + 1) \times (N_\eta + 1)$ [59]. Similarly,

$$\left.\frac{\partial f}{\partial \xi}\right|_{(x_j, y_i)} \approx 2 \sum_{q=0}^{N_\xi} d_{iq} \mathbf{F}_q \quad \text{and} \quad \left.\frac{\partial^2 f}{\partial \eta \partial \xi}\right|_{(x_j, y_i)} = 2 \sum_{q=0}^{N_\xi} d_{iq} \mathbf{DF}_q,$$

where d_{iq} are the entries of the standard $(N_\xi + 1) \times (N_\xi + 1)$ Chebyshev differentiation matrices and

$$\mathbf{F}_i = [f(x_0, y_i), (x_1, y_i), \cdots, f(x_{N_\eta - 1, y_i}), f(x_{N_\eta}, y_i)]^T.$$

Higher order derivatives are given by the formulas

$$\left.\frac{\partial^n f}{\partial \eta^n}\right|_{(x_j, y_i)} \approx \left(\frac{2}{L_\infty}\right)^n \sum_{p=0}^{N_\eta} D_{jp}^n f(x_p, y_i) \quad \text{and} \quad \left.\frac{\partial^n f}{\partial \xi^n}\right|_{(x_j, y_i)} \approx 2^n \sum_{p=0}^{N_\eta} d_{iq}^n f(x_p, y_q).$$

Derivatives of $\theta(\eta,\xi)$ and $\phi(\eta,\xi)$ with respect to η and ξ are defined in a similar fashion. Applying spectral collocation to Eqns (5.4.20), (5.4.21) and (5.4.22) we get

$$[\mathbf{a}_{0,r}\mathbf{D}^4+\mathbf{a}_{1,r}\mathbf{D}^3+\mathbf{a}_{2,r}\mathbf{D}^2+\mathbf{a}_{3,r}\mathbf{D}+\mathbf{a}_{4,r}]\mathbf{F}_{r+1,i}+\mathbf{a}_{5,r}\boldsymbol{\theta}_{r+1,i}+\mathbf{a}_{6,r}\boldsymbol{\phi}_{r+1,i}$$
$$+\sum_{q=0}^{N_\xi}[\mathbf{a}_{7,r}\mathbf{D}^3+\mathbf{a}_{8,r}\mathbf{D}^2+\mathbf{a}_{9,r}\mathbf{D}+\mathbf{a}_{10,r}]d_{iq}\mathbf{F}_{r+1,q}=\mathbf{R}_{1,r}, \tag{5.4.25}$$

$$[\mathbf{b}_{0,r}\mathbf{D^2}+\mathbf{b}_{1,r}\mathbf{D}]\boldsymbol{\theta}_{r+1,i}+[\mathbf{b}_{2,r}\mathbf{D}+\mathbf{b}_{3,r}]\mathbf{F}_{r+1,i}+\mathbf{b}_{4,r}\sum_{q=0}^{N_\xi}d_{iq}\mathbf{F}_{r+1,q}$$
$$+\mathbf{b}_{5,r}\sum_{q=0}^{N_\xi}d_{iq}\boldsymbol{\theta}_{r+1,q}=\mathbf{R}_{2,r}, \tag{5.4.26}$$

$$[\mathbf{c}_{0,r}\mathbf{D^2}+\mathbf{c_{1,r}}\mathbf{D}+\mathbf{c_{2,r}}]\boldsymbol{\phi}_{r+1,i}+[\mathbf{c}_{3,r}\mathbf{D}+\mathbf{c}_{4,r}]\mathbf{F}_{r+1,i}+\mathbf{c}_{5,r}\sum_{q=0}^{N_\xi}d_{iq}\mathbf{F}_{r+1,q}$$
$$+\mathbf{c}_{6,r}\sum_{q=0}^{N_\xi}d_{iq}\boldsymbol{\phi}_{r+1,q}=\mathbf{R}_{3,r}. \tag{5.4.27}$$

The system of Eqs (5.4.25)-(5.4.27) can be written in vector matrix form as

$$\begin{bmatrix}\mathbf{A}_{0,0} & \mathbf{A}_{0,1} & \cdots & \mathbf{A}_{0,N_{\xi-1}} & \mathbf{A}_{0,N_\xi}\\ \mathbf{A}_{1,0} & \mathbf{A}_{1,1} & \cdots & \mathbf{A}_{1,N_{\xi-1}} & \mathbf{A}_{1,N_\xi}\\ \vdots & \vdots & \ddots & \vdots & \vdots\\ \mathbf{A}_{N_{\eta-1},0} & \mathbf{A}_{N_{\eta-1},1} & \cdots & \mathbf{A}_{N_{\eta-1},N_{\xi-1}} & \mathbf{A}_{N_{\eta-1},N_\xi}\\ \mathbf{A}_{N_\eta,0} & \mathbf{A}_{N_\eta,1} & \cdots & \mathbf{A}_{N_\eta,N_{\xi-1}} & \mathbf{A}_{N_\eta,N_\xi}\end{bmatrix}\begin{bmatrix}\boldsymbol{\Theta}_{r+1,0}\\ \boldsymbol{\Theta}_{r+1,1}\\ \vdots\\ \boldsymbol{\Theta}_{r+1,N_\eta-1}\\ \boldsymbol{\Theta}_{r+1,N_\eta}\end{bmatrix}=\begin{bmatrix}\mathbf{R}_r^{(0)}\\ \mathbf{R}_r^{(1)}\\ \vdots\\ \mathbf{R}_r^{(N_\xi-1)}\\ \mathbf{R}_r^{(N_\xi)}\end{bmatrix} \tag{5.4.28}$$

where

$$\mathbf{A}_{i,i}=\begin{bmatrix}\mathbf{a}_{0,r}\mathbf{D}^4+\mathbf{a}_{1,r}\mathbf{D}^3+\mathbf{a}_{2,r}\mathbf{D}^2+\mathbf{a}_{3,r}\mathbf{D}+\mathbf{a}_{4,r} & \mathbf{a}_{5,r} & \mathbf{a}_{6,r}\\ +(\mathbf{a}_{7,r}\mathbf{D}^3+\mathbf{a}_{8,r}\mathbf{D}^2+\mathbf{a}_{9,r}\mathbf{D}+\mathbf{a}_{10,r})\mathbf{d}_{i,i} & & \\ \mathbf{b}_{2,r}\mathbf{D}+\mathbf{b}_{3,r}+\mathbf{b}_{4,r}\mathbf{d}_{i,i} & \mathbf{b}_{0,r}\mathbf{D}^2+\mathbf{b}_{1,r}\mathbf{D}+\mathbf{b}_{5,r}d_{i,i} & \mathbf{0}\\ \mathbf{c}_{3,r}\mathbf{D}+\mathbf{c}_{4,r}+\mathbf{c}_{5,r}d_{i,i} & \mathbf{0} & \mathbf{c}_{0,r}\mathbf{D}^2+\mathbf{c}_{1,r}\mathbf{D}\\ & & +\mathbf{c}_{2,r}+\mathbf{c}_{6,r}\mathbf{d}_{i,i}\end{bmatrix},$$

$$\mathbf{A}_{i,j} = \begin{bmatrix} (\mathbf{a}_{7,r}\mathbf{D}^3 + \mathbf{a}_{8,r}\mathbf{D}^2 + \mathbf{a}_{9,r}\mathbf{D} + \mathbf{a}_{10,r})\mathbf{d}_{i,j} & \mathbf{0} & \mathbf{0} \\ \mathbf{b}_{4,r}\mathbf{d}_{i,j} & \mathbf{b}_{5,r}\mathbf{d}_{i,j} & \mathbf{0} \\ \mathbf{c}_{5,r}\mathbf{d}_{i,j} & \mathbf{0} & \mathbf{c}_{6,r}\mathbf{d}_{i,j} \end{bmatrix},$$

$\mathbf{\Theta}_{r+1,0} = [\mathbf{F}_{r+1,0}, \boldsymbol{\theta}_{r+1,0}, \boldsymbol{\phi}_{r+1,0}]^T$, $\mathbf{R}_r^{(0)} = [\mathbf{R}_{1,r}^{(0)}, \mathbf{R}_{2,r}^{(0)}, \mathbf{R}_{3,r}^{(0)}]$ and $\mathbf{0}$ is a zero matrix of order $(N_\eta+1)\times(N_\eta+1)$. Solving the linear system of Eqns (5.4.28), after applying the appropriate boundary conditions gives the approximate solutions of $\mathbf{F}_{r+1}$, $\mathbf{G}_{r+1}$ and $\mathbf{H}_{r+1}$.

5.5 Results and discussions

The nonlinear partial differential equations in this study are solved using the BSQLM. We show the accuracy and convergence of the BSQLM solutions using the following respective approaches as in Oyelakin *et al.* [125]:

- use of infinity norms
- use of residual errors.

The infinity norms are defined as the differences between the successive approximate solutions iteration levels r and $r+1$

$$\text{Error}_f = \max_{0\leqslant i\leqslant N_\eta} ||\mathbf{F}_{r+1,i} - \mathbf{F}_{r,i}||_\infty,\ \text{Error}_\theta = \max_{0\leqslant i\leqslant N_\eta} ||\boldsymbol{\theta}_{r+1,i} - \boldsymbol{\theta}_{r,i}||_\infty,\ \text{Error}_\phi = \max_{0\leqslant i\leqslant N_\eta} ||\boldsymbol{\phi}_{r+1,i} - \boldsymbol{\phi}_{r,i}||_\infty,$$

The infinity norms of the residual errors are defined by

$$\begin{aligned} ||Res(f)||_\infty &= \Big|\Big|\frac{1}{1+\lambda}f''' + 3ff'' - 2(f')^2 + \frac{De}{1+\lambda}\Big[(f'')^2 - 2f'f''' - 3ff^{iv}\Big] + \theta + K\phi \\ &- 2\xi\Big[f'\frac{\partial f'}{\partial \xi} - f''\frac{\partial f}{\partial \xi} - \frac{De}{1+\lambda}\Big(f'\frac{\partial f'''}{\partial \xi} + f''\frac{\partial f''}{\partial \xi} - f'''\frac{\partial f'}{\partial \xi} - f^{iv}\frac{\partial f}{\partial \xi}\Big)\Big]\Big|\Big|_\infty, \\ ||Res(\theta)||_\infty &= ||\Big(\frac{1}{Pr} + \frac{4}{3F}\Big)\theta'' + 3f\theta' - 2\xi\Big(f'\frac{\partial \theta}{\partial \xi} - \theta'\frac{\partial f}{\partial \xi}\Big)||_\infty, \\ ||Res(\phi)||_\infty &= ||\frac{1}{Sc}\phi'' + 3f\phi' - \Delta\phi - 2\xi\Big(f'\frac{\partial \phi}{\partial \xi} - \phi'\frac{\partial f}{\partial \xi}\Big)||_\infty. \end{aligned}$$

For all the results discussed in this section, the number of collocation points used was $N_\eta = 60$ and $N_\xi = 10$ and the tolerance level was set to be $\epsilon = 10^{-7}$. The default parameters considered, unless otherwise specified, are $De = 0.1$, $Pr = 0.71$, $Sc = 0.6$, $K = 0.5$, $Q = 0.1$, $\Delta = 0.1$ and $\lambda = 0.2$.

Figure (5.1) shows that error norms decrease with the increasing number of iterations and converge after 5^{th}

iteration. Figure (5.2) shows that the residual errors of less than 10^{-4}, 10^{-7} and 10^{-8} for $f(\eta,\xi)$, $\theta(\eta,\xi)$ and $\phi(\eta,\xi)$, respectively, are achieved after 5 iterations. Figures (5.1) and (5.2) confirm the convergence and accuracy of the BSQLM solutions of the partial differential equations in this study.

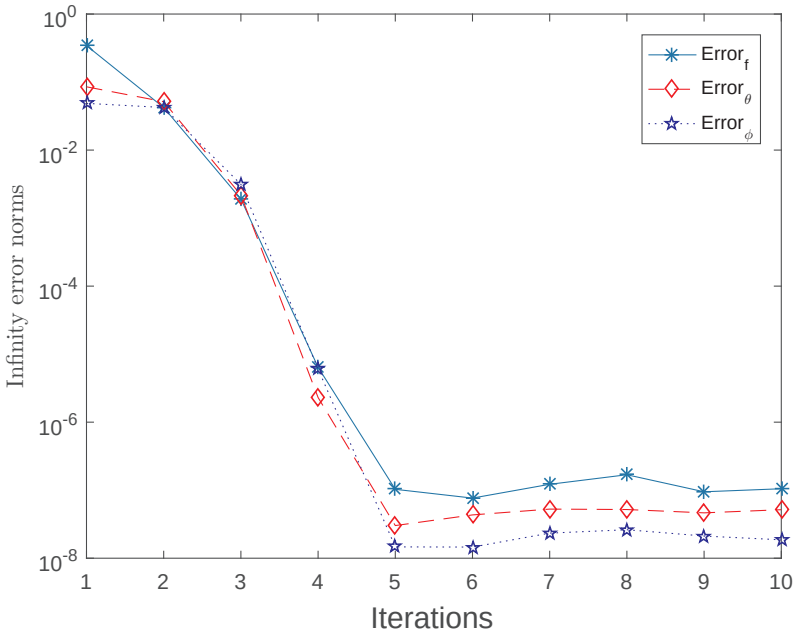

Figure 5.1: Convergence graphs for $f(\eta,\xi)$, $\theta(\eta,\xi)$ and $\phi(\eta,\xi)$.

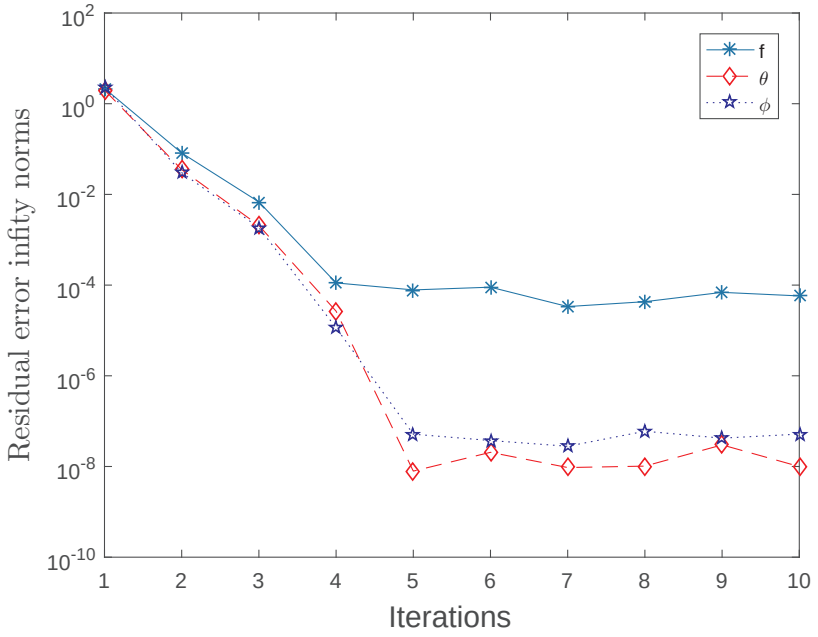

Figure 5.2: The residual error infinity norms of $f(\eta,\xi)$, $\theta(\eta,\xi)$ and $\phi(\eta,\xi)$.

When a fluid is deformed, the time it takes to return to its equilibrium state is called the relaxation time. Retardation time is the time required to balance the applied shear stress by the opposing force produced in the fluid due to the applied shear stress. Figures (5.3) - (5.5) show the influence of the ratio of relaxation to retardation times (λ) on the dimensionless velocity $(f'(\eta,\xi))$, temperature $(\theta(\eta,\xi))$ and concentration $(\phi(\eta,\xi))$ functions respectively. From the graphs presented, we note that velocity is increased significantly with an increase in λ. Both the fluid temperature and concentration are slightly depressed with an increase in the ratio of relaxation to retardation times.

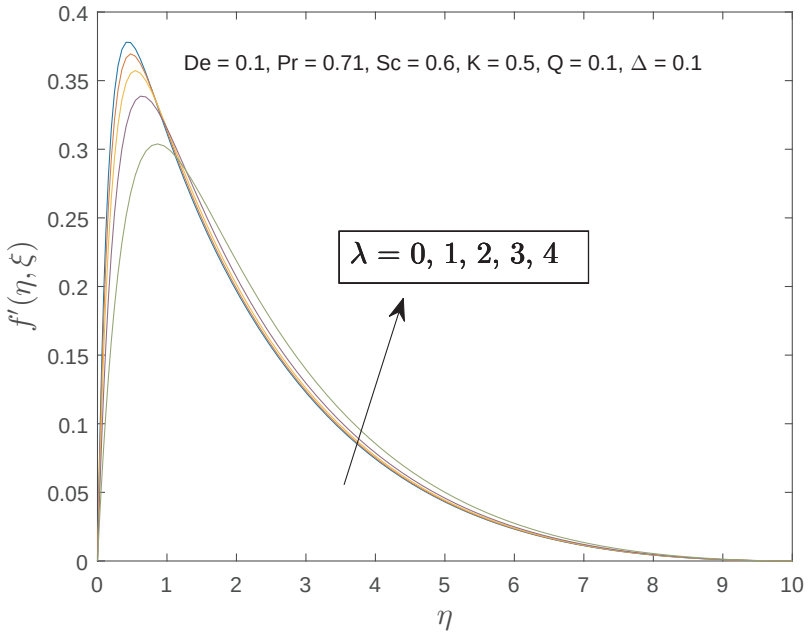

Figure 5.3: The effects of λ on the velocity profiles.

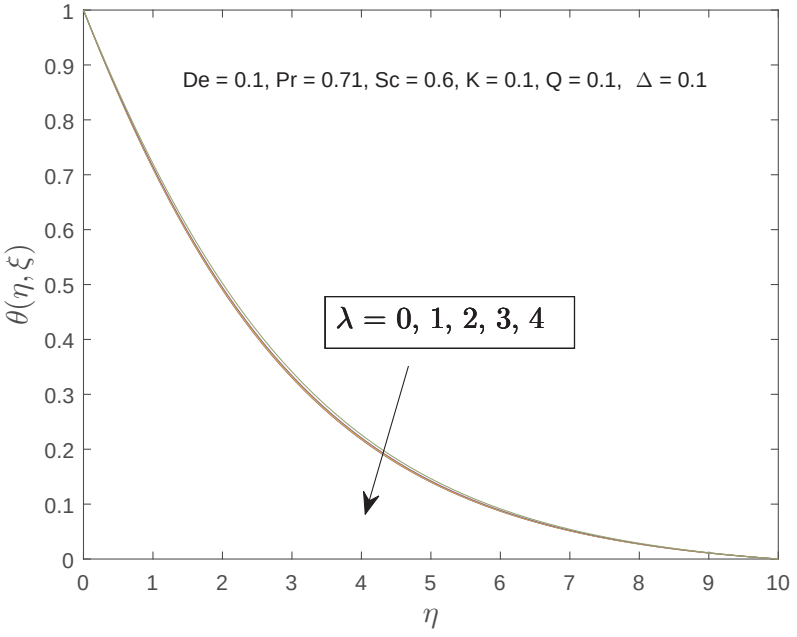

Figure 5.4: The effects of λ on the temperature profiles.

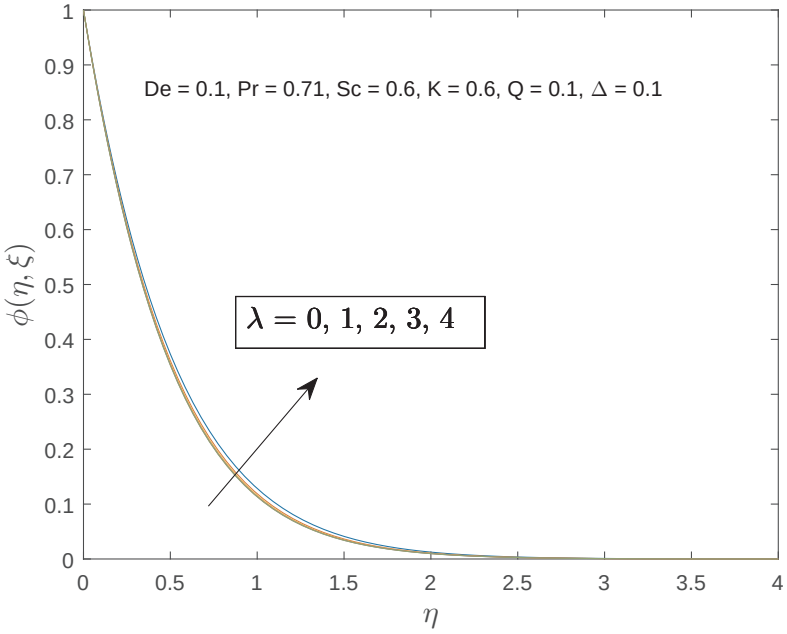

Figure 5.5: The effects of λ on the concentration profiles.

Figures (5.6)-(5.8) show the effects of the thermal radiation parameter Q on the velocity, temperature and concentration profiles of the Jeffrey fluid flowing past a vertical porous plate. The Jeffrey fluid is greatly accelerated with an increase in the thermal radiation parameter. Increasing the thermal radiation parameter produces significant increases in thermal conditions of the fluid temperature which cause more fluid in the boundary layer due to buoyancy effect, causing the velocity to increase. Figure (5.7) show that increasing the thermal radiation parameter decrease the fluid temperature. This is due to the fact that increasing the radiation parameter increases conduction effects of the fluid and hence higher surface heat flux which in turn will decrease the temperature of the fluid.

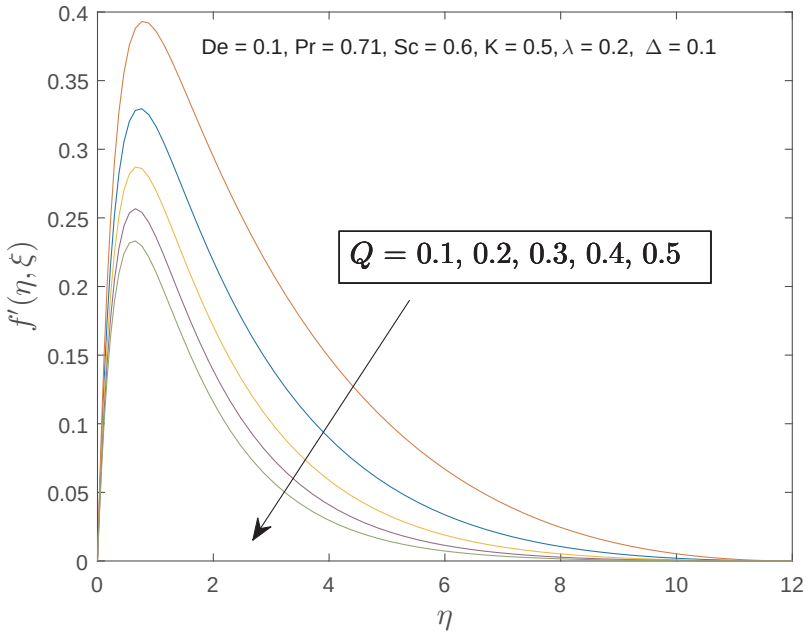

Figure 5.6: The effects of Q on the velocity profiles.

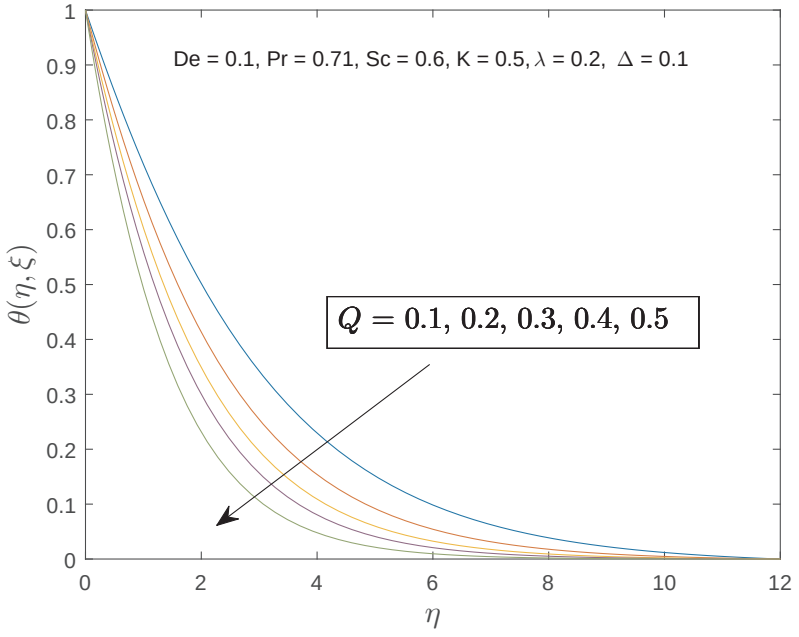

Figure 5.7: The effects of Q on the temperature profiles.

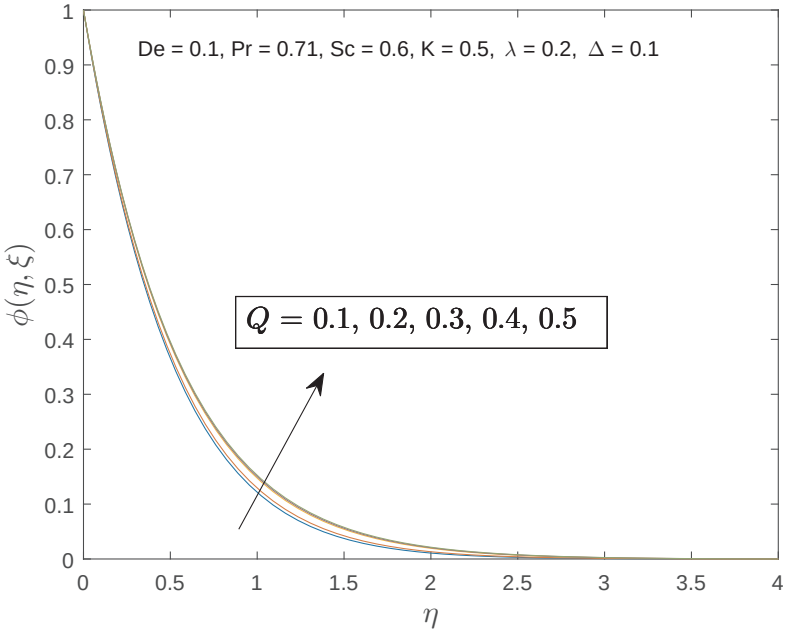

Figure 5.8: The effects of Q on the concentration profiles.

The effects of the Prandtl number on the velocity, temperature and concentration functions are shown in Figures (5.9) - (5.11), respectively. The velocity and temperature profiles are both decreased with an increase in the Prandtl number. On the other hand, the concentration of the Jeffrey fluid is slightly increased with an increase in the Prandtl number.

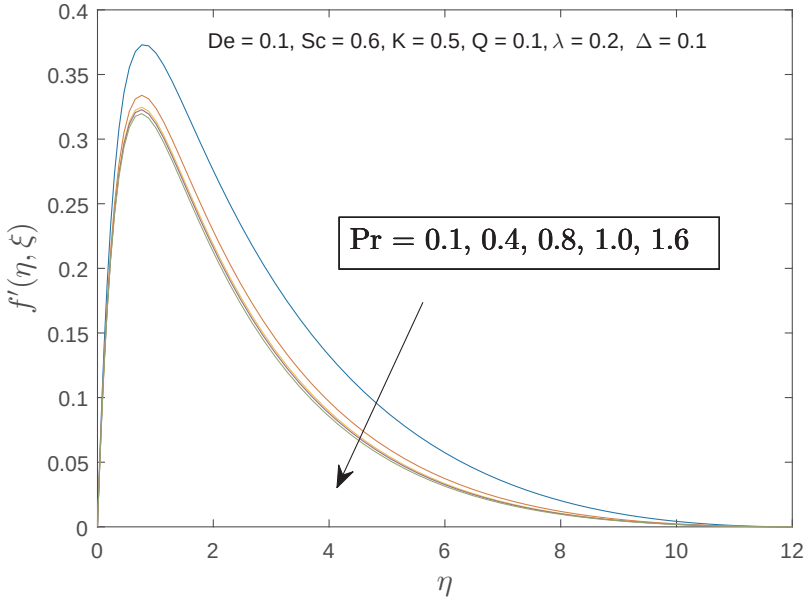

Figure 5.9: The effects of Pr on the velocity profiles.

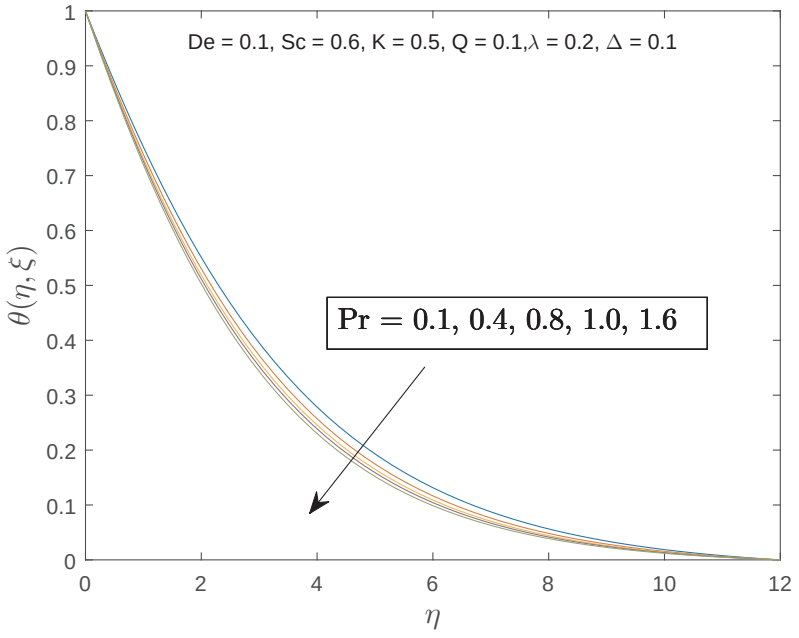

Figure 5.10: The effects of Pr on the temperature profiles.

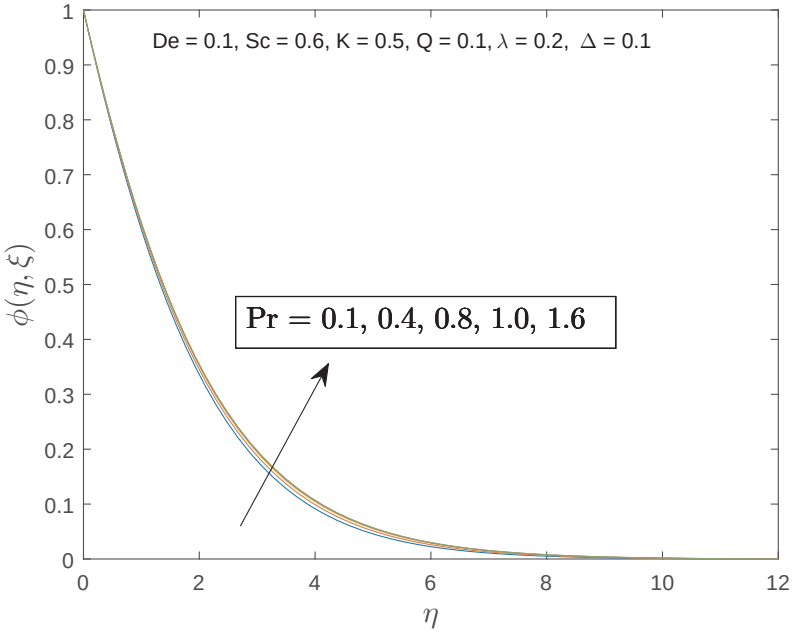

Figure 5.11: The effects of Pr on the concentration profiles.

Figures (5.12) - (5.14) show that increasing the Debora number has the effect of decelerating the Jeffrey fluid flow whilst the fluid temperature and concentration are slightly increased.

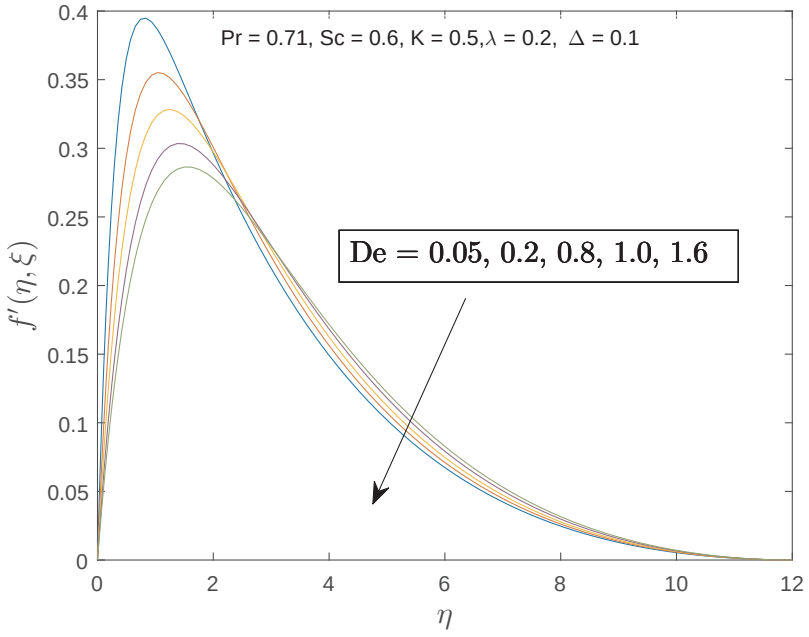

Figure 5.12: The effects of De on the velocity profiles.

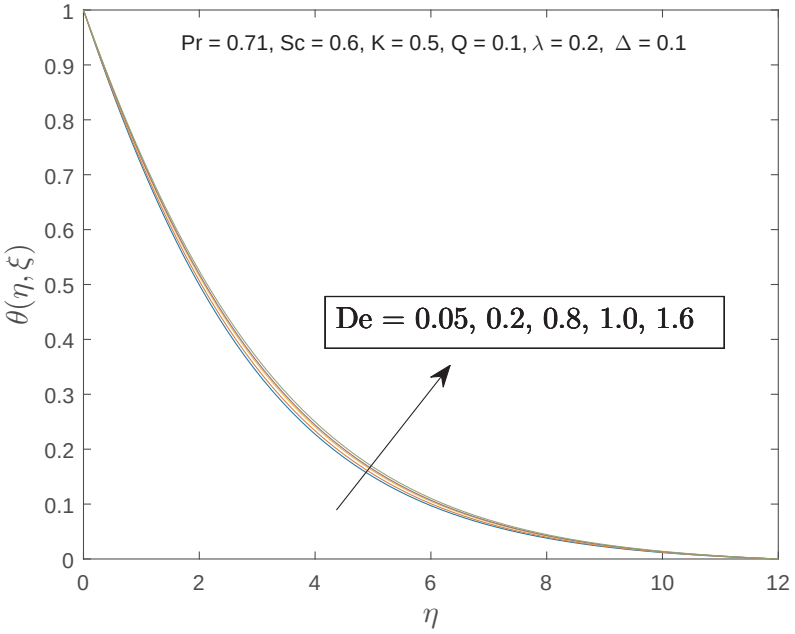

Figure 5.13: The effects of De on the temperature profiles.

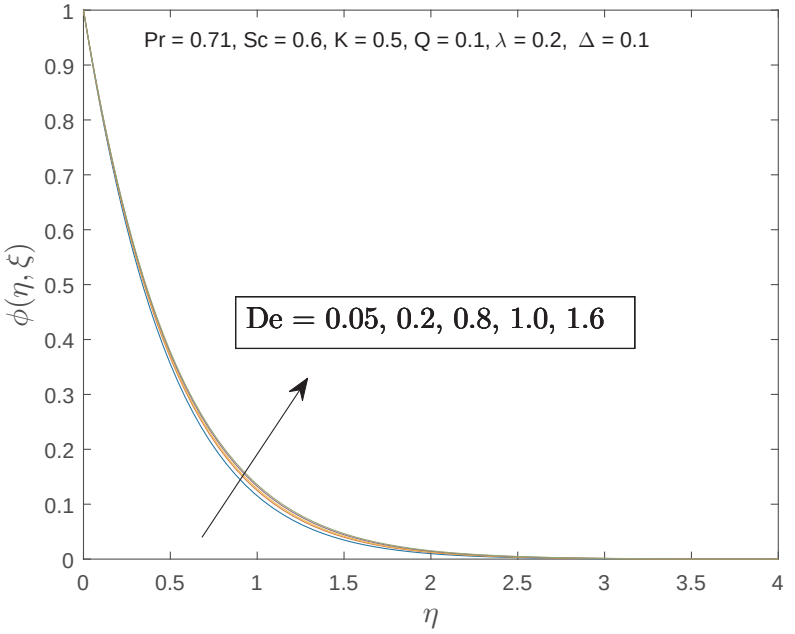

Figure 5.14: The effects of De on the concentration profiles.

The effect of the Schmidt number on the velocity, temperature and concentration profiles is shown in Figures (5.15)-(5.17) respectively. The Schmidt number is used to characterize fluid flow in which there are simultaneous

momentum and mas diffusion. It physically relates to the relative thickness of the velocity boundary layer and mass transfer boundary layer. Figure (5.15) shows that the Jeffery fluid flow is decelerated when the Schmidt is increased. The fluid temperature is slightly enhanced with an increase in the Schmidt number as shown by Figure (5.16). Figure (5.17) shows that the concentration function is greatly depressed with increased values of Schmidt number.

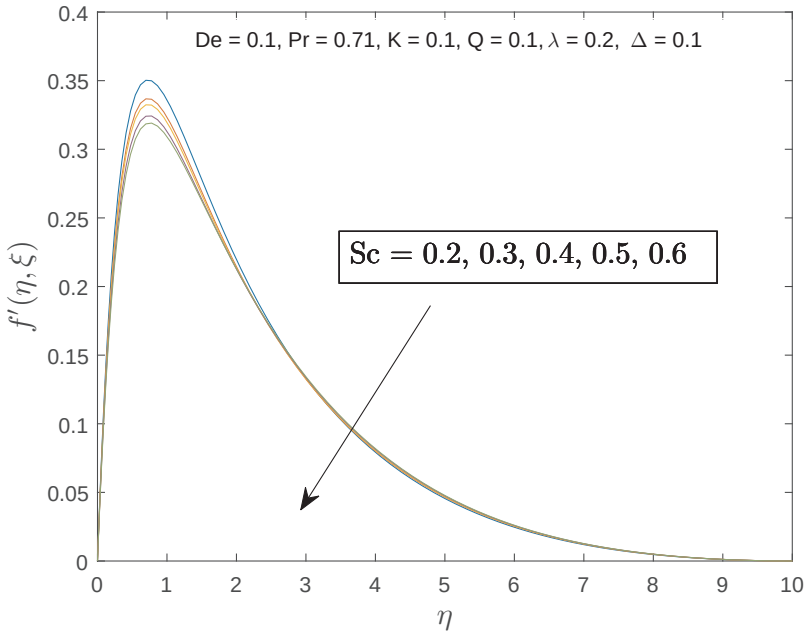

Figure 5.15: The effects of Sc on the velocity profiles.

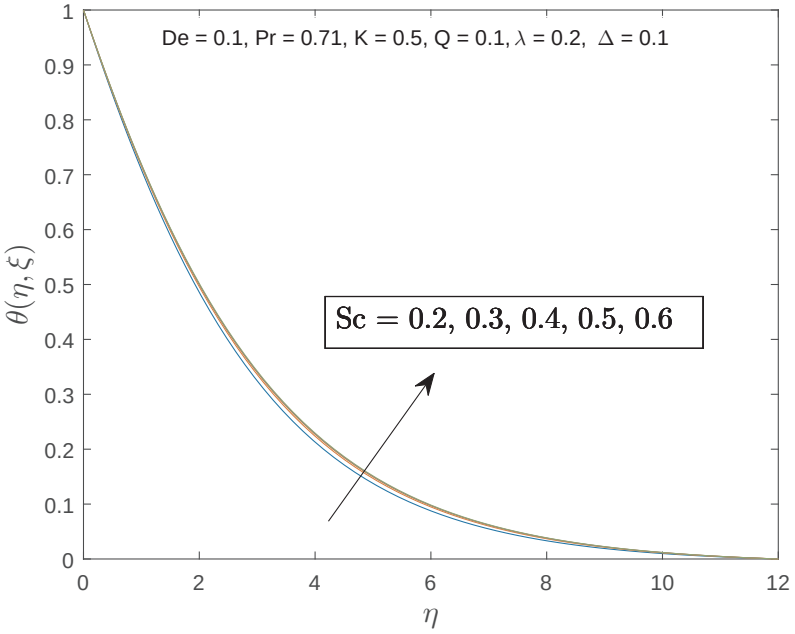

Figure 5.16: The effects of Sc on the temperature profiles.

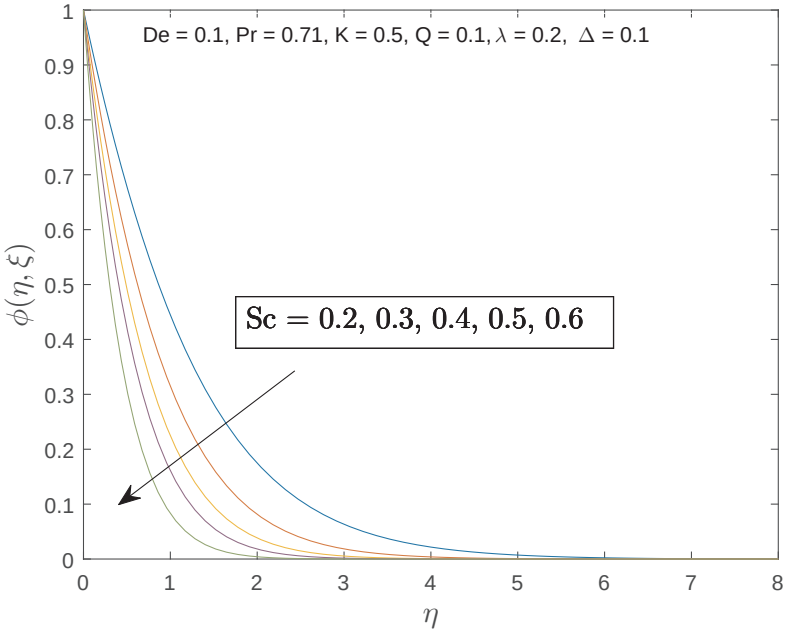

Figure 5.17: The effects of Sc on the concentration profiles.

Figures (5.18) - (5.20) show how the chemical reaction parameter affects the velocity, temperature and concentration profiles. The fluid velocity is slightly decreased with an increase in the chemical reaction parameter whilst the fluid temperature and concentration are greatly decreased.

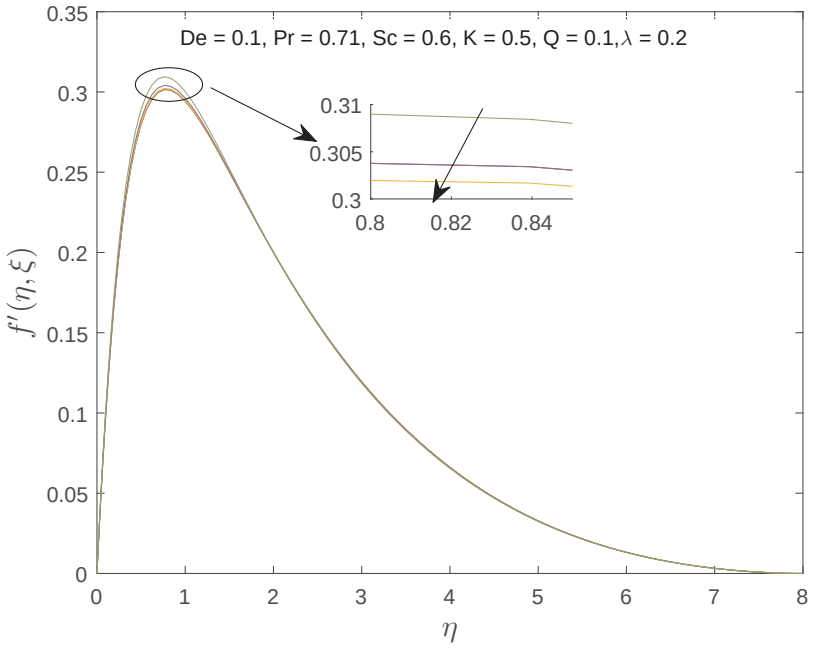

Figure 5.18: The effects of Δ on the velocity profiles.

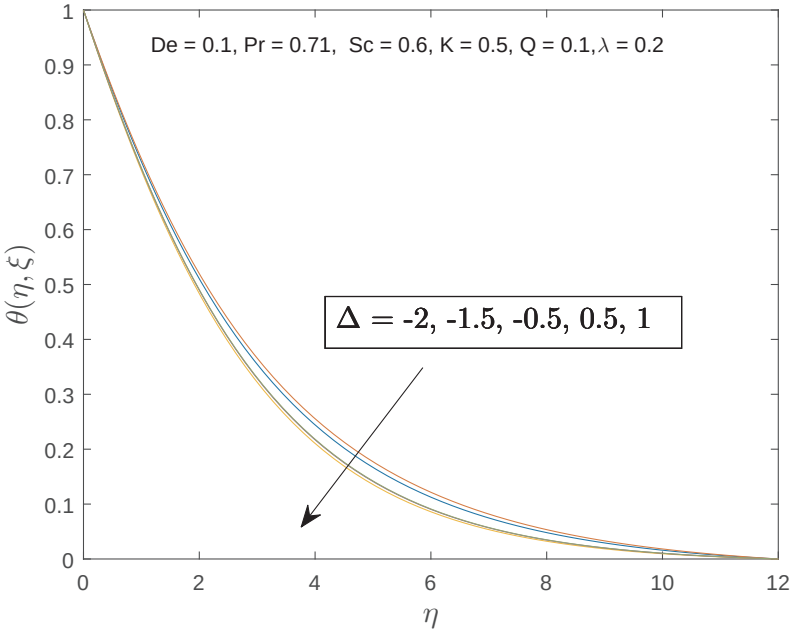

Figure 5.19: The effects of Δ on the temperature profiles.

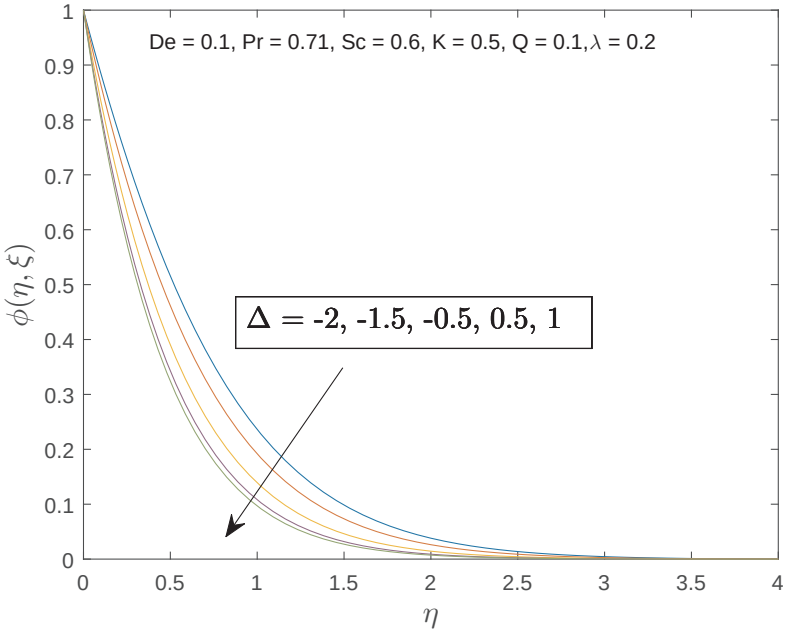

Figure 5.20: The effects of Δ on the concentration profiles.

Table (5.1) shows the influence of λ, Pr, De and Sc on the dimensionless local skin friction coefficient, the heat transfer rate and the mass transfer rate. It is observed that increasing the ratio of relaxation to retardation times

has the effect of increasing the skin friction, the heat transfer rate and the mass transfer rate at the plate surface. It has been shown in Figure (5.3) that the ratio of relaxation to retardation times increases fluid velocity. Higher the velocity means higher the mass flow rate which leads to higher the heat transfer coefficient hence higher the heat transfer rate. An increase in Pr causes an decrease in skin friction and the mass transfer rate whilst the heat transfer rate is increased. This is due to the fact that smaller values of Pr are equivalent to increasing the thermal conductivities, and therefore heat is able to diffuse away the heated plate more rapidly than for higher values of Pr. Increasing both De and Sc decrease the skin friction and the heat transfer rate whilst the mass transfer rate is enhanced. The Schmidt number defined as the ratio of momentum diffusivity and mass diffusivity quantifies the effectiveness of momentum and mass transport by diffusion in the velocity and concentration boundary layers.

Table 5.1: The values of $f''(0,\xi)$, $-\theta'(0,\xi)$ and $-\phi'(0,\xi)$ for different values of the parameters when $\xi = 0.1$.

λ	Pr	De	Sc	$f''(0,\xi)$	$-\theta'(0,\xi)$	$-\phi'(0,\xi)$
0	0.71	0.1	0.6	1.063208	0.309054	1.989794
1				1.666955	0.314015	2.020411
2				2.145467	0.316278	2.036779
3				2.555033	0.317646	2.047521
4				2.919135	0.318586	2.055319
0.2	0.1	0.1	0.6	1.326036	0.231334	2.015877
	0.4			1.221108	0.296032	2.001172
	0.8			1.196212	0.312777	1.997620
	1.0			1.190865	0.316452	1.996854
	1.6			1.182590	0.322196	1.995666
0.2	0.71	0.05	0.6	1.448951	0.313258	2.012246
		0.2		0.947905	0.306715	1.980696
		0.8		0.528923	0.295591	1.940415
		1.0		0.475971	0.293340	1.933769
		1.6		0.377612	0.288177	1.920027
0.2	0.71	0.1	0.2	1.314063	0.315052	0.786595
			0.3	1.267095	0.312732	1.097880
			0.4	1.236869	0.311591	1.401174
			0.5	1.215506	0.310930	1.700629
			0.6	1.199535	0.310508	1.998095

Conclusion

The bi-variate spectral quasi-linearization method was used to solve a system of transformed partial differential equations that model the flow of a Jeffrey fluid through a vertical porous plate in the presence of thermal radiation and chemical reaction. The following are the significant observations from the study

- Increasing the parameter ratio of relaxation to retardation times (λ) increases the flow velocity of the Jeffrey fluid, the local skin friction coefficient, heat transfer rate and the mass transfer rate whilst the temperature and the concentration are slightly depressed.
- Increasing the thermal radiation parameter has an effect of decelerating the fluid flow whilst the temperature and the concentration are slightly enhanced.
- Increasing the Prandtl number causes a reduction in the velocity and temperature of the fluid whilst the concentration is slightly increased. Also, the local skin friction coefficient and the mass transfer rate are depressed with an increase in Pr whilst the heat transfer rate is increase.
- Increasing the Deborah number decreases the fluid flow velocity, local skin friction coefficient, heat transfer rate, mass transfer rate and slightly increase both the temperature and the concentration of the fluid.
- Increasing the Schmidt number has the effect of increasing the fluid concentration, local skin friction coefficient, heat transfer rate, mass transfer rate whilst the fluid velocity and temperature are decreased.
- Increasing the chemical reaction decreases the fluid velocity, temperature and the concentration.

Chapter 6

DISCUSSION AND CONCLUSION

In this work we presented the numerical solutions of nonlinear differential problems that arise from fluid flow. The Bratu problem is a highly nonlinear differential problem which besides being a tool for testing nonlinear solvers, is also used to model problem in radiative heat transfer. The spectral quasi-linearization method (SQLM) was used to solve the one-dimensional Bratu problem. The Bratu problem was solved for different values of the physical parameter $\lambda(= 0.0001, 0.001, 1, 2, 3.51)$. Results obtained were compared against the exact solution and those from published literature, that is, the B-spline method, iterative finite difference method. The SQLM produced results which were correct upto 10 decimal places of the exact solution. The SQLM poduced the solution of the Bratu problem even at the critical value $\lambda = 3.51$ where even some highly accurate methods fail, Temimi and Ben-Romdhane [51]. From these findings we conclude that the SQLM is a relatively reliable numerical technique that can be used to solve nonlinear models in fluid dynamics.

The second part of the thesis dealt with the solution of the two-dimensional Bratu problem using the bivariate spectral quasi-linearization method (BSQLM). The results obtained using the BSQLM were compared with those obtained using the finite difference method, weighted residual method, optimal homotopy analysis method and the wavelet homotopy analysis method. It was found that the results are in good agreement. The results were also compared against the Chebyshev spectral collocation (CSCM-K) that make use of Kronecker multiplication which is known to be highly accurate. The results obtained from the BSQLM are found to agree to 5 decimal places of the results from CSCM-K. Also, it is observed that BSQLM takes less time and fewer iterations to converge to the solution than CSCM-K.

The third problem is the numerical study of a non-Newtonian fluid past a vertical porous plate with heat and mass transfer in the fluid flow. The fluid flow is modeled by a coupled system of nonlinear differential equations. Similarity transformations were introduced to transform the nonlinear system into a coupled system of linear partial

differential equations which which were solved using the bivariate spectral quasi-linearization method (BSQLM). The error norms and residual error norms were used to show the convergence and accuracy of the bivariate spectral quasi-linearization method, respectively. The error norms and residual error norms in each of the functions (f, ϕ, θ) is observed to decrease with an increase in the number of iterations and this suggests the convergence and accuracy of the method. The values of the local skin friction, Nusselt number and the Sherwood number were computed and compared against those from previous studies. It was found out that there is a good agreement between the results. The effects of some non-dimensionless physical parameters namely the ratio of relaxation to retardation times, Prandtl number and Schmidt number on the velocity, temperature and concentration profiles were investigated. The results were presented graphically.

The last problem was the extension of the non-Newtonian Jeffrey model to include the effects of chemical reaction and thermal radiation in fluid flow. The error norms and residual error norms where used to show that the method is both convergent and accurate, respectively. This was shown by the decrease in the errors of the functions (f, θ, ϕ) with an increase in the number of iterations. In this work, it is noted that local skin friction coefficient, heat and mass transfer rate are increased with increasing ratio of relaxation to retardation times parameter whilst the fluid concentration is depressed. Increasing the Prandtl number causes a reduction in the velocity and temperature of the fluid whilst the concentration is increased. Also, the local skin friction coefficient and the mass transfer rates are depressed with an increase in the Prandtl number. An increase in the chemical reaction parameter decreases the fluid velocity, temperature and the concentration. Increasing the thermal radiation parameter has an effect of decelerating the fluid flow whilst the temperature and the concentration are slightly enhanced.

6.1 What is new in this study

The methods used to solve the differential equations are available in literature. Also, the problems under consideration have been previously studied. The original part of this thesis is the use of the methods to solve the differential equations under study.

6.2 Future work

In this work we applied the SQLM and the BSQLM to solve both the one-dimensional and two-dimensional Bratu problems, respectively. We also applied the BSQLM to study numerically the flow of a non-Newtonian fluid past a vertical porous plate. It will be of interest in future work to apply another spectral method like the multi-domain bivariate spectral quasi-linearization method Magagula *et al.*[126] to analyze the flow of a non-Newtonian fluid in porous media. The numerical method is known to be easy to use, converges rapidly and give accurate results.

Bibliography

[1] Chhabra, R. P. (1993). Fluid Flow, Heat, and Mass Transfer in Non-Newtonian Fluids: Multiphase Systems. Advances in Heat Transfer, 187–278.

[2] Koplik, J., & Banavar, J. R. (1997). Reentrant corner flows of Newtonian and non-Newtonian fluids. Journal of Rheology, 41(3), 787–805.

[3] Kaur, N., Singh, R., & Wanchoo, R. K. (2011). Flow of Newtonian and Non-Newtonian Fluids Through Packed Beds: An Experimental Study. Transport in Porous Media, 90(2), 655–671.

[4] Nouri, J. M., & Whitelaw, J. H. (1994). Flow of Newtonian and Non-Newtonian Fluids in a Concentric Annulus With Rotation of the Inner Cylinder. Journal of Fluids Engineering, 116(4), 821.

[5] Akbar, N. S., Nadeem, S., & Lee, C. (2013). Characteristics of Jeffrey fluid model for peristaltic flow of chyme in small intestine with magnetic field. Results in Physics, 3, 152–160.

[6] Akbar, N. S., Nadeem, S., & Ali, M. (2011). Jeffrey fluid model for blood flow through a tapered artery with a stenosis. Journal of Mechanics in Medicine and Biology, 11(03), 529-545.

[7] Sharma, B. D., Yadav, P. K., & Filippov, A. (2017). A Jeffrey-fluid model of blood flow in tubes with stenosis. Colloid Journal, 79(6), 849–856.

[8] Paul, A.; Laurila, T.; Vuorinen, V.; Divinski, S. V. Fick's Laws of Diffusion.; Springer: Berlin, Gemany, 2014.

[9] Gür, H. B., & Eyi, S. (2018). CFD Analyses of Hypersonic Flow Regimes with Stephan-Maxwell Diffusion Equation. 2018 Fluid Dynamics Conference.

[10] Guo, Z., & Zhao, T. S. (2003). Explicit finite-difference lattice Boltzmann method for curvilinear coordinates. Physical Review E, 67(6).

[11] Xu, A. (2005). Finite-difference lattice-Boltzmann methods for binary fluids. Physical Review E, 71(6).

[12] Gabbanelli, S., Drazer, G., & Koplik, J. (2005). Lattice Boltzmann method for non-Newtonian (power-law) fluids. Physical Review E, 72(4).

[13] Wang, C.-H., & Ho, J.-R. (2011). A lattice Boltzmann approach for the non-Newtonian effect in the blood flow. Computers & Mathematics with Applications, 62(1), 75–86.

[14] Omosebi, O. A., & Akabogu, A. K. (2017). Application of the Galerkin's Finite Element Method to the Flow of Power-Law Non-Newtonian Fluids through Porous Media. SPE Western Regional Meeting.

[15] Chung, E. T., Iliev, O., & Vasilyeva, M. V. (2016). Generalized multiscale finite element method for non-Newtonian fluid flow in perforated domain.

[16] Tanner, R. I., Nickell, R. E., & Bilger, R. W. (1975). Finite element methods for the solution of some incompressible non-Newtonian fluid mechanics problems with free surfaces. Computer Methods in Applied Mechanics and Engineering, 6(2), 155–174.

[17] Böhme, G., & Rubart, L. (1989). Non-Newtonian flow analysis by finite elements. Fluid Dynamics Research, 5(3), 147–158.

[18] Salahuddin, T., Malik, M. Y., Hussain, A., Awais, M., & Bilal, S. (2017). Mixed Convection Boundary Layer Flow of Williamson Fluid with Slip Conditions Over a Stretching Cylinder by Using Keller Box Method. International Journal of Nonlinear Sciences and Numerical Simulation, 18(1).

[19] Liao SJ. (1992). The proposed homotopy analysis technique for the solution of nonlinear problems. PhD thesis. Shanghai Jiao Tong University.

[20] Esmaeilpour, M., Domairry, G., Sadoughi, N., & Davodi, A. G. (2010). Homotopy Analysis Method for the heat transfer of a non-Newtonian fluid flow in an axisymmetric channel with a porous wall. Communications in Nonlinear Science and Numerical Simulation, 15(9), 2424–2430.

[21] Ellahi, R. (2012). A Study on the Convergence of Series Solution of Non-Newtonian Third Grade Fluid with Variable Viscosity: By Means of Homotopy Analysis Method. Advances in Mathematical Physics, 2012, 1–11.

[22] Rashidi, M. M., Rastegari, M. T., Asadi, M., & Bég, O. A. (2012). A study of non-Newtonian flow and heat transfer over a non-thermal wedge using the homotopy analysis method. Chemical Engineering Communications, 199(2), 231–256.

[23] G. Adomian. (1994), Solving Frontier Problems of Physics: The Decomposition Method, vol. 60 of Fundamental Theories of Physics, Kluwer Academic, Dordrecht, The Netherlands.

[24] Shakeri Aski, F., Nasirkhani, S. J., Mohammadian, E., & Asgari, A. (2014). Application of Adomian decomposition method for micropolar flow in a porous channel. Propulsion and Power Research, 3(1), 15–21.

[25] Siddiqui, A. M., Hameed, M., Siddiqui, B. M., & Babcock, B. S. (2012). Adomian decomposition method applied to study nonlinear equations arising in non-newtonian flows. Applied Mathematical Sciences, 6(97-100), 4889-4909.

[26] Alam, M. K., Rahim, M. T., Avital, E. J., Islam, S., Siddiqui, A. M., & Williams, J. J. R. (2013). Solution of the steady thin film flow of non-Newtonian fluid on vertical cylinder using Adomian Decomposition Method. Journal of the Franklin Institute, 350(4), 818–839.

[27] He, J.H. (1997) A New Approach to Nonlinear Partial Differential Equations. Communications in Nonlinear Science and Numerical Simulation, 2, 230-235.

[28] Siddiqui, A., Farooq, A., Haroon, T., Rana, M., & Babcock, B. (2012). Application of He's Variational Iterative Method for Solving Thin Film Flow Problem Arising in Non-Newtonian Fluid Mechanics, World Journal of Mechanics, Vol. 2 No. 3. 138-142.

[29] Farooq, A., Siddiqui, A. M., Rana, M. A., & Haroon, T. (2012). Application of He's Method in Solving a System of Nonlinear Coupled Equations Arising in Non-Newtonian Fluid Mechanics. International Journal of Applied Mathematical Research, 1(2).

[30] Moosavi, M., Momeni, M., Tavangar, T., Mohammadyari, R., & Rahimi-Esbo, M. (2016). Variational iteration method for flow of non-Newtonian fluid on a moving belt and in a collector. Alexandria Engineering Journal, 55(2), 1775–1783.

[31] RamReddy, C., & Pradeepa, T. (2016). Spectral Quasi-linearization Method for Homogeneous-Heterogeneous Reactions on Nonlinear Convection Flow of Micropolar Fluid Saturated Porous Medium with Convective Boundary Condition. Open Engineering, 6(1).

[32] Shateyi, S. & Marewo, G. (2018). Numerical solution of mixed convection flow of an MHD Jeffery fluid over an exponentially stretching sheet in the presence of thermal radiation and chemical reaction. Open Physics, 16(1), pp. 249-259.

[33] Shateyi, S., Mabood, F., & Marewo, G. T. (2016). On a New Numerical Approach on Micropolar Fluid, Heat and Mass Transfer Over an Unsteady Stretching Sheet Through Porous Media in the Presence of a Heat Source/Sink and Chemical Reaction. Numerical Simulation - From Brain Imaging to Turbulent Flows.

[34] Motsa, S. S. (2013). A New Spectral Local Linearization Method for Nonlinear Boundary Layer Flow Problems. Journal of Applied Mathematics, 2013, 1–15.

[35] Goqo, S. P., Oloniiju, S. D., Mondal, H., Sibanda, P., & Motsa, S. S. (2018). Entropy generation in MHD radiative viscous nanofluid flow over a porous wedge using the bivariate spectral quasi-linearization method. Case Studies in Thermal Engineering.

[36] Abbas, Z., Sheikh, M., & Motsa, S. S. (2016). Numerical solution of binary chemical reaction on stagnation point flow of Casson fluid over a stretching/shrinking sheet with thermal radiation. Energy, 95, 12–20.

[37] Motsa, S.S., & Mohammad, S. A. (2015). Unsteady boundary layer flow and heat transfer of Oldroyd-B nanofluid towards a stretching sheet with variable thermal conductivity. Thermal Science 19.suppl, 1239-248.

[38] Motsa, S. S., Magagula, V. M., & Sibanda, P. (2014). A Bivariate Chebyshev Spectral Collocation Quasi-linearization Method for Nonlinear Evolution Parabolic Equations. The Scientific World Journal, 2014, 1-13.

[39] Bratu. G, Sur les equation integrals non-lineaires, Bull. Math. Soc. France 42 (1914):pp 113-142.

[40] Mounim, A. S., & de Dormale, B. M. (2006). From the fitting techniques to accurate schemes for the Liouville-Bratu-Gelfand problem. Numerical Methods for Partial Differential Equations, 22(4), 761–775.

[41] Jacobsen, J., & Schmitt, K. (2002). The Liouville–Bratu–Gelfand Problem for Radial Operators. Journal of Differential Equations, 184(1), 283–298.

[42] Luo, Q., Liang, D., & Mo, S. (2015). Numerical Calculation of the Critical Parameters of Frank-Kamenetskii Equation in Spontaneous Combustion Theory. Numerical Heat Transfer, Part B: Fundamentals, 68(5), 403–417.

[43] Mohsen, A. (2014). A simple solution of the Bratu problem. Computers & Mathematics with Applications, 67(1), 26–33.

[44] Adesanya, S. O., Arekete S. A. & Babadipe E. S.(2013). A new result on adomian decomposition method for solving Bratu's problem, Math. Theory Model 3.1.

[45] Kafri, H. Q., & Khuri, S. A. (2016). Bratu's problem: A novel approach using fixed-point iterations and Green's functions. Computer Physics Communications, 198, 97–104.

[46] Boyd, J. P. (1986). An analytical and numerical study of the two-dimensional Bratu equation. Journal of Scientific Computing, 1(2), 183–206.

[47] Liao, S., & Tan, Y. (2007). A General Approach to Obtain Series Solutions of Nonlinear Differential Equations. Studies in Applied Mathematics, 119(4), 297–354.

[48] Wan, Y.-Q., Guo, Q.,& Pan, N. (2004). Thermo-electro-hydrodynamic model for electrospinning process. International Journal of Nonlinear Sciences and Numerical Simulation, 5(1).

[49] Motsa, S. S., & Sibanda, P. (2012). Some modifications of the quasilinearization method with higher-order convergence for solving nonlinear BVPs. Numerical Algorithms, 63(3), 399–417.

[50] Semary, M. S., & Hassan, H. N. (2015). A new approach for a class of nonlinear boundary value problems with multiple solutions. Journal of the Association of Arab Universities for Basic and Applied Sciences, 17(1), 27–35.

[51] Temimi, H., & Ben-Romdhane, M. (2016). An iterative finite difference method for solving Bratu's problem. Journal of Computational and Applied Mathematics, 292, 76–82.

[52] Hassan, H.N.,& Semary, M.S., (2013). Analytic approximate solution for Bratu's problem by optimal homotopy analysis method. Commun. Numer. Anal. 2013, 1–14.

[53] Abbasbandy, S., Hashemi, M. S., & Liu, C.-S. (2011). The Lie-group shooting method for solving the Bratu equation. Communications in Nonlinear Science and Numerical Simulation, 16(11), 4238–4249.

[54] Buckmire, R. (2003). Investigations of nonstandard, Mickens-type, finite-difference schemes for singular boundary value problems in cylindrical or spherical coordinates. Numerical Methods for Partial Differential Equations, 19(3), 380–398.

[55] Hassan, H. N., & El-Tawil, M. A. (2011). An efficient analytic approach for solving two-point nonlinear boundary value problems by homotopy analysis method. Mathematical Methods in the Applied Sciences, 34(8), 977–989.

[56] Syam, M. I., & Hamdan, A. (2006). An efficient method for solving Bratu equations. Applied Mathematics and Computation, 176(2), 704–713.

[57] Motsa, S. S., Dlamini, P. G., & Khumalo, M. (2014). Spectral Relaxation Method and Spectral Quasilinearization Method for Solving Unsteady Boundary Layer Flow Problems. Advances in Mathematical Physics, 2014, 1–12.

[58] Bellman, R. E. and Kalaba, R. E, Quasilinearization and nonlinear boundary-value problems. Elsevier, New York (1965).

[59] Trefethen. L.N, Spectral methods in MATLAB, SIAM, Philadelphia, 2000.

[60] Caglar, H., Caglar, N., Özer, M., Valarıstos, A., & Anagnostopoulos, A. N. (2010). B-spline method for solving Bratu's problem. International Journal of Computer Mathematics, 87(8), 1885–1891.

[61] Boyd, J. P. (2003). Chebyshev polynomial expansions for simultaneous approximation of two branches of a function with application to the one-dimensional Bratu equation. Applied Mathematics and Computation, 143(2-3), 189–200.

[62] Slunyaev, A. V., & Shrira, V. I. (2013). On the highest non-breaking wave in a group: fully nonlinear water wave breathers versus weakly nonlinear theory. Journal of Fluid Mechanics, 735, 203–248.

[63] Sibanda, P., Motsa, S., & Makukula, Z. (2012). A spectral-homotopy analysis method for heat transfer flow of a third grade fluid between parallel plates. International Journal of Numerical Methods for Heat & Fluid Flow, 22(1), 4-23.

[64] He, J. H. (2005). Homotopy Perturbation Method for Bifurcation of Nonlinear Problems. International Journal of Nonlinear Sciences and Numerical Simulation, 6(2).

[65] Adomian, G. (1991). A review of the decomposition method and some recent results for nonlinear equations. Computers & Mathematics with Applications, 21(5), 101–127.

[66] Mohan, C., & Al-Bayaty, A. R. (1980). Power-series solutions of the Lane-Emden equation. Astrophysics and Space Science, 73(1), 227–239.

[67] Lyapunov, A. M. (1992). The general problem of the stability of motion. International Journal of Control, 55(3), 531–534.

[68] Ji-huan, H. (2002). A note on delta-perturbation expansion method. Applied Mathematics and Mechanics, 23(6), 634–638.

[69] Argyris, J., & Haase, M. (1987). An engineer's guide to soliton phenomena: Application of the finite element method. Computer Methods in Applied Mechanics and Engineering, 61(1), 71–122.

[70] Vliegenthart, A. C. (1971). On finite-difference methods for the Korteweg-de Vries equation. Journal of Engineering Mathematics, 5(2), 137–155.

[71] Temimi, H., & Ben-Romdhane, M. (2016). An iterative finite difference method for solving Bratu's problem. Journal of Computational and Applied Mathematics, 292, 76–82.

[72] Caglar, H., Caglar, N., Özer, M., Valarıstos, A., & Anagnostopoulos, A. N. (2010). B-spline method for solving Bratu's problem. International Journal of Computer Mathematics, 87(8), 1885–1891.

[73] Mohsen, A., Sedeek, L. F., & Mohamed, S. A. (2008). New smoother to enhance multigrid-based methods for Bratu problem. Applied Mathematics and Computation, 204(1), 325–339.

[74] Chang, S.-L., & Chien, C.-S. (2003). A Multigrid-Lanczos algorithm for the numerical solutions of nonlinear eigenvalue problems. International Journal of Bifurcation and Chaos, 13(05), 1217–1228.

[75] Odejide, S. A., & Y. A. S. Aregbesola. (2006). A note on two dimensional Bratu problem. Kragujevac Journal of Mathematics 29.29. 49-56.

[76] Yang, Z., & Liao, S. (2017). A HAM-based wavelet approach for nonlinear partial differential equations: Two dimensional Bratu problem as an application. Communications in Nonlinear Science and Numerical Simulation, 53, 249–262.

[77] Raja, M. A. Z., Ahmad, S.-I., & Samar, R. (2014). Solution of the 2-dimensional Bratu problem using neural network, swarm intelligence and sequential quadratic programming. Neural Computing and Applications, 25(7-8), 1723–1739.

[78] Motsa, S. S., Magagula, V. M., & Sibanda, P. (2014). A Bivariate Chebyshev Spectral Collocation Quasi-linearization Method for Nonlinear Evolution Parabolic Equations. The Scientific World Journal, 1–13.

[79] Liu, F., Ye, X., & Wang, X. (2011). Efficient Chebyshev spectral method for solving linear elliptic PDEs using quasi-inverse technique. Numer. Math. Theor. Meth. Appl, 4, 197-215.

[80] Sochi, T. (2010). Non-Newtonian flow in porous media. Polymer, 51(22), 5007–5023.

[81] Hussanan, A., Zuki Salleh, M., Tahar, R. M., & Khan, I. (2014). Unsteady Boundary Layer Flow and Heat Transfer of a Casson Fluid past an Oscillating Vertical Plate with Newtonian Heating. 9(10), e108763.

[82] Yilmaz, N., Bakhtiyarov, A. S., & Ibragimov, R. N. (2009). Experimental investigation of Newtonian and non-Newtonian fluid flows in porous media. Mechanics Research Communications, 36(5), 638–641.

[83] Kozicki, W., & Tiu, C. (1988). A unified model for non-Newtonian flow in packed beds and porous media. Rheologica Acta, 27(1), 31–38.

[84] Pearson, J. R. A., & Tardy, P. M. J. (2002). Models for flow of non-Newtonian and complex fluids through porous media. Journal of Non-Newtonian Fluid Mechanics, 102(2), 447–473.

[85] Sadowski, T. J., & Bird, R. B. (1965). Non-Newtonian Flow through Porous Media. I. Theoretical. Transactions of the Society of Rheology, 9(2), 243–250.

[86] Liu S & Masliyah JH (1998). On non-Newtonian fluid flow in ducts and porous media-optical rheometry in opposed jets and flow through porous media. Chem Eng Sci;53(6):1175-201.

[87] Hosseini, M., Sheikholeslami, Z., & Ganji, D. D. (2013). Non-Newtonian fluid flow in an axisymmetric channel with porous wall. Propulsion and Power Research, 2(4), 254–262.

[88] Debruge, L. L., & Han, L. S. (1972). Heat Transfer in a Channel with a Porous Wall for Turbine Cooling Application. Journal of Heat Transfer, 94(4), 385-390.

[89] Qasim, M (2013) Heat and mass transfer in a Jeffrey fluid over a stretching sheet with heat source/sink. Alexandria Engineering Journal (52): 571–575.

[90] Khan I, Fakhar K, Anwar MI (2012) Hydromagnetic rotating flows of an Oldroyd-B fluid in a porous medium. Special Topics and Review in Porous Media (3): 89–95.

[91] Khan I, Farhad A, Samiulhaq, Sharidan S (2013) Exact solutions for unsteady MHD oscillatory flow of a Maxwell fluid in a porous medium. Zeitschrift Fur Naturforschung A (68): 635–645.

[92] Hayat T, Khan I, Ellahi R, Fetecau C (2008) Some unsteady MHD flows of a second grade fluid through porous medium. Journal Porous Media (11): 389–400.

[93] Pop, I., Watanabe, T.: The effects of suction or injection in boundary layer flow and heat transfer on a continuous moving surface. Techn. Mechanik13, 49–54 (1992).

[94] Ellahi R., Rahman S.U., Nadeem S., Blood flow of Jeffrey fluid in a catherized tapered artery with the suspension of nanoparticles, Phys. Lett. A, 2014, 378, 2973-2980.

[95] Afsar Khan, A., Ellahi, R., & Vafai, K. (2012). Peristaltic Transport of a Jeffrey Fluid with Variable Viscosity through a Porous Medium in an Asymmetric Channel. Advances in Mathematical Physics, 2012, 1–15.

[96] Kothandapani, M., & Srinivas, S. (2008). Peristaltic transport of a Jeffrey fluid under the effect of magnetic field in an asymmetric channel. International Journal of Non-Linear Mechanics, 43(9), 915–924.

[97] Hayat, T., Shehzad, S. A., Qasim, M., & Obaidat, S. (2012). Radiative flow of Jeffery fluid in a porous medium with power law heat flux and heat source. Nuclear Engineering and Design, 243, 15–19.

[98] S.S. Motsa, et al., A Bivariate Chebyshev Spectral Collocation Quasilinearization Method for Nonlinear Evolution Parabolic Equations, The Scientific World Journal, 2014 (2014), ID 581987.

[99] Nazari,M., Salah, F., & Z. A. Aziz. (2012). Analytic approximate solution for the KdV equation with the homotopy analysis method, Matematika, 28(1), 53–61.

[100] J. W. Cahn and J. E. Hillard, "Free energy of a nonuniform system. I. Interfacial free energy," J. Chem. Phys. 28, 258 (1958).

[101] Vinay Chandraker, Ashish Awasthi, Simon Jayaraj, (2016), "Numerical Treatment of Burger-Fisher equation", Procedia Technology 25 (2016) 1217–1225.

[102] Muzara, H., Shateyi, S. & Tendayi Marewo, G. (2018). On the bivariate spectral quasi-linearization method for solving the two-dimensional Bratu problem. Open Physics, 16(1), pp. 554-562.

[103] Nadeem, S., & Akbar, N. S. (2009). Peristaltic Flow of a Jeffrey Fluid with Variable Viscosity in an Asymmetric Channel. Zeitschrift Für Naturforschung A, 64(11): 713-722.

[104] Ramachandra Prasad, V., Abdul Gaffar, S., Keshava Reddy, E., Anwar Bég, O., & Krishnaiah, S. (2013). A Mathematical Study for Laminar Boundary-Layer Flow, Heat, and Mass Transfer of a Jeffrey Non-Newtonian Fluid Past a Vertical Porous Plate. Heat Transfer-Asian Research, 44(3), 189–210.

[105] Gaffar SA, Prasad VR, Reddy EK (2017) Computational study of Jeffrey's non-Newtonian fluid past a semi-infinite vertical plate with thermal radiation and heat generation/absorption. Ain Shams Eng J 8(2):277–294

[106] Ahmad, B., Nieto, J. J., & Shahzad, N. (2001). The Bellman–Kalaba–Lakshmikantham Quasilinearization Method for Neumann Problems. Journal of Mathematical Analysis and Applications, 257(2), 356–363.

[107] Shamsi, M., & Dehghan, M. (2006). Recovering a time-dependent coefficient in a parabolic equation from overspecified boundary data using the pseudospectral Legendre method. Numerical Methods for Partial Differential Equations, 23(1), 196–210.

[108] S.S. Motsa and M.S. Ansari, Unsteady Boundary Layer Flow and Heat transfer of Oldroyd-B Nanofluid towards a Stretching Sheet with Variable Thermal Conductivity, Thermal Science, 19(1), pp. s239–s248(2015).

[109] Khan, Y., Wu, Q., Faraz, N., Yıldırım, A., & Mohyud-Din, S. T. (2012). Heat Transfer Analysis on the Magnetohydrodynamic Flow of a Non- Newtonian Fluid in the Presence of Thermal Radiation: An Analytic Solution. Zeitschrift Für Naturforschung A, 67(3-4).

[110] Srinivasacharya, D., & Upendar, M. (2013). Thermal radiation and chemical reaction effects on MHD mixed convection heat and mass transfer in micropolar fluid. Mechanics, 19(5).

[111] Ganapathirao, M., Ravindran, R., & Momoniat, E. (2014). Effects of chemical reaction, heat and mass transfer on an unsteady mixed convection boundary layer flow over a wedge with heat generation/absorption in the presence of suction or injection. Heat and Mass Transfer, 51(2), 289–300.

[112] Vajravelu, K., Prasad, K. V., & Prasanna Rao, N. S. (2011). Diffusion of a chemically reactive species of a power-law fluid past a stretching surface. Computers & Mathematics with Applications, 62(1), 93–108.

[113] Postelnicu, A. (2006). Influence of chemical reaction on heat and mass transfer by natural convection from vertical surfaces in porous media considering Soret and Dufour effects. Heat and Mass Transfer, 43(6), 595–602.

[114] El-Sayed, M. F., Eldabe, N. T. M., Ghaly, A. Y., & Sayed, H. M. (2011). Effects of Chemical Reaction, Heat, and Mass Transfer on Non-Newtonian Fluid Flow Through Porous Medium in a Vertical Peristaltic Tube. Transport in Porous Media, 89(2), 185-212.

[115] Srinivasacharya, D., & Swamy Reddy, G. (2016). Chemical reaction and radiation effects on mixed convection heat and mass transfer over a vertical plate in power-law fluid saturated porous medium. Journal of the Egyptian Mathematical Society, 24(1), 108-115.

[116] Gorla, R. S. R., Asghar, S., Hossain, M. A., Khan, W., & Mukhopadhyay, S. (2014). Heat and Mass Transfer in Non-Newtonian Fluids. Advances in Mechanical Engineering, 6, 1043-92.

[117] Xie, Y., Zhang, Z., Shen, Z., & Zhang, D. (2015). Numerical Investigation of Non-Newtonian Flow and Heat Transfer Characteristics in Rectangular Tubes with Protrusions. Mathematical Problems in Engineering, 2015, 1-11.

[118] Sojoudi, A., Mazloomi, A., Saha, S. C., & Gu, Y. T. (2014). Similarity Solutions for Flow and Heat Transfer of Non-Newtonian Fluid over a Stretching Surface. Journal of Applied Mathematics, 2014, 1-8.

[119] Oyelakin, I.S.; Mondal, S.; Sibanda, P. (2017) . Unsteady mixed convection in nanofluid flow through a porous medium with thermal radiation using the Bivariate Spectral Quasilinearization method. J. Nanofluids, 6, 273–281.

[120] Muzara, H., Shateyi, S., & Tendayi Marewo, G. (2018). On the bivariate spectral quasi-linearization method for solving the two-dimensional Bratu problem. Open Physics, 16(1), 554-562.

[121] Devakar, M., Ramesh, K., Chouhan, S., & Raje, A. (2017). Fully developed flow of non-Newtonian fluids in a straight uniform square duct through porous medium. Journal of the Association of Arab Universities for Basic and Applied Sciences, 23(1), 66-74.

[122] El-Aziz, M. A., & Yahya, A. S. (2017). Heat and Mass Transfer of Unsteady Hydromagnetic Free Convection Flow Through Porous Medium Past a Vertical Plate with Uniform Surface Heat Flux. Journal of Theoretical and Applied Mechanics, 47(3), 25–58.

[123] Abdul Gaffar, S., Ramachandra Prasad, V., & Keshava Reddy, E. (2017). Computational study of Jeffrey's non-Newtonian fluid past a semi-infinite vertical plate with thermal radiation and heat generation/absorption. Ain Shams Engineering Journal, 8(2), 277–294.

[124] Magagula, V. M., Motsa, S. S., Sibanda, P., & Dlamini, P. G. (2016). On a bivariate spectral relaxation method for unsteady magneto-hydrodynamic flow in porous media. SpringerPlus, 5(1).

[125] Oyelakin, I. S., Mondal, S., & Sibanda, P. (2017). A multi-domain spectral method for non-Darcian mixed convection flow in a power-law fluid with viscous dissipation. Physics and Chemistry of Liquids, 1–19.

[126] Magagula, V. M., Motsa, S. S., & Sibanda, P. (2016). A Multi-Domain Bivariate Pseudospectral Method for Evolution Equations. International Journal of Computational Methods, 14(04), 1750041.